MONTHLY NOTICES

OF THE

ROYAL ASTRONOMICAL SOCIETY

CONTAINING

PAPERS, ABSTRACTS OF PAPERS, AND REPORTS
OF THE PROCEEDINGS OF THE SOCIETY

1949

VOL. 109

Published and Sold by the
ROYAL ASTRONOMICAL SOCIETY
BURLINGTON HOUSE
LONDON, W. 1
1949

Printed in London by
TAYLOR & FRANCIS, LIMITED

MONTHLY NOTICES

OF THE

ROYAL ASTRONOMICAL SOCIETY

Vol. 109 No. 1

MEETING OF 1949 JANUARY 14

Professor W. M. H. Greaves, President, in the Chair

The election by the Council of the following Fellows was duly confirmed:—

David William Glyn Arthur, 35 Vastern Road, Reading, Berkshire (proposed by H. P. Wilkins);

Alwyn John Ashmore, 17 Hampden Road, Malvern Link, Worcestershire (proposed by A. W. Lane Hall);

Robert Ion Beverley Cooper, Ph.D., Trinity College, Cambridge (proposed by B. C. Browne);

John Frederick Griffiths, B.Sc., 29 Ingleton Avenue, Welling, Kent (proposed by D. Brunt);

Caroline Winifred Herschel, 10 Polstead Road, Oxford (proposed by Rev. Sir John Herschel, Bt.);

James Chisholm Johnston, 34 Minto Street, Edinburgh (proposed by W. M. H. Greaves);

Claude Lipman Lyons, B.Sc., 1 Goodyers Gardens, Brent Green, London, N.W. 4 (proposed by J. M. F. Dumphreys);

Cyril Thomas Moss, 58 Garden Road, Brighouse, Yorkshire (proposed by H. Dingle);

Roderick McIver Paton, 63 Second Avenue, Chelmsford, Essex (proposed by H. W. Newton);

William Herschel Ward, 14 Kent Road, St. John's Hill, Wanganui, New Zealand (proposed by D. C. Berry); and

James Leslie White, 132 By Pass Road, Ewell, Surrey (proposed by J. G. Porter).

The election by the Council of the following Junior Members was duly confirmed:—

Raymond Douglas Manners, Khanspur, Mansfield Road, Bognor Regis, Sussex (proposed by Lydia A. Brown);

William Theodore Roach, Kentish House, Kentish Lane, Hatfield, Hertfordshire (proposed by M. W. Ovenden); and

John Bertram Slayton, 1a Grosvenor Hill, The Ridgeway, Wimbledon, S.W. 19 (proposed by E. A. Milne).

Eighty-two presents were announced as having been received since the last meeting, including:—

S. A. Mitchell, *History of the Leander McCormick Observatory of the University of Virginia* (presented by the author);

P. Herget, *The Computation of Orbits* (presented by Dr G. Merton);

G. Keller, *On the Physical and Chemical Composition of the Sun* (presented by the author); and

W. Stewart Wallace, *Royal Canadian Institute, Centennial Volume*, 1849–1949 (presented by the Royal Canadian Institute).

The President announced that the Council had awarded the Gold Medal of the Society to Professor Sydney Chapman, Sedleian Professor of Natural Philosophy in the University of Oxford, for his contributions to geophysics and solar physics, and particularly to the theory of geomagnetic phenomena.

The President announced that the Council had awarded a Jackson-Gwilt Medal and Gift to Mr Algernon Montagu Newbegin, for his observations of solar phenomena during the past forty years.

CHARACTERISTIC PROPERTIES OF CHROMOSPHERIC FLARES

M. A. Ellison

(Communicated by the Astronomer Royal for Scotland)

(Received 1949 January 5)

Summary

Characteristic properties of flares, derived from visual and photographic records extending over nine years, are briefly summarized.

While the *areas* of the flare filaments provide a rough index of *importance*, the *development curves*, obtained by plotting *effective line-widths* of the $H\alpha$ emission against time, provide a simple measure of the intensity changes and give a fuller quantitative basis for the classification of flares. The geophysical (ultra-violet) effects of flares can be closely correlated with the line-width curves. They also indicate that the peak of the flare emission is sometimes of such short duration and high intensity that it may correctly be described as a *flash* of radiation, a result which lends strong support to the discharge mechanism of flare formation advocated by Giovanelli.

Flares occur close to sunspots (within a radius of 10^5 km.) and most frequently between the two main spots of a bi-polar group. The emission patches are relatively stationary both in the horizontal and vertical directions, but evidence is given for variability of height as between one flare and another.

High-velocity *absorption filaments* are ejected from more than 50 per cent of the Class 2 and Class 3 flares near the times of their maximum brightness. A detailed study of this process has been carried out visually in $H\alpha$ light and by photographic photometry from calibrated spectrograms. Following Newton, the flare filaments are identified with the larger limb *surges* (discovered at McMath-Hulbert Observatory and well shown in the Menzel films) and it is proved that they must differ fundamentally from other prominence types.

From a discussion of *emission line intensities* it is concluded that flares of comparable $H\alpha$ intensity produce similar, though by no means identical, spectra. The *He* I lines of helium and the D lines of sodium exhibit the most outstanding anomalies, reasons for which are suggested.

Line *profiles* of $H\alpha$ during flares have been plotted, showing that a great expansion of the emission line wings occurs (possibly as a result of Stark effect) as soon as the central intensity surpasses approximately 150 per cent of the continuous spectrum. These profiles also confirm the absence of appreciable Doppler shifts in the emission lines, a result which is consistent with all the earlier visual measures made with the spectrohelioscope.

An analysis of over 500 measures of the wave-lengths of the red and blue wings of the $H\alpha$ emission line, made with two different instruments at Sherborne and Edinburgh respectively, confirm the existence of an *asymmetry* (first described in 1943) in the widened emission wings. Absorption of light from the blue wing is considered to be the cause of asymmetry; the hypothesis is advanced that this arises from H atoms which have been previously excited to the 2-quantum state in sufficient numbers by the enhanced $L\alpha$ radiation from the flare, the atoms being thereby accelerated radially away from the flare region near the time of peak emission intensity.

This effect (clearly distinguishable from the flare surges which return to the chromosphere) in all probability represents the initial departure from the Sun of the *aurora-generating particles* at a time before they have reached their terminal velocity.

1. *Introduction.*—The object of this paper is to summarize the detailed records of 162 chromospheric flares observed by the author at Sherborne in the years 1939–47. With the discontinuance of the observing programme and the removal of the spectrohelioscope and spectrograph to a new site, the time seems appropriate for a presentation and discussion of the accumulated material. The known properties of flares will be reconsidered in the light of these and other recent results, but the paper is chiefly concerned with the primary phenomenon at the solar end rather than with its secondary (geophysical) effects. Some more recent results obtained at Edinburgh in 1948 are also described.

2. *Methods of observation.*—Throughout the greater part of this period a standard observational procedure was adopted, designed to collect information under the following headings:

(*a*) estimated time (U.T.) of beginning, end and peak intensity of the flare,

(*b*) precise location of the flare emission patches in relation to associated sunspots and neighbouring bright hydrogen flocculi and dark filaments of quiescent type,

(*c*) an estimate by means of an eyepiece graticule of the maximum area of the emission region in millionths of the Sun's hemisphere,

(*d*) a series of measures with the line-shifter (at approximately one-minute intervals) of the *effective line-width* (so-called *visibility range*) of the $H\alpha$ emission contour, as described more fully in Section 5,

(*e*) notes and sketches of associated active dark filaments of short life showing large components of velocity in the line of sight with (when possible) measures of their sightline * velocities at frequent intervals.

From 1943 onwards a wedge photometer was occasionally employed, following Newton's method (1), to obtain direct readings of the central intensity of the $H\alpha$ emission line in terms of the intensity of the adjacent continuous spectrum of the disk. In 1946 and 1947 the main emphasis was laid upon securing spectrograms of the flare emission and of the associated active dark filaments. In this work the spectrohelioscope was used mainly as a "scouting" device for picking up flares in their early stages so as to enable the spectrograph slit to be centred upon them. Some sacrifice of completeness in the observational records was inevitable during this period.

3. *Essential characteristics.*—A flare may be described as a sudden, short-lived increase of monochromatic radiation occurring in a limited region of the chromosphere and in the vicinity of an active sunspot group. These flare emission patches possess the following properties:—

(*a*) their areas lie within the range 0–5000 millionths of the Sun's hemisphere, i. e. they are comparable in area with their associated sunspots;

(*b*) with rare exceptions they are located within a radius of 10^5 km. (one-seventh of the Sun's radius) of a visible spot;

(*c*) while they are normally confined to chromospheric levels there is some evidence for considerable variations in level as between one flare and another;

(*d*) they develop out of pre-existent "normal" bright hydrogen flocculi;

(*e*) their rise to peak intensity may be extremely rapid, sometimes occurring as a "flash" of radiation followed by a slow decay;

* I owe the use of this term to F. J. Sellers. When dealing with velocities inferred from Doppler displacements of spectral lines in the chromosphere, it is less ambiguous than the term *radial velocity* which it displaces.

(*f*) the duration of the peak intensity is very short (<5 minutes), though the total life of an intense flare may be many hours;

(*g*) their spectra exhibit bright reversals in the Balmer absorption lines of hydrogen, in neutral helium and in the lines of ionized calcium, iron, silicon and a few other metallic atoms (*Ti* II, *Sr* II, *Sc* II, etc.), but there is much variation in detail;

(*h*) in a few instances an increase in brightness of the continuous spectrum has been recorded which probably renders the greatest (3^+) flares visible for a short time in integrated (white) light;

(*i*) they are essentially stationary in height as well as in the horizontal plane relative to other chromospheric markings;

(*j*) a majority of the brighter flare patches eject prominences of *surge* type which subsequently appear to fall back towards the chromosphere;

(*k*) the probability of a flare occurring varies with the type of associated sunspot, increasing as we progress from the simple unipolar (α-type) spot through the bi-polar types (β and $\beta\gamma$) to the magnetically much more complex type, γ (**2**).

(*l*) small flares are most frequent during the stages of rapid growth (**2**) or decay of a sunspot, but the most intense flares seem to favour the mature stage of spot development (**3**);

(*m*) secondary geophysical effects arise from the emission of both *wave* and *corpuscular* radiation at the time and place of the more intense (3 and 3^+) flares (**4**);

(*n*) characteristic "bursts" of radio noise of short duration, as discovered by Hey and his colleagues, have been found to coincide approximately in time with the flash of visible radiation from the more intense flares (**5**). Whether the radio noise is a primary or secondary effect of the flare emission is, as yet, undetermined.

In the recognition of flares and their subsequent classification these properties should be continually borne in mind. For example, one sometimes observes an unusually intense (>50 per cent of the continuous spectrum) region in the bright hydrogen flocculi within a spot group which, at first glance, may have all the appearances of a Class 1 flare, whereas more prolonged study will show that it remains sensibly constant in brightness and does not exhibit the characteristic sequence of intensity changes referred to in (*e*) and (*f*) above. It should not, then, be rated as a flare.

Again, at the limb, a flare normally appears as a brilliant, rounded elevation in the chromosphere. Without photometric measures it is no easy matter to distinguish this from the very similar appearance of a low-lying metallic prominence of abnormal brightness, such as one occasionally finds in the vicinity of an active group of spots. As mentioned in (*j*), the flare patch itself frequently ejects a prominence of surge type at about the time of its peak intensity, and these surges have in the past been confused with the flare emission which occurs at a lower chromospheric level. In either case, the absence of any appreciable sightline component of velocity in the emission lines of the flare (*i*) will assist in distinguishing it from a metallic prominence on the one hand, or from a surge on the other. Available evidence also suggests that, unlike the flares, neither the metallic prominences nor the surges emit sufficient ultra-violet radiation to cause ionospheric anomalies, crochets or fade-outs, nor corpuscular streams of sufficient intensity to generate magnetic storms.

The occurrence of characteristic "bursts" of radio noise radiated from the flare region, as well as the long-wave ionospheric anomalies (ultra-violet effect)

recently described by Ratcliffe, Bracewell and Straker at the Cavendish Laboratory (**6**), may in the future be found to provide a sure criterion for distinguishing between flares and prominences when these occur at the limb. When seen against the background of the disk there is, of course, no risk of confusing the two phenomena.

4. *Areas of flares.*—Observers who cooperate in supplying the flare data for inclusion in the *Quarterly Bulletin on Solar Activity*, published by the I.A.U., have been accustomed to classify flares on the scale of importance, 1 (smallest) to 3 (largest)*. By reason of the exceedingly short duration of peak intensity of flares and the difficulty of obtaining photometric measures of brightness which refer to this early phase, it has been considered better to adhere to the system of area classification. This system, however, is by no means widely used, and so it is not surprising to find that much diversity of classification exists between the practice of different flare observers. The following figures, kindly supplied by M. d'Azambuja, give the number of flares recorded per hour of actual observation in 1947 by a few of the cooperating observatories: Arcetri 4·6; Cambridge 1·0; Greenwich 0·26; Kodaikanal 0·26; McMath-Hulbert 2·8; Meudon 0·40; Mt. Wilson 0·04; Muswell Hill 0·70; Sherborne 0·30; Zürich 0·55. Such comparisons suggest that some of the observers must include large numbers of the smallest observable (1^-) flares which by others are neglected.

At Sherborne and Edinburgh, flares having an area lying within the range $\geqslant 100 \leqslant 300$ millionths of the Sun's hemisphere were rated as Class 1; $>300 \leqslant 750$ millionths as Class 2; >750 millionths as Class 3 or 3^+. In a few instances flares have been rated above, or below, the importance corresponding to the measured area because they exhibited a maximum intensity, or an emission line-width, considerably greater, or less, than that which was judged normal for the class. Except in special circumstances, flares of area <100 millionths have not been recorded in detail; for it has been found difficult to draw any clear line of demarcation between these small flares of the 1^- category and the ever-present fluctuations of brightness observable under good conditions of seeing in the smaller bright flocculi of an active spot group.

The area estimates have been made by means of a photographic graticule placed immediately in front of the viewing slit of the spectrohelioscope, and the probable error of a single measurement is of the order of 20 per cent. The measured areas have, like those of sunspots, been corrected for foreshortening in accordance with the secant law. It now (1948) seems probable that the flare emission region is in no real sense a plane area parallel to the Sun's surface and the application of the secant law to the measured areas may not be valid. If this is the case, it follows that flares occurring near the limbs will have been over-rated in importance by comparison with those seen near the centre of the disk.

In respect of the 91 flares whose areas have been measured, Table I records the mean areas for each class together with similar figures for comparison, as published by Waldmeier and Giovanelli. It will be noted that, especially for flares of lesser importance, the tendency has been to underestimate the importances by comparison with the results of these two observers.

From Fig. 1, which illustrates the frequency of occurrence of areas lying within successive intervals of 100 units of area, it will be seen that flares having areas between 100 and 300 units are by far the most common. It should be

* A fourth category (3^+) has been introduced by H. W. Newton (*M.N.*, **103**, 244, 1944) to designate those flares of outstanding importance, as judged mainly by their geophysical effects.

TABLE I

Importance	Author		Waldmeier		Giovanelli	
	No.	Mean Area	No.	Mean Area	No.	Mean Area
1	48	217	70	120	78	106
2	35	570	37	380	66	326
3	6	1266	8	1020	4	800
3^+	2	2350	...	...	...	...

remembered that "microscopic" flares (area <100 millionths) have not been fully recorded. Under the most perfect conditions of seeing their recorded frequency might exceed that of any other group.

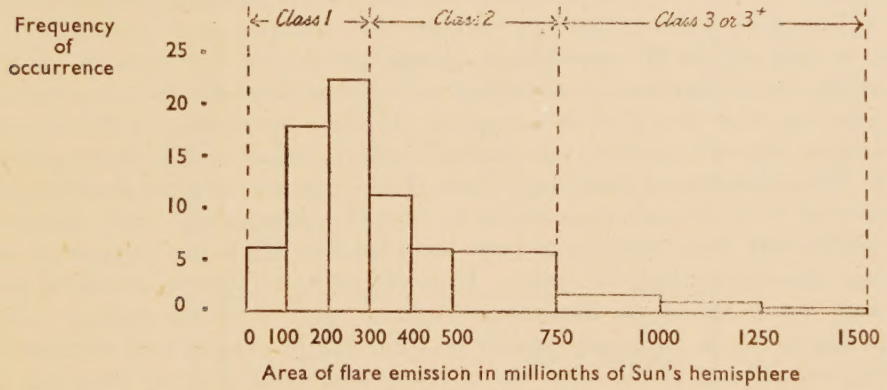

FIG. 1.—*Frequency Distribution for Flares of Different Areas.*

Analysis of 91 flares. The ordinates give the number of observed flares within the corresponding area range (abscissae). Areas have been measured by means of a graticule and are expressed in millionths of the Sun's visible hemisphere, corrected for foreshortening.

5. *The development of flares.*—Apart from a simple photometric technique, the most satisfactory method available at present for following the development of a flare consists in measuring, at intervals of about one minute, the effective line-width (visibility range) of the $H\alpha$ emission. This method has been employed by Waldmeier (**25**) and by Giovanelli (**2**), and I have described the method in detail in an earlier paper (**7**), where a number of such development curves showing variations of line-width against time will be found (**7, 8**). Briefly described, the method is as follows. Using the line-shifter of the spectrohelioscope, the $H\alpha$ line is centred upon the second slit in the position which yields the darkest field of view. The line-shifter is then rotated until the bright flare filament can no longer be seen by contrast with its surroundings, first one setting on the blue side and then one on the red side of the line centre. In both cases the direction of motion of the line-shifter is outwards from the centre of $H\alpha$ to avoid systematic errors. These two settings are referred to as the *extinction values* for the flare patch and their wave-length interval in angstroms I have called the *effective width* of the emission line.

A further series of development curves for the years 1946–48 is reproduced in Fig. 2 (Plate 1), so that these may be available for comparative purposes to workers who are engaged in the measurement of radio-noise bursts (**5**) or of ionospheric

anomalies (ultra-violet effects) (**6**). It should be emphasised that these curves also represent in a general way the changes which take place in monochromatic light intensity during the life-time of a flare. For, whatever may be the precise nature of the function connecting the central intensity of the emission profile with its line-width (see Section 12 and Fig. 8B), it is reasonably certain, from a number of simultaneous measures of both quantities, that the peak of light intensity for the centre of the line coincides in time with the moment of maximum line-width.

It is convenient, in view of the form of the curves, to divide the life-history of a flare into three distinct phases, which we may denote by A (the rapid rise to peak intensity), B (the brief period of maximum) and C (the more gradual return to the pre-flare brightness). An analysis of the 23 curves available for study gives a mean ratio $A/C = 0{\cdot}29$ with a range between extremes of 0·08 to 1·0. Thus, while we may say that the chief characteristics of light variation are a rapid rise followed by a slower decline, yet there are evidently many cases, like the flares of 1946 July 25 (**8**), 1946 March 29 and 1947 August 9, to quote only a few, where the rise to maximum is so sudden and so short-lived that we may correctly describe the effect as a *flash* of radiation. In these circumstances the duration of the peak phase B is probably momentary and is certainly shorter than 1 minute.

6. *Mean duration of flares.*—In Table II are recorded the mean durations of a number of flares of each class, together with the greatest and least durations. Naturally, only those flares have been included for which the beginnings and endings have been clearly observed. It should be noted that the probable error is much less in timing the beginning of a flare than it is for the ending. If the beginning is seen at all it may usually be fixed within 1–2 minutes, whereas the ending, on account of the slow rate of decay and uncertainty of what was the pre-flare brightness of the region, may be in doubt by as much as 5–10 minutes, or more for the long-lived flares.

TABLE II

Importance	No.	Mean duration	Greatest and Least values
1	41	17^m	$43^m - 4^m$
2	18	29^m	$90^m - 10^m$
3	21*	62^m	$155^m - 20^m$
3+	29†	$\sim 3^h$	$> 7^h{\cdot}2 - 0^h{\cdot}9$

* Derived from the lists of flares in the *Quarterly Bulletin on Solar Activity*, 1935–47.

† Twenty-seven flares included in Newton's list (1943) and two observed subsequently (1946 February 6, of duration $2^h\ 10^m$; 1946 July 25, duration $4^h\ 15^m$).

It will be seen from these figures that the average duration of a flare increases by a factor of approximately two as we pass from one class to the next‡. In any one class, however, the duration may vary within wide limits, those of shortest life lasting for about one-tenth of the longest.

7. *The location of flares in relation to sunspots.*—It has been my practice to record in red pencil the shape and position of every flare emission region

‡ Since this was written, an analysis by M. Waldmeier of flares for the period 1935–44 has been received, which gives the following mean durations: Class 1, 20·3 minutes; Class 2, 33·4 minutes; and Class 3, 62·4 minutes. (*Statistische Untersuchungen an chromosphärischen Eruptionen*: Astronomische Mitteilungen der Eidgenössischen Sternwarte Zürich, 1948.)

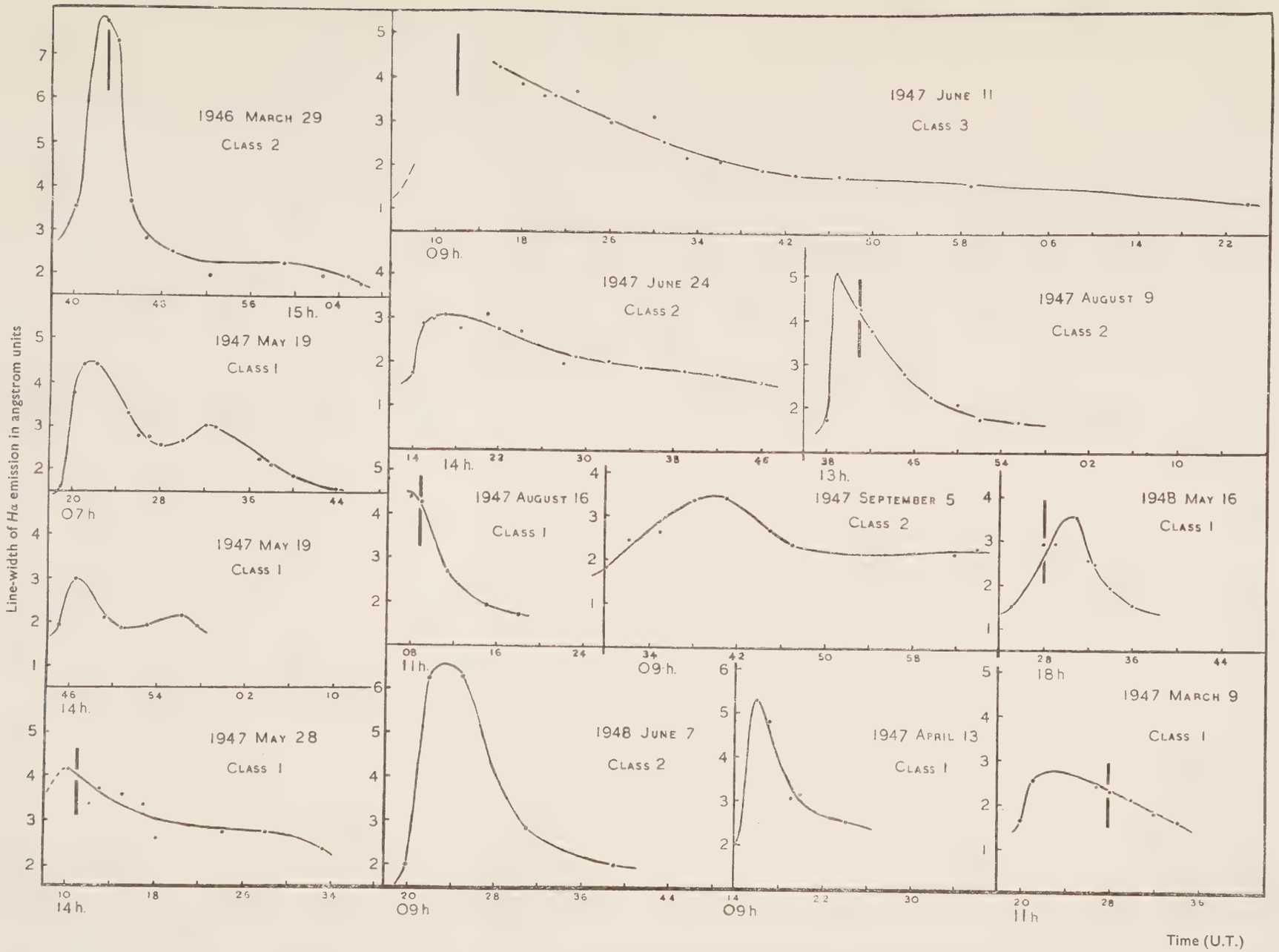

FIG. 2.—*Development Curves for Flares.*

These curves show the effective line-widths in angstroms of the Hα emission against time. The method of measurement is that described in M.N., **103**, 3, 1943, *where a number of similar curves are given. Vertical strokes drawn in some cases near the times of maximum line-widths indicate the first appearances of active prominences of* surge *type, as described in Section* 10.

relative to the neighbouring spots and pores. To do this, a movement of the line-shifter of the spectrohelioscope 2 A. away from the centre of the $H\alpha$ absorption line brings clearly into view the background of the sunspot umbrae. The flare may then be located and entered in upon a drawing of the Sun's disk which has been previously prepared and oriented on the projection board of the 6-inch refractor. An eyepiece graticule which can be held in front of the oscillating viewing slit has been found very useful for this purpose and for measuring distances in the chromosphere. If the graticule is such that the side of one square represents 30,000 km. ($2\frac{1}{2}°$) at the centre of the solar image, the scale will be found most convenient.

A few of these drawings, relating to Class 3 and Class 3^+ flares, are reproduced in Fig. 3. It is at once noticeable, when one studies the whole material, that the long ribbon-like emission filaments, which characterize the most intense flares (109 and 147), pass right across the associated spot group, often obscuring many of the largest umbrae and passing far beyond the visible boundaries of the penumbra. Lesser flares, on the contrary, are rarely seen superimposed upon the umbrae of the principal spots, though they undoubtedly show a preference for the small spots and pores in the vicinity of the larger ones. The emission filaments stand out like "white-hot" ropes in the field of the spectrohelioscope and one gains the impression that they are at a higher level than the umbrae which they obscure. Yet, they do not show any preferential motion towards certain umbrae of the group like that which is observed in connection with the high-level dark filaments (sunspot prominences seen in plan) which can be observed discharging themselves into spots at speeds of the order of 50 km./sec. (**9**). When the bright filaments are seen in plan view near the centre of the disk, they appear to be floating, possibly at different levels, in the chromosphere above the spot. But a scrutiny of the few spectroheliograms we possess * of 3^+ flares also suggests that they are closely associated with, we might almost say "anchored" in, the well-known vortex structure exhibited by the less conspicuous bright and dark flocculi which are visible in the best $H\alpha$ photographs.

The great flares of 1942 February 28 and 1946 July 25 in their fully developed stages each comprised two such bright filaments crossing the spot group and running roughly parallel to one another. In the latter case the channel separating the filaments coincided almost exactly with the line of demarcation between the regions showing N. and S. polarity in this complex $\beta\gamma$-type spot, as determined at Mount Wilson†. Other 3^+ flares which have shown the arrangement of double parallel filaments similar to that of 1946 are those of 1926 February 22 (Plate 2) and 1870 September 28‡. Carrington's observation of a flare seen in integrated light on 1859 September 1 is also consistent with the "two filament" type, for, it will be remembered, he observed *two* brilliant patches over the spot group lasting for several minutes. With our present knowledge we must suppose these bright patches to have been enhancements of the continuous spectrum arising from the central parts of two flare filaments where they crossed the region of high excitation over the sunspot. A similar phenomenon (one bright area) was

* See, for example, *Ap. J.*, **73**, 379, 1931; *P.A.S.P.*, **58**, 87, 1946, and **58**, 317, 1946; *l'Astronomie*, Septembre–Octobre, 1946.

† Compare, for example, Plate XXIa, *P.A.S.P.*, October 1946 with the Meudon spectroheliograms published in *l'Astronomie*, Septembre-Octobre, 1946.

‡ See *Early Visual Observations of Bright Chromospheric Eruptions on the Sun's Disk:* H. W. Newton, *J.B.A.A.*, **50**, 273, 1940.

observed in white light by du Martheray in connection with the flare of 1946 March 5 (**10**) and the continuous spectrum of another flare was recorded at Sherborne on 1946 July 25 (**8**) on a spectrogram of the region near $\lambda 6000$.

In his valuable theoretical discussion on *Chromospheric Flares* (**11**), Giovanelli draws attention to another pattern assumed by the bright filaments and one which

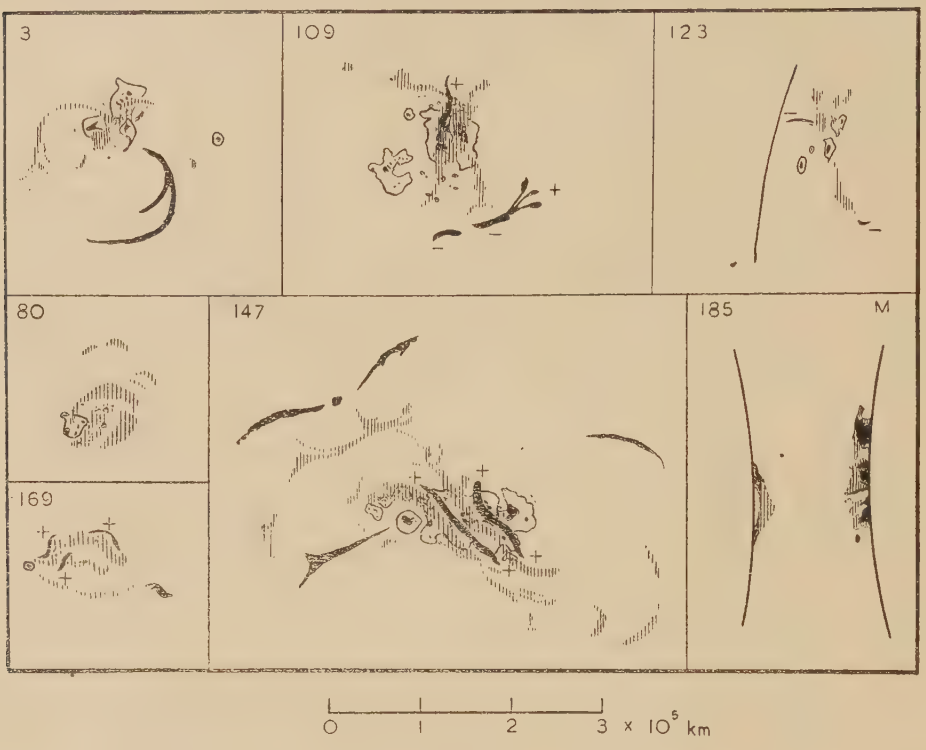

FIG. 3.—*The Location of the Bright Filaments of Intense Flares (Class 3 and 3⁺) in relation to Sunspots.*

Bright filaments are represented by shading with vertical lines. The dark filaments are prominences of quiescent type seen in plan: where + or − signs are attached, active prominences of surge *type are indicated. East is to* right, *and West to* left, *except for M which is in reverse.*

No. 3. 1940 *March* 27^d 17^h 10^m; $+12°$, *W.* 19°. *Class* 3; *area* 1200 *millionths.*

80. 1941 *June* 6^d 16^h 41^m; $+12°$, *E.* 34°. *Class* 3; *area* 1500 *millionths.*

109. 1942 *February* 28^d 12^h 42^m; $+07°$, *E.* 04°. *Class* 3^+; *area* 2200 *millionths. Observed independently at Greenwich* (The Observatory, **64**, 260, 1942).

123. 1942 *November* 7^d 10^h 20^m; $-12°$, *W.* 64°. *Class* 3; *area* 1800 *millionths.*

147. 1946 *July* 25^d 17^h 30^m; $+22°$, *E.* 15°. *Class* 3^+; *area* 2500 *millionths. The dark filaments shown were descending into the Sun with sightline velocity* +75 *km./sec. at* 17^h 50^m. *This flare was also observed at Cambridge, Meudon, Mt. Wilson, Wendelstein and Zürich.*

169. 1947 *June* 11^d 09^h 06^m; $+15°$, *W.* 11°. *Class* 3; *area* 650 *millionths. Also observed at Greenwich, Schauinsland and Zürich.*

185. 1947 *August* 23^d 16^h 55^m; $+23°$, *E.* 90°. *An intense flare detached from the limb at a height of* 30,000 *km., connected by fainter prominence streamers to the chromosphere below. I am indebted to M. d'Azambuja for copies of spectroheliograms in Hα, taken at Meudon at* 17^h 04^m *and* 17^h 08^m *on this day: they confirm the above particulars and show that the flare was fading rapidly at the time.* (*See also* The Observatory, **67**, 206, 1947 *and* **68**, 70, 1948.)

M. 1942 *February* 21^d 14^h 25^m; *E. limb. For comparison with* 185, *an intense flare at the limb, as photographed in Hα at Meudon. Greatest height of the emission was about* 40,000 *km.* (*See* J.B.A.A., **57**, 56, 1947.) *This* 3^+ *flare occurred over the same spot as No.* 109, *observed at Sherborne one week later.*

has been photographed in connection with several intense 3^+ flares. That of 1917 February 7, for example, showed a large number of closely bunched short filaments connecting the umbrae of the leader and follower of a bi-polar group. There were also filaments connecting each of the main umbrae to smaller umbrae of opposite magnetic polarity lying between them. When sufficient material becomes available there is evidently an important field for study in comparing the pattern exhibited by the bright filaments with the detailed distribution of the magnetic lines of force which can be inferred from the Mount Wilson polarity diagrams. The material at present available is too small in amount to enable any conclusions to be drawn as to the relative frequency of occurrence of the two pattern types.

In this connection it seems desirable to make an appeal to workers with spectroheliographs and monochromatic filters who may have the opportunity of consciously recording an intense flare. All the spectroheliograms of these phenomena which we at present possess are in the nature of things greatly over-exposed, so much so, that the merging images of the filaments cannot be separated from one another and, even when single, they appear many times broader than their real width. At maximum brightness the filaments are known to be 10 or 20 times more intense in $H\alpha$ than the chromospheric background *: a small neutral screen allowing about 10 per cent transmission would, if placed over the primary image of the spot group, provide approximately the correct exposure for the bright filaments without at the same time reducing the exposure below the normal value for the remainder of the solar disk.

When we come to analyse the locations of the less intense flares (Classes 1 and 2) we find a noticeable avoidance of those areas over the larger umbrae and a preference for the regions of the smaller spots and pores in the central and eastern parts of the groups. This tendency is brought out in Fig. 4, where the locations of 90 flares (69 Class 1; 21 Class 2) have been plotted in terms of distance and position angle measured from the leading umbra of the spot group. It is clear that the most favoured location is the central region of the group at a mean distance of about 50,000 km. following the leading spot. The filamentary nature of these smaller flares is also less obvious: the majority consist of small oval or irregular patches and the smallest of all are often fairly round points of light.

Thus the observed location of the flares of lesser intensity, occurring mainly in the central regions of bi-polar spot groups, together with their characteristic sudden rise followed by a slow decline of light intensity, seem both to favour the Giovanelli discharge mechanism of flare formation. But it still remains very difficult on this theory to account for the enormously extended bright filaments ($\sim 10^5$ km. in length) such as have been observed in some of the most intense 3^+ flares. In addition to which, as pointed out by H. W. Newton (3), the great flares tend to occur during the mature phase of development of the great sunspots when their *rate* of growth is a minimum, unlike the lesser flares whose frequency is greatest during the first few days of rapid spot development.

8. *The location of flares in height.*—Much less is known about the vertical distribution of flares in the chromosphere. For this purpose limb observations in elevation are necessary; the plan view on the disk merely indicates that the

* The brightness of the chromosphere in the spectrohelioscope is determined by the central intensity of $H\alpha$ absorption, i. e. about 25 per cent (15 per cent corrected) of the adjacent continuous spectrum.

flare emission is situated above the level of the umbra and penumbra of a sunspot, since these are sometimes completely obscured by a bright filament, but how much above this level is uncertain.

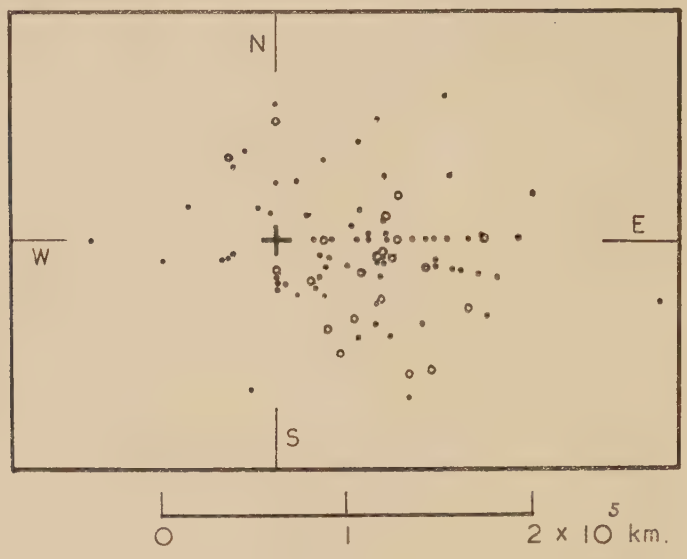

FIG. 4.—*Distribution of Flares in Bi-polar Spot Groups.*
The diagram shows the location in a horizontal plane of 69 Class 1 flares (dots) and of 21 of Class 2 (circles). The cross represents the position of the leading umbra in each associated group. The mean location is about 50,000 km. east of this umbra, i. e. it coincides approximately with the centre of the group. I am grateful to Miss M. Conway for compiling the material required by this diagram.

The probability of observing a flare of any kind at the limb (say in longitude 85° to 95°) is about one-tenth that of observing the corresponding phenomenon on the disk. It is not surprising, therefore, that only two records are available of intense flares seen in elevation, the accompanying geophysical effects * in both cases being such as to leave no doubt that both phenomena were, in fact, flares and not bright metallic prominences. The first was recorded at Meudon on 1942 February 21 over a great spot group on the east limb (**12**). It showed on the $H\alpha$ spectroheliograms as a brilliant fringe or crown to some prominence material, and rose slowly during the 92 minutes to a height of 40,000 km. (see *M*, Fig. 3). This gives a mean outward velocity of 7 km./sec., which is quite consistent with the low values of sightline velocity (<18 km./sec.) exhibited by the flare emission patches when these are observed in plan near the centre of the disk. A similar observation was made at Sherborne on 1947 August 23 and the spectrum of this flare has been described elsewhere (**13**). There is evidence that the emission region on this occasion had passed its maximum intensity when it was observed completely detached from the limb at a height of 30,000 km. It was still connected to the chromosphere by a few threads of fainter prominence material (No. 185, Fig. 3). Six lesser flares seen near the limb have not been detached but have given the appearance of luminous dome-shaped elevations rising to heights of no more than 10,000 km.

* These were: 1942 February 21, an intense radio fade-out on the Earth's sunlit hemisphere, and a characteristic "crochet" disturbance on the magnetic traces at Abinger; 1947 August 23, an extensive fade-out reported by Cable and Wireless Ltd., and a dip in the received galactic radio-noise (12½-metre wave-length) reported by J. S. Hey (privately communicated).

Evidence from the line profiles of $H\alpha$ also seems to indicate that flare emission regions can occur at very different levels in the chromosphere. In Plate 3: (1) is a typical $H\alpha$ line reversal in a Class 2 flare; (2) shows a less common type in which there is a central absorption in the bright reversal, in this case 0·6 A. wide, separating the brighter wings of the emission; (3) is probably an extreme case of (2) and is the type of reversal recorded in one of the so-called "solar hydrogen bombs", first photographed by Ellerman (**14**). Ellerman describes a "bomb" as the sudden appearance of a "very brilliant and very narrow band extending four or five angstroms on either side of the line ($H\alpha$), but not crossing it". The duration is "only a few minutes—from one to three on the average, and from five to ten minutes rarely". He notes that "the regions where bombs are likely to appear are around and among active spot-groups, especially groups which are developing and composed of many members". Although many other lines were examined, he says "none but the hydrogen lines have shown the band".

In the course of this work one of these bombs, probably a minor one, has been observed in the spectrohelioscope and it might be described as a flare which could only be seen when the line-shifter was displaced 1 A. or more to the blue or to the red, but was unobservable on the centre of the line; the spectrum of another was photographed at $H\beta$, and is somewhat similar to Ellerman's description. It is clear that these bombs are of much greater rarity even than flares and I suggest that the bomb phenomenon can be most readily explained if we assume that it represents the "flash" phase of an intense flare occurring at an abnormally low level in the chromosphere, in fact below the reversing layer. During this phase, which we have shown lasts for a few minutes only near the beginning of an intense flare, the wings of the emission are greatly widened (**15**), possibly as a result of the Stark mechanism arising from electronic fields. The light from the widened emission wings will, therefore, suffer relatively much less absorption in passing out through the chromospheric hydrogen than will the centre of the line. A deeply located flare at peak intensity should present just the appearance which Ellerman has described. It is to be noted especially that, unlike flares, the bombs have been observed only in the hydrogen lines, that is to say in the only flare reversals in which the Stark broadening is appreciable.

It should be possible from a single spectrogram showing all the principal Balmer reversals simultaneously in a major flare to decide whether the sudden broadening of the hydrogen lines in the "flash" stage is due to Stark effect or not. The Stark effect operates to a different extent in the various members of the series. Finally, it should be remarked that Giovanelli's theory (**11**) predicts the likelihood of flares occurring at different chromospheric levels.

9. *Stationary nature of flare emission regions.*—In Section 13 (Fig. 10) is given an analysis of 434 measures of wave-length of the $H\alpha$ emission line (disk observations) made at Sherborne, together with a further 106 measures made with a different instrument at Edinburgh, the full material relating to 99 different flares. These measures, which have been obtained by the method described in Section 5, give the mean wave-length $(R + B)/2$, where R and B stand for the wave-lengths of the observed extremities, red and blue respectively, of the wings of the emission line. We must not assume that $(R + B)/2$ coincides with the wave-length of the point of maximum intensity of the emission profile; for, as we shall see later, there is considerable evidence that the wings are slightly unsymmetrical at the time of greatest flare brightness.

Notwithstanding this, the most striking feature of these measures is the absence of any *large* Doppler shifts in the emission line (of the order of + or − 100 km./sec.) such as one commonly records in the *Hα* absorption line of the small, active, dark filaments near sunspots (i.e. sunspot prominences of Pettit's types III a, b, c and d, seen in plan on the disk). As explained in Section 13, the shifts in the emission line $(R+B)/2$, which *have* been observed, are found to be a function of the line-widths and evidence is there given that they cannot arise predominantly from Doppler displacements due to sightline motion. Even if we were to interpret them as such, we should be forced to conclude that the maximum sightline component of velocity observed in the most intense flares is only of the order +18 km./sec. (0·4 A.), a view which is confirmed by the line profiles for several flares as reproduced in Fig. 8A.

The spectroscopic evidence, gained from the low values of sightline velocity (dz/dt), is entirely consistent with the absence of large horizontal movements (x- and y-coordinates) in long-lived flares seen near the centre of the disk. Examples were quoted in an earlier paper (**7**), where it was remarked that, while the luminous points and bright filaments are thin and sharply outlined in the initial stages of a flare, once the greatest intensity is past a broadening and outward diffusion is observable in each filament without any certain movement as a whole. As the flare develops, another curious feature is the fading of the earlier filaments and the "lighting up" of new ones farther from the spot centre, a process which, if not continuously followed in detail, may easily lead one to suppose that mass motion of the filaments has taken place from the centre outwards.

These characteristics are well brought out in the *Hα* spectroheliograms of a Class 3+ flare which occurred near the centre of the disk on 1926 February 22. This (at present) unique series (Plate 2), taken by Professor Royds at Kodaikanal, covers nearly the whole life-history of the flare from its commencement at 8^h03^m (I.S.T.) to the last stages at about 11^h18^m *. The associated sunspot, Greenwich 9881 (+23°; W. 10°), although of small area (390 millionths), was the fourth return of a region producing great spots. As Greenwich 9861 in the previous rotation (January 18–31), it had a mean area of 3285 millionths and was thus the largest group in the Greenwich records until displaced by the great spots of 1946 and 1947. The faculae associated with this active region could be traced until Rotation 974, that is to six rotations later †.

In the photograph taken at 8^h03^m (Plate 2) two filaments can be seen developing from the pre-existent bright hydrogen flocculi, located about 30,000 km. south-east and south-west of the main spot respectively. By 8^h08^m these had much increased in brightness, and two other small points were beginning to brighten at *E*. By 8^h36^m the south-west filament had elongated at both ends, partly obscuring the main umbra, and the bright dots at *E* had developed into a complex pattern. Three other points *A*, *B* and *C* had "lit up" in patches of normal bright hydrogen far removed from the centre, *A* being 280,000 km. from the umbra. At 9^h04^m the filaments had become thicker and their outer edges were both sharper and brighter than the inner. By 11^h18^m the innermost parts of the filaments had faded out, but leaving the outer edges still sharply

* The filaments have been described by Professor Royds (*M.N.*, **86**, 380, 1926), but their significance (as an intense chromospheric flare) was not realized at the time. I am indebted to Mr Evershed for the loan of the plates from which copies have been made.

† I am indebted to H. W. Newton for this information.

H_α 8·03

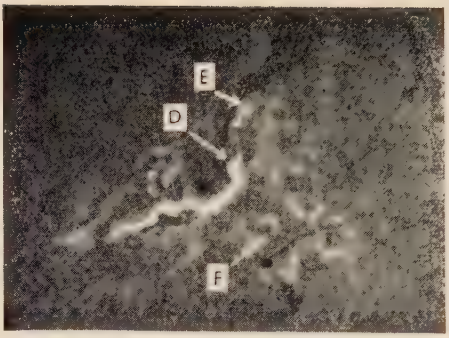

H_α 8·08

H_α 8·36

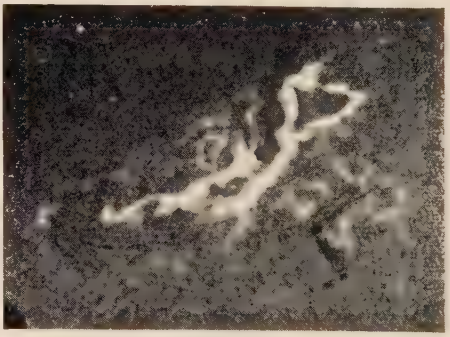

H_α 9·04

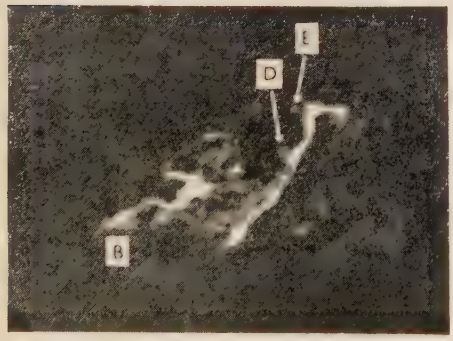

H_α 11·18

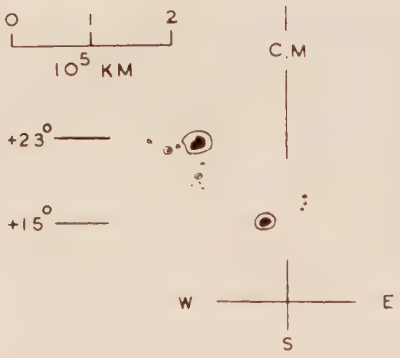

ASSOCIATED SUNSPOTS

Chromospheric Flare : Kodaikanal, 1926 February 22.

1. 1948 *June* 7^{d} 09^{h} 29^{m}. *Hα after the maximum of a Class 2 flare. Corrected central intensity 71 per cent of the continuous spectrum for the adjacent disk.*

2. 1948 *March* 11^{d} 12^{h} 47^{m}. *End of Class 3 flare. Central absorption in Hα is 67 per cent as against 81 per cent for the brighter wing. The bright band above the penumbral spectrum is 104 per cent of the disk continuum and seems to represent an abnormally bright region of the photosphere at the boundary of the sunspot.*

3. *An Ellerman "bomb", showing the extended bright wings of Hα and the deep central absorption (from* Ap. J., **46,** 298, 1917). *The scale is about twice that of Nos. 1 and 2.*

4. 1946 *July* 25^{d} 16^{h} 37^{m}. *Wide wings of Hα during the "flash" phase of a* 3^{+} *flare. Here there is no trace of central absorption in the emission; possibly a high-level flare.*

5. 1948 *April 5. Chromospheric emission in He* λ 6678·1 *over an active spot group on the E. limb; central intensity 5 per cent of the continuum at the centre of the disk. The blended Fraunhofer line is Fe* I λ 6678·0.

6. 1921 *May* 14^{d} 08^{h} 12^{m}. *Reversals of Ca* II H *and Hε as recorded by Evershed. Note the wide wings of Hε as compared with Ca* II H.

7. 1921 *May* 14^{d} 08^{h} 12^{m}. *Same plate as last, showing the Ca* II K *line. There is also a faint band of emission in the continuous spectrum from the flare filament.*

8. 1947 *August* 23^{d} 16^{h} 58^{m}. *Class 3 (?) flare above the E. limb (see Fig. 3, No. 185). The centre of Hα is indicated and the wings can be traced 12 A. to the red and 8 A. to the blue in the original. Intensity >200 per cent of the centre of disk continuum. There is no evidence of Doppler shift of the peak of the profile.*

9. 1948 *April 2. Hα line of "blow off"* prominence, *10,000 km. above the E. limb. The displacements of 3 A. to blue and 1 A. to red are caused by sightline motions in the prominence material. Distortions of this type have not been photographed in the emission lines of any of the flares under review. Corrected central intensity is 20 per cent of the continuum at the centre of the disk.*

10. 1948 *February* 18^{d} 12^{h} 55^{m}. *Hα line of a normal quiescent limb prominence for comparison with Nos. 4, 8 and 9. A faint Fraunhofer spectrum has been superimposed in order to bring out the narrowness of the prominence line and the absence of Doppler shift. Corrected central intensity is 7 per cent.*

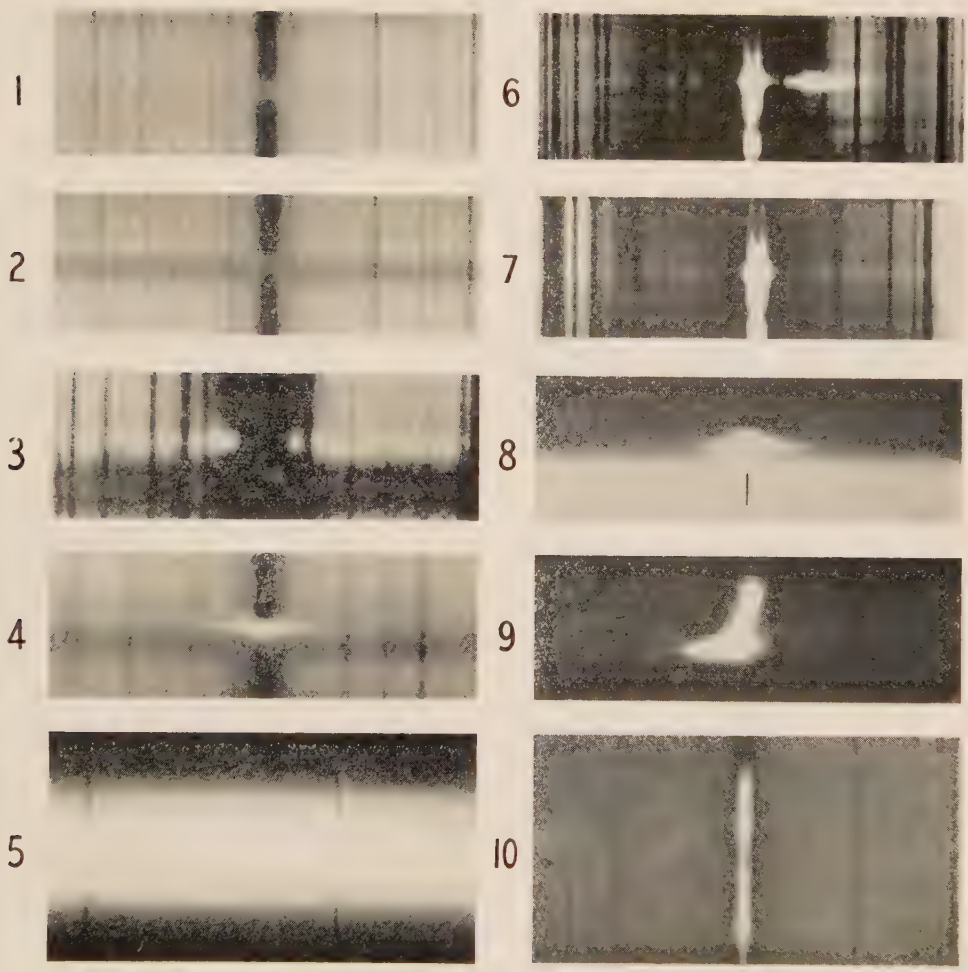

Emission lines of Flares and Prominences.

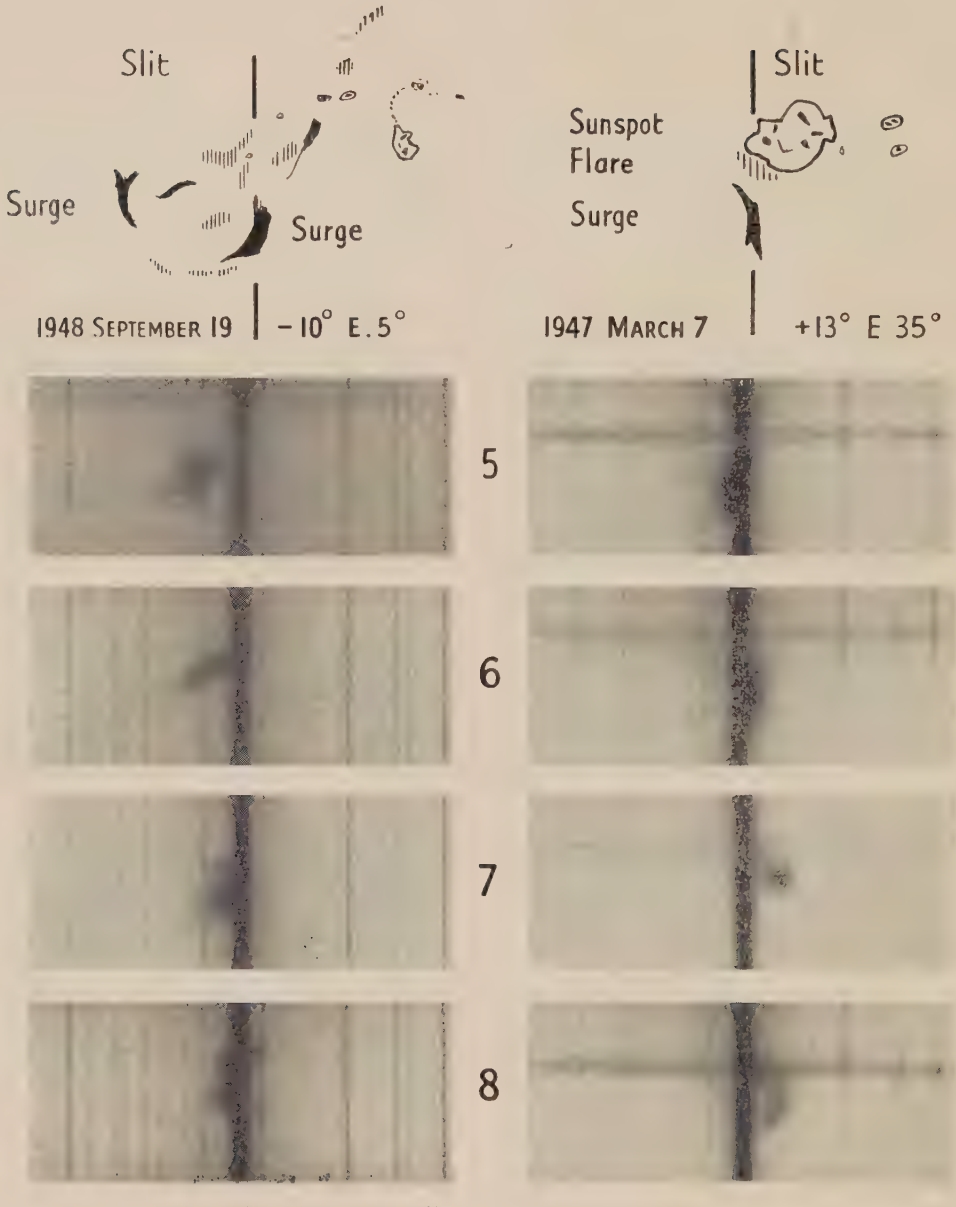

Hα "Motion Forms" of Surges ejected by Flares.

defined. Easily identifiable features, like the points *D* and *E*, can be traced right from start to finish, as they brighten and then fade without any appreciable lateral displacements during the period of three hours. Some normal bright flocculi, like *F*, remain unaffected throughout. Even among the less certain features there is none which admits of a horizontal motion exceeding 30,000 km. in the interval of 195 minutes. We may say, therefore, that, so far as this flare is concerned, there were no observable horizontal velocity components in excess of about 3 km./sec., a conclusion which is also consistent with the records of the 3+ flares of 1942 February 28 and 1946 July 25 made at Sherborne, as well as with the evidence from sightline velocities already mentioned.

In conclusion, reference should be made to the early spectroscopic observations of Young, Maunder and others, some of which would appear to indicate genuine Doppler displacements (~100 km./sec.) in the bright reversals (C, F and *He* λ6678) of intense flares. The matter has been raised by Evershed in a recent correspondence in *The Observatory* (**16**), and it may be said that the answer to the problem remains somewhat in doubt why these large sightline velocities have not been recorded in the *emission* lines of intense flares in recent years.

10. *Surges ejected from flares.*—High-velocity absorption markings associated with disk flares have been described by Giovanelli (**2**), and detailed studies of their life-histories and characteristic sightline velocity sequences have been made by H. W. Newton (**17**) and the author (**18**). These studies lead to the conclusion that active dark filaments of this kind, which make their appearance suddenly within a few minutes of the time of peak intensity (see Fig. 2) of the flare, are to be identified with the characteristic limb prominences of short life (type III d), first discovered at the McMath-Hulbert Observatory and designated "surges"*. This identification has been strikingly confirmed by the Menzel films of sunspot prominences taken at Climax, in which many surges are to be seen. They may be described as jets of luminous material rising in nearly vertical trajectories (sometimes curved) to heights of 100,000 km. or more. The ascent is followed by a slower recoil *along the same trajectory*. McMath and Mohler have also recorded in a series of K_{232} spectroheliograms the complete development of a flare just inside the limb, showing also the surge ejected from it, which appears as a prominence against the sky (**19**). Since it is by no means certain that all surge prominences arise from flares, we shall refer to these as *flare surges*.

In Plate 4 are reproduced some spectrograms of the *Hα* absorption line of the flare surges as seen against the background of the disk. These were recorded during 1947–48 with a view to investigating the validity of the measures of sightline velocity of such objects which had previously been obtained visually by means of the line-shifter of the spectrohelioscope. When a surge is generated in this way by a disk flare, the typical sequence of events as seen in the spectrohelioscope may be described as follows. During the few minutes following the peak intensity of the emission a dense absorption filament makes its appearance within a radius of 100,000 km. of the emission patch and exhibits a sightline velocity of approach of the order 100 to 200 km./sec. This early phase can only be observed at all by continually "hunting" to and fro with the line-shifter: it is also difficult to photograph because the Doppler displacement (~4 A.) of the moving gases

* It seems very probable that "surges" are also to be identified with the solitary brilliant jets "often found away from sunspots as well as over them", described by Mr and Mrs John Evershed (*Memoir*, 1917) as occurring on the Kodaikanal plates.

throws the $H\alpha$ line right off the second slit of the spectroheliograph. As shown in the earlier paper (**18**), the initial high speed of ascent is subject to a retardation of the same order of magnitude as the value of solar gravity. This retardation decreases with time (or height) and brings the moving gases to rest at the highest point of their trajectory. Thereafter, they sink back with a smaller velocity of descent. The spectra, Nos. 1–4, taken at approximately 3-minute intervals, show a surge rising with an initial velocity of 150 km./sec. and reaching the top of its trajectory (zero displacement of the line) after about 10 minutes. It is difficult to follow the material of the moving gases through the stationary point owing to the lack of contrast between its absorption line and that of the surrounding background (see Section 11), and in default of a complete series of spectra the downward motion is illustrated by Nos. 5–8, of a different date. These show both the remains of the emission from the flare filament and the "motion forms" of the surge ejected by it, the sightline velocity having altered in this case from −40 km./sec. to +100 km./sec. in a period of 22 minutes.

It is now possible to compare the movements of the surges seen on the disk with those which have been recorded at the limb. In Fig. 5 are given side by side the typical sequence of sightline velocity measures (B) for some of the flare surges I have observed on the disk (mean of six cases), together with the velocity-

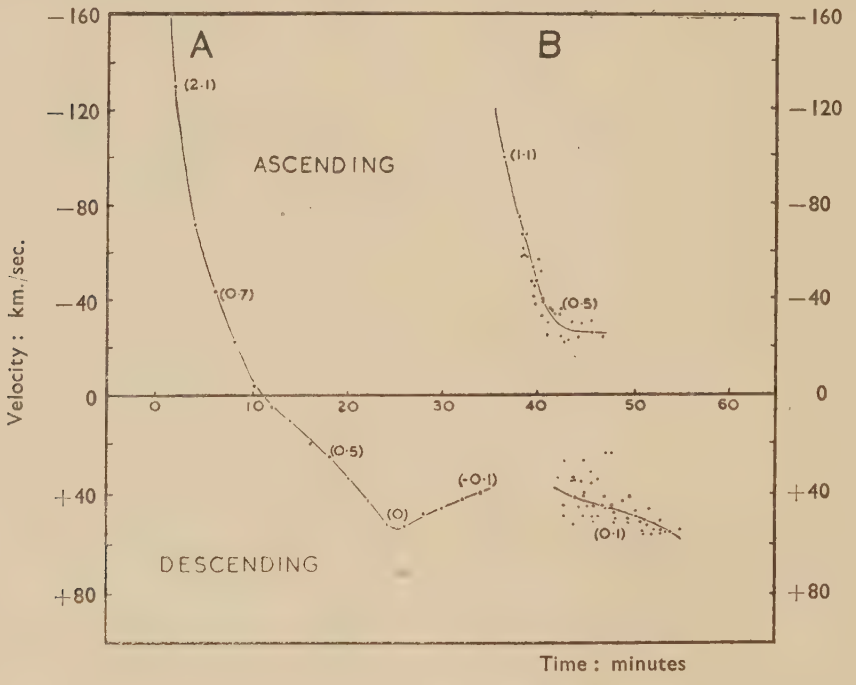

FIG. 5.—*Velocity-time Curves for Limb and Disk Surges ejected by Flares.*

A. *Velocity-time curve for the apex of a surge, deduced from McMath and Mohler's height-time diagram for a limb surge accompanying a flare* (The Observatory, **68**, 110, 1948).

B. *The mean velocity-time curve for six disk surges connected with flares observed at Sherborne. These curves have been plotted from direct measures of the velocity (sightline component) of the moving gases, made by determining the Doppler displacements with the line-shifter of the spectrohelioscope (see Plate 4 and Fig. 7). The gap between the ascending and descending branches arises from the lack of contrast between the Hα line of the moving gases and that of the chromosphere, here seen as background. The quantities in brackets are the deduced accelerations, the unit being the value of solar gravity, 0·274 km./sec.².*

time curve for a limb surge accompanying a flare, as observed by McMath and Mohler (**19**). The velocity-time curve (A) for the apex of the limb surge has been derived by drawing tangents at 2-minute intervals to McMath and Mohler's height-time diagram, which for this purpose was reproduced on a large scale. The correction for "projection factor" is unknown, but is unlikely to be large, since the majority of surges move along nearly vertical trajectories. The numbers in brackets close to each curve give the deduced accelerations, expressed as fractions of solar gravity ($27{\cdot}9g = 0{\cdot}274$ km./sec.^{2}) for a number of points in the upward and downward motions: while these values are inherently subject to very large uncertainties, they provide interesting data for a discussion of the forces acting upon the surge prominences. The general similarity between curves A and B certainly supports the identity, first proposed by H. W. Newton (**17**), of the flare absorption markings and the limb surges. The spectrohelioscope sketches of Fig. 6 (A, B and C) show cases of flare emission patches occurring just inside the limb together with the surges ejected by them.

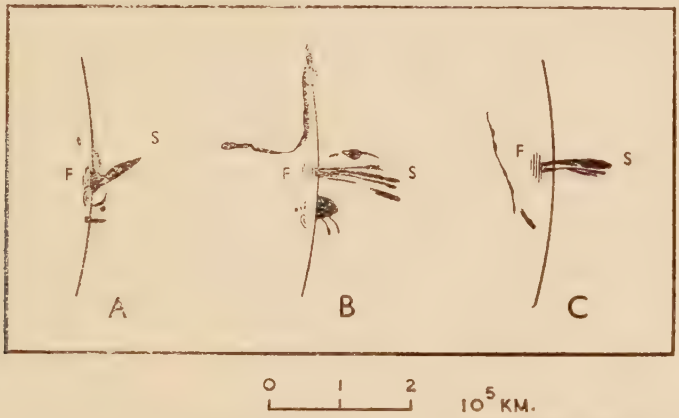

FIG. 6.—*Some Flares near the Limb and the Surges ejected by them.*

A. 1940 *August* $29^d\ 17^h\ 18^m$; $+11°$, *E. limb. Average velocity component for the surge at right angles to the line of sight was 97 km./sec. outwards from the limb.*

B. 1946 *March* $29^d\ 14^h\ 52^m$; $+32°$, *E. limb. Average outward velocity of the apex of the surge was 150–200 km./sec. The flare patch was an intense one, having a momentary line-width in Hα of 7·7* A.

C. 1947 *May* $28^d\ 14^h\ 29^m$; $-35°$, *E. limb. Average outward velocity 150 km./sec. Maximum Hα line-width for flare emission, 4·1* A.

Not every flare generates a surge: in Table III are given particulars of the percentage association for the period during which a special watch has been kept. The figures show that the number (expressed as a percentage) of flares which generate surges increases with the importance (and therefore brightness) of the flare emission, a conclusion in agreement with Newton's results (**17**).

TABLE III

Class of flare (Importance)	No. of flares	No. of flares generating surges	Surges / Flares (Percentage)
1	142	44	31
2	45	23	51
3 and 3^+	9	7	78

These percentages in the last column should be regarded as minimum values, since it is inevitable that some of the surges escape detection when the observer may be preoccupied with other things: as mentioned earlier, they can only be seen at all by constantly hunting to and fro with the line-shifter on either side of the $H\alpha$ line.

11. *The photometry of a flare surge.*—When plotting the curves of sightline velocity against time (Fig. 5B) for flare surges seen on the disk, a very peculiar fact was discovered independently by Newton (**17**) and the author (**18**). The surge cannot be seen in the spectrohelioscope at the top of its trajectory. As the dense absorption filament approaches its greatest height and its velocity has fallen to about −20 km./sec., it fades from sight, later to reappear on the downward path at about +20 km./sec. These events were observed on so many occasions that there could be little doubt of the reality of the phenomenon.

The cause of the fading was briefly discussed at the time (**20**) in terms of the *contrast effect*, and it appeared that there were two extreme possibilities, namely: (1) Let us suppose, for the sake of example, that the absorption line of a surge has at any moment a displacement of 2 A. to the blue and that its absolute central intensity at this velocity (91 km./sec.) is 15 per cent of the continuous spectrum. If it were a cloud of no great vertical thickness, *absorbing quanta mainly from below*, it would now be receiving light from the wings of the $H\alpha$ line, where the intensity is about 80 per cent, and re-emitting 15 per cent in the direction of observation, i.e. its central opacity would be 15/80ths. As its profile, with decreasing Doppler shift, approaches the centre of undisplaced $H\alpha$ for the disk, we should expect its absolute intensity to diminish in order that it shall maintain a constant opacity of 15/80ths. Therefore, in the undisplaced position it should have an absolute central intensity of 3 per cent (15/80ths of 15 per cent) and when seen in the spectrohelioscope it should stand out in strong contrast against the background, in a similar manner to the common quiescent filaments of great density. (2) On the contrary view, let us imagine that the surge is a long dense column of chromospheric matter projected upwards in a nearly vertical direction and that it is being viewed from on top. It may be expected that on this model the surge will carry its "background" along with it, that is to say, the top of the surge will receive light not from the chromosphere but from the moving column itself, thus maintaining a constant absolute intensity independent of its velocity for much of its life-time. If it is first observed with an intensity of, again let us say, 15 per cent at a displacement of 2 A., it will appear with the same contrast intensity as in (1); but in this case as the contour approaches the position of normal $H\alpha$ its monochromatic brightness relative to the neighbouring portion of the disk will decrease while its absolute brightness remains the same. The quantity $\log(I_s/I_b)$ or $\log C$, which by Fechner's law determines the visual appreciation of the surge against the background, has been calculated as a function of the displacement of the contour (**20**). $\log C$ shows a comparatively sudden change of 53 per cent as the displacement varies from 30 to 10 km./sec., and it may well be that this would cause the apparent extinction of the surge in the region of 20 km./sec. At zero displacement there will, of course, be no visible contrast between the surge and the surrounding disk, both being equally bright.

It has now become possible to put this matter to the test by the photometry of the series of calibrated plates obtained on 1948 September 19 (Nos. 1, 2, 3 and 4 of Plate 4). These plates were taken in the second order of the 16-foot grating spectrograph at Edinburgh (linear dispersion 1·7 A./mm.), while the surge

itself was kept under observation in the same instrument used as a spectrohelioscope. The plates were calibrated in the usual manner on the centre of the solar disk, the light being stepped down through a high-speed rotating sector.

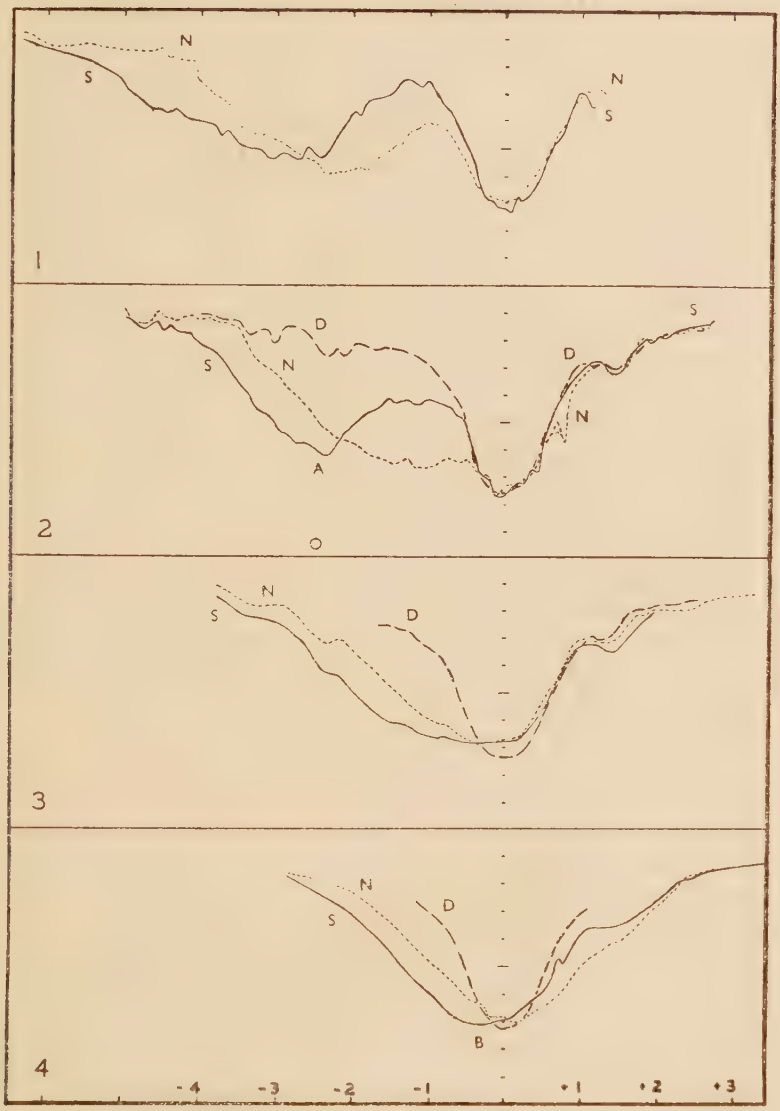

FIG. 7.—*Profiles of Hα for a moving Surge.*

Nos. 1–4 are profiles across the Hα line at the north (*N, N*) *and* south (*S, S*) *ends of the surge represented in Plate 4 (1–4). D, D is the profile of normal Hα absorption for the adjacent disk.* Abscissae *are angstroms from the centre of normal Hα, to red + to blue −.* Ordinates: *100 per cent equals adjacent disk continuum.*

In Fig. 7 are given profiles derived from microphotometer measures showing the densest parts of the surge, corresponding to the various displacements of the line, as depicted in Plate 4 (Nos. 1–4). The profiles give true intensities, but have not been corrected for heterochromatic light*. Corrections for slit

* The spectra were recorded through a Schott R.G.2 screen in order to eliminate light from the overlapping third order spectrum. The difference between the observed central intensity of $H\alpha$ (24 per cent) and the corrected value (15 per cent) therefore arises from scattering into the centre of the line by ghosts and other instrumental causes.

width are negligible in the second order. It is clear that the opacity of this surge diminishes from a value of about 0·5 (the ratio OA/OD of No. 2) to zero as its velocity decreases from −120 km./sec. to zero. At the top of its trajectory (zero displacement, B in No. 4) it is actually about 2 per cent brighter than the surrounding chromosphere. The *absolute brightness* of the surge was therefore approximately *independent of its velocity*, a result which is in complete accord with the earlier visual records obtained with the spectrohelioscope. It is, therefore, suggested that these high-velocity dark filaments consist of dense chromospheric material whose emission during motion is not governed by the "Doppler brightness" of the solar surface beneath it. Such a view is consistent with the identity already proposed between the flare filaments (Plate 4) and the limb surges (Fig. 6). Lastly, it is attractive to consider the possibility that the mechanism, pressure of $L\alpha$ radiation, or whatever it may be, by which the surge is "punched out" near the time of peak intensity of the flare, may be the same as that which is responsible for the ejection of the aurora-generating particles. However, the available evidence gained from these spectra makes it clear that the greater part of the surge returns to the chromosphere. The only direct evidence we have at present of material particles leaving the Sun at these times comes from the asymmetry observed in the $H\alpha$ emission, to be discussed in Section 13, and from the absorption reported near H and K at the times of magnetic storms by Richardson (**26**) and by Brück and Rutllant (**27**).

12. *Emission line spectrum of flares.*—The early work of Richardson and Minkowski (**22**), that of Allen (**23**) and the more recent spectra obtained during the great flare of 1946 (**8, 24**) are in general agreement as to the emission lines usually observed in flare spectra. But when we come to study the changes in relative intensity of particular lines between one flare and another, as well as between different areas in the same flare filament, some surprising anomalies are encountered. These discrepancies are much too great to be ascribed to errors of observation or photometry.

Let us take the D_3 line (λ5876) of *He* I as an illustration. In spectrograms of six minor (Class 1 and 2) flares on the disk, recorded at Sherborne and Edinburgh, D_3 has appeared dark in absorption from that part of the filament which showed the brightest emission in $H\alpha$. In the 3^+ flares, on the other hand, recorded visually by Young, Maunder, Evershed and others (**4**), D_3 is referred to as "brilliantly reversed", usually over the sunspot *umbra*. During the 3^+ flare of 1946 July 25, D_3 was photographed both in emission and in absorption in different parts of the same flare. The emission was confined to two very limited regions, namely the central parts of the two long filaments where they passed directly over some of the umbrae of the spot group. Between these an extensive region, equal to about one-half the area of the sunspot and extending out over the photosphere, showed D_3 in dense absorption.

The helium line λ6678 has never been observed in absorption on the Sun's disk. In emission it has been reported in some metallic prominences at the limb; and on the disk during a few only (**4, 8, 23**) of the most intense flares. More recently I have photographed it at Edinburgh as a *chromospheric* emission line at the limb (Plate 3, No. 5). The emission was equally intense (central intensity about 5 per cent of the continuous spectrum at the centre of the disk) over an arc of the limb 160,000 km. long. The region was one which coincided with an active spot group departing round the west limb (1948 April 5, +15°).

Some small surges and other sunspot-type prominences were seen here later, but at the time ($09^h\ 14^m$) it was clear that there were no prominences contributing to the emission in λ6678. A similar effect has been noticed over two recent spot groups on the limb, although other apparently active groups have failed to show it. Finally, M. and Mme d'Azambuja have found (**28**) that *He* λ10830 absorbs strongly over some spot groups and in prominence filaments projected against the disk: it has been photographed (**22**) in emission from at least one Class 3 flare on the disk. Such facts are an indication that the *He* I lines are peculiarly sensitive to differences of excitation, such as we might expect to exist locally and in the immediate vicinity of a sunspot, and this may account for their very variable intensities in flares.

The D lines of sodium have also shown great variations between flares which, judged by the geophysical and other effects associated with them, must have been of comparable *Hα* intensity. Newton (**4**) lists many references to "brilliant reversals" of D_1 and D_2 over the umbra of a sunspot during 3^+ flares. On the contrary, the 3^+ flare of 1946 July 25, perhaps one of the greatest on record, showed no emission or appreciable filling in of either line, even from that region of the spot which gave D_3 brighter than the continuous spectrum (**8**). Waldmeier, who has studied the intensities of D_2 and D_3 visually in 50 flares (**25**), finds anomalies very similar to those mentioned above and he gives schematic curves representing the intensities of both lines as a function of the intensity of *Hα*. In support of this conclusion, I give, for a few lines in the red, Allen's intensity estimates from various flares (**23**) against my own measures for the 3^+ flare of 1946 July 25 (the zero entries for the D lines mean that there was no filling in of the normal Fraunhofer profile):

	He λ 5876	*Na* λ 5890	*Na* λ 5896	*Fe*$^+$ λ 6456	*H* λ 6563	*He* λ 6678
Allen (visual estimates; Rowland intensities)	50	6	6	1	800	20
Author (photometric measures of central intensities; percentages of continuum)	120	0	0	100	300	150

Even if we make all possible allowances for errors of estimation and photometry we cannot reconcile these observations with the concept of a standard type of flare spectrum which differs only in intensity between flares of Class 1 and Class 3. There are evidently great differences in the relative intensities of different lines, arising perhaps from variations in chromospheric level, or of excitation, which are in need of investigation by accurate photometry. For this purpose calibrated plates giving a *simultaneous* record of wide regions of the spectrum are preferable to a succession of plates of higher dispersion which will inevitably record different places and phases of the flare development.

Since it is likely that the peak central intensity of the *Hα* emission will be generally accepted as the most reliable index of flare intensity for geophysical purposes, I give in Fig. 8A some profiles of the emission lines for a number of flares and bright filaments. A simpler measurement which can be carried out by most observers is that of effective line-width, a method which has been briefly described in Section 5 and more fully in an earlier paper (**7**). In Fig. 8B I have attempted to express the line-width as a function of the corrected central intensity for the *Hα* emission. The central intensities, plotted as ordinates in this graph,

have been obtained either by visual measurement with the wedge photometer, following Newton's method (**1**), or by photographic photometry of calibrated plates. In each case the observed values have been corrected to allow for the effect of instrumental scattering by the use of Woolley and Newton's formula (**29**),

$$r = \frac{r' - \alpha}{1 - \alpha},$$

where r' and r are the observed and corrected central intensities respectively, and α is a constant for the instrumental working conditions whose value may be derived from the observed central intensity of the normal $H\alpha$ absorption line. The level 100 per cent is that of the continuous spectrum 15 A. from $H\alpha$ for the adjacent disk. The number of occasions for which accurate simultaneous

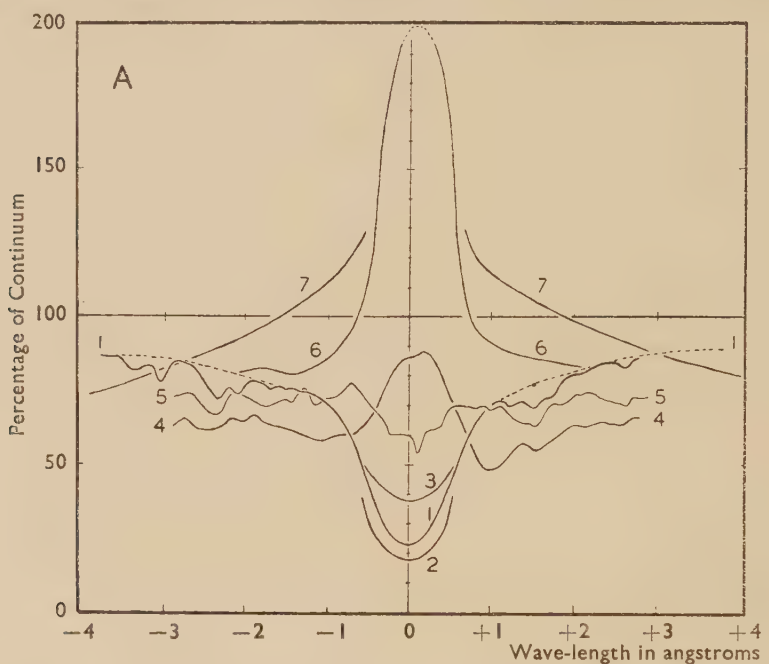

FIG. 8A.—*Flare Emission Line Profiles in Hα.*

1. *Profile of normal Hα absorption line at undisturbed centre of disk;* ordinates *are true intensities but uncorrected for heterochromatic light.*

2. *Profile for quiescent dark filament; central intensity* 8 *per cent* (*corrected for heterochromatic light by Woolley and Newton's method* (**29**)).

3. *Bright hydrogen of quiescent type in spot group; corrected central intensity* 31 *per cent.*

4. *End stages of Class* 3^+ *flare of* 1946 *July* $25^d\ 17^h\ 15^m$. *Note the absorption of the red side of the reversal at* +1 A., *caused by descending dark filaments which were observed visually in the spectrohelioscope. The flare was overlying the penumbra of a spot, which accounts for the low intensity level in the wings.*

5. *End of Class* 3 *flare of* 1948 *March* $11^d\ 12^h\ 47^m$. *Note the bright wings and central absorption. This is a profile of Plate* 3, *No.* 2, *also overlying the penumbra of a spot.*

6. *Early stage* (2 *minutes before peak intensity*) *of Class* 3^+ *flare of* 1946 *July* $25^d\ 16^h\ 25^m$. *The central intensity* (*corrected*) *is* 224 *per cent, but this is subject to a probable error of* ±10 *per cent due to the density of the image. Note that the blue wing gives lower intensities than the red, quite apart from any small shift of the line centre.*

7. *Emission wings at the time of peak intensity. Same flare as last but taken two minutes later at* $16^h\ 27^m$. *If extrapolated to penumbral intensity these wings are* 16 A. *wide. Central intensity at this time probably* >300 *per cent.*

(*In the above profiles the* ordinate 100 *per cent refers to the level of the continuous spectrum of the adjacent undisturbed disk.*)

measures of line-width and intensity are available is not large, but the plotted points suggest that the line-width is roughly proportional to the central intensity up to intensity values about 150 per cent of the continuum. Thereafter, there is some evidence that with the appearance of the wide wings the line-width increases more rapidly with increasing central intensity.

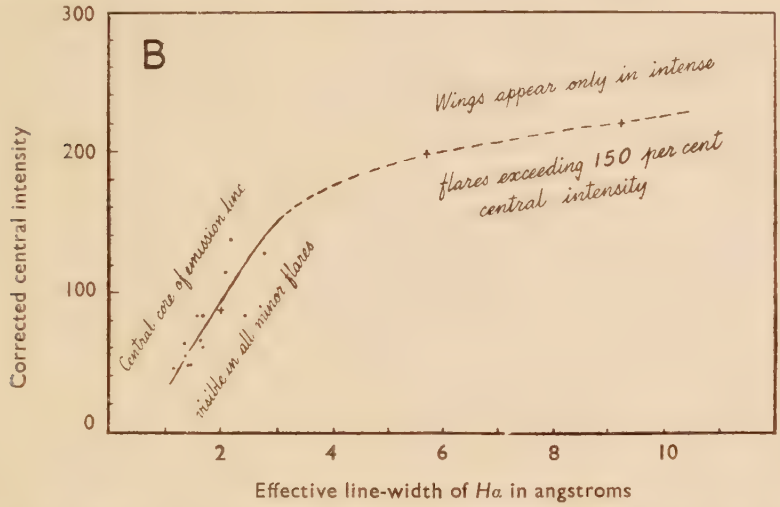

FIG. 8B.—*Effective Line-width of Hα Emission plotted as a Function of Central Intensity.*

The ordinates *are corrected central intensities (see text of Section* 12), 100 *per cent being the level of the continuous spectrum* 15 A. *from Hα for the adjacent undisturbed disk.*

The measures of central intensity, represented by circles, have been obtained with a wedge photometer applied to the spectroheliоscope (Newton's method). Line-widths were measured simultaneously with the line-shifter (as described in Section 5). *The crosses represent photographic determinations and these three points refer to one flare only—that of* 1946 *July* 25. *The two highest points may be in error by* ±10 *per cent.*

It is considered that the change of gradient at about 150 *per cent central intensity is a real effect and corresponds to the "emergence" of the wings of the emission line above the level of the continuum. In a flare on the disk the visibility of the wings is confined to the "flash" phase and at other times only the narrow central core of the emission can be seen: in a detached flare at the limb* (1947 *August* 23) *the wings were photographed to better advantage, in absence of the continuous spectrum* (*Plate* 3, *No.* 8).

Accurate central intensity measures for the H and K lines of *Ca* II would be of great value for comparison with those of *Hα*, but so far the only measures published are those of Partridge (**24**). Looking through Mr Evershed's very extensive collection of unusual chromospheric spectra we were able to pick out an H and K spectrum, taken by him on 1921 May 14, which evidently recorded an intense flare filament. This is reproduced, by his kindness, in Plate 3 (Nos. 6 and 7). The relative widths of H (0·7 A.) and *Hε* (2·5 A.) should be noted and compared with Partridge's photograph*. In both cases there is evidence for a small increase in the brightness of the continuous spectrum, in addition to the monochromatic emissions.

13. *Asymmetry of the Hα emission line near the time of peak intensity.*—The behaviour of the emission profile during the progress of a flare is one of the most interesting results which have emerged from the detailed work on flare spectra. Preliminary measures, first published in 1943 (**7**), showed that the red wing of the broadened emission persistently extends farther than the blue wing from

* *The Observatory*, **68**, 68, 1948.

the centre of normal *Hα*, by an amount which is approximately proportional to the line-width and therefore to the brightness of the flare.

We now have 540 measures of line-width available for discussion, relating to 99 different flares. While the method of measurement (**7**), briefly described in Section 5, has remained uniform throughout, two different instruments have been employed: the majority (434) of the measures were made at Sherborne and the remainder (106) with the new instrument at Edinburgh, employing an entirely different grating and collimator. Both series of measures are consistent with one another, to such an extent that we may safely disregard the possibility that the asymmetry is instrumental in origin, arising perhaps from defects in the grating or from a similar cause.

In Fig. 9 are shown typical records of the changes in wave-length of the red and blue wings of the emission line during the life-times of a number of flares. It is evident that at the time of greatest total line-width the red wing has a greater extension from the wave-length of normal *Hα* (λ6562·8) than the blue wing. As the flare subsides this asymmetry disappears and at line-widths of from 1·5 to 2 A. both wings of the emission contour are equally extended.

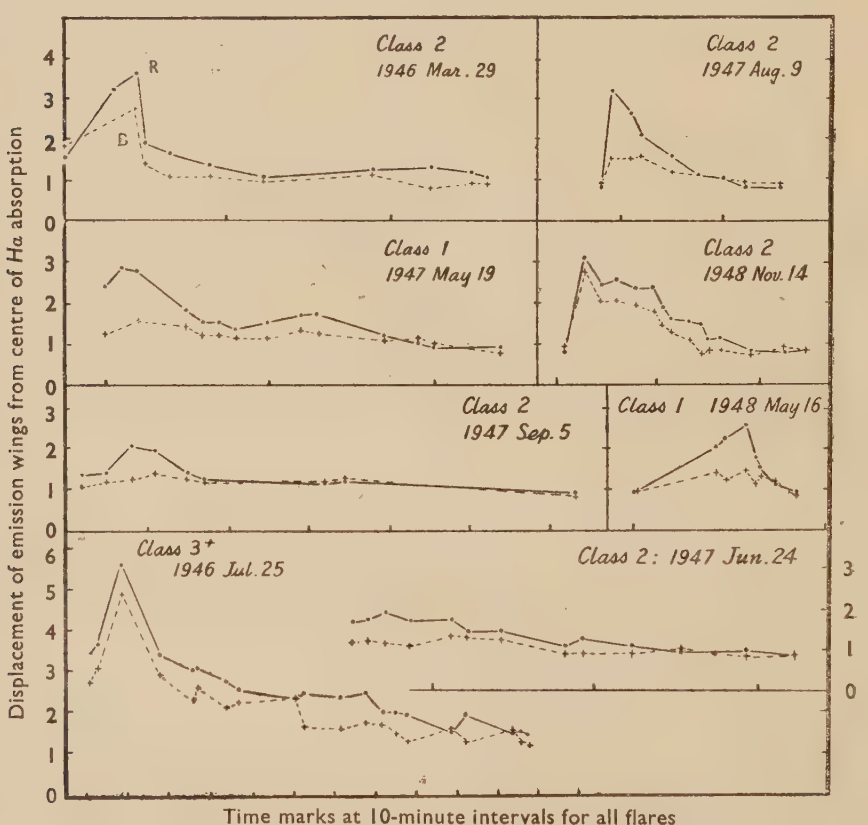

FIG. 9.—*Wave-lengths of the Emission Line Wings during Flares.*

The full lines refer to the red wing; the broken lines to the blue wing. Ordinates *are arbitrary units* (1 *unit* = 10° *of the line-shifter scale* = 1 A., *nearly*). *The zero in every case is the wave-length of the Hα absorption line* (*darkest field*) λ 6562·8. Abscissae *are marked at* 10-*minute intervals.*

The greatest difference (*red* minus *blue*) *occurs at the time of greatest total line-width, or intensity, and is always positive.*

We must next consider what happens to the central peak of the line profile; is this likewise shifted to the red, or are we concerned only with an asymmetry in the wings? In none of the 99 flares so far considered has the centre of the emission profile (line-shifter position of greatest flare intensity in the spectrohelioscope) shown any certain displacement from the position of normal $H\alpha$ (darkest background in the field of the spectrohelioscope). The emission line is admittedly broad and the test is consequently not a very sensitive one, but experience gained during some hundreds of measures on the absorption lines of moving prominences seen against the disk, in which a shift of 0·1 A. can be easily detected, suggests that it would be quite impossible to miss a displacement of the centre of the emission line of as much as 0·5 A. This conclusion is supported by the profiles of Fig. 8A, especially those of the flare of 1946 July 25 (**8**) in which the wings only were asymmetrical and the centre of the line was not appreciably displaced.

The orderly sequence of these variations in red shift, depending as they do upon the intensity of the flare emission, is further strong evidence that we must seek some explanation other than that of a Doppler displacement of the emitting atoms in the line of sight. If the effect were due to line-of-sight motions the integrated effect over the total life-time of a flare would be of the order of 50,000 km.: So large an *inward* movement for a flare seen near the centre of the disk would be quite inconsistent with our observations of flares occurring at the limb, where the motions have usually been slowly outwards, if observed at all. To test the matter further, the material has been divided into two groups: (1) measures relating to central flares, i.e. those occurring within 60° heliocentric angle from the centre of the disk, and (2) measures relating to limb flares, lying between 60° and 90° from the centre. The results of this analysis are embodied in Fig. 10B, from which we infer that the relationship between red shift and line-width is independent of the heliocentric angle of the flare: it cannot, therefore, arise from vertical movements of the flare material in the chromosphere. This does not rule out the possibility, however, that part of the scatter of the individual measures shown in Fig. 10A may be due to small Doppler shifts caused by *random* movements of the flare filaments, but if this is the case, such motions cannot be in excess of about ± 5 km./sec.

The probable error in the individual values of red shift, as plotted in the scatter diagram of Fig. 10A, has been the subject of a separate investigation. Combining suitably the probable errors determined by experiment for the three line-shifter settings involved (see Section 5), a value of 0·04 A. was obtained for the probable error of a single determination of red shift by an experienced observer.

The proposal, first advanced in 1943 (**7**), that the asymmetry arises from absorption superimposed upon the blue wing of the emission line seems to be even more probable now than it did then, as a consequence of Kahn's recent investigations (**21**) into the density and composition of the aurora-generating particle stream at various distances from the Sun following its ejection from the flare. The chances of observing the particles spectroscopically appear to be greatest during and immediately following the flare and before they have acquired their terminal velocity. Let us suppose that during the flare they form a cone-shaped cloud which is in process of *accelerating* outwards. If this cloud carries a sufficient concentration of hydrogen atoms in the 2-quantum state, which is

highly probable, since it is then absorbing $L\alpha$ radiation from the flare below it, we should expect its absorption effect upon the emission contour to reduce the intensity of the blue wing but not of the red. We might also expect such a mechanism to contribute its greatest effect at and shortly after the time of peak intensity of the flare. Once the emission in $L\alpha$ and $H\alpha$ has begun to subside, there will be fewer atoms in the 2-quantum state and by this time the cloud will in any case have accelerated to such a velocity that its absorption line will be well displaced to the blue.

Alternatively, there is to be considered the possibility that the asymmetry may arise from an *unsymmetrical* Stark effect. Very great fields appear to be

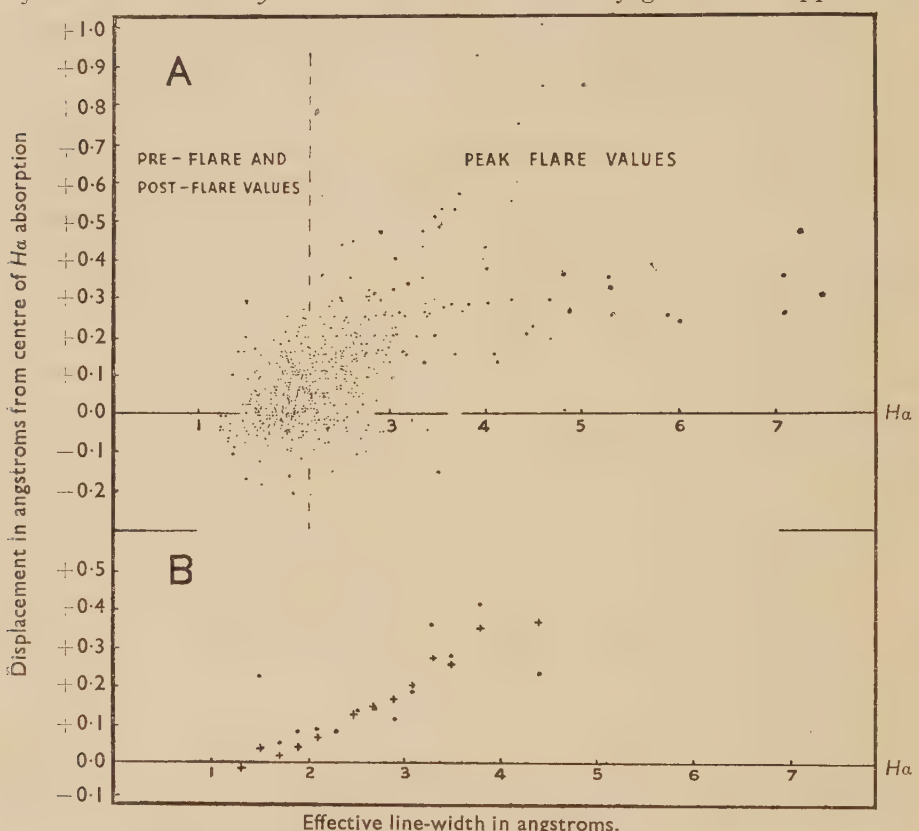

FIG. 10.—*The Red Shift expressed as a Function of Line-width.*

A. *The mean wave-length of the emission line extremities* $(R+B)/2$ *is here plotted as a function of the total line-width of the Hα emission. The* 540 *plotted measures refer to* 99 *different flares, including those* (8) *of Fig.* 9. *It will be seen that the mean wave-length is displaced to the red for all values of line-width in excess of about* 3 A., *that is to say, at the times of peak intensity of all bright flares.* Ordinates *show displacement in angstroms from normal Hα (darkest field), redward being* +. Abscissae *show line-widths in angstroms.*

B. *The* 540 *measures have been divided into two categories,* centre *and* limb, *according to the location of the flare on the solar disk, the division having been fixed at* 60° *heliocentric angle, and the mean displacements calculated for intervals of* 0·2 A. Crosses *represent the mean displacements for the measures* (451) *on central flares,* circles *for the measures* (89) *on limb flares.*

There is clearly no significant difference in the magnitude of the wing asymmetry between the two categories. It is inferred that the asymmetry cannot arise from Doppler shifts of the whole profile, such as might derive from vertical motions of the flare filaments downwards *in the chromosphere at about the time of greatest flare intensity. (A Doppler shift of* 1 A. *at Hα represents a sightline velocity of* 45·7 *km./sec.)*

The diagrams of Fig. 10 *have been kindly prepared by Mr H. Schneider.*

required: that such fields do occur in the flash phases of intense flares is suggested by the enormously wide emission wings which have been photographed both on the disk and at the limb (**15**). For example, the wings shown in Fig. 8A (No. 7) cover a wave-length interval of 16 A., although the central thermal Doppler core is only 1 A. wide. In the limb flare of 1947 August 23 (Plate 3, No. 8) the wings can be traced 12 A. to red and 8 A. to blue.

A simultaneous photograph of the whole Balmer series from an intense flare would probably be of great value in settling the origin of the observed effects.

In conclusion, I wish to record my indebtedness to Professor Greaves for stimulating discussions and advice in connection with this paper; to Miss M. Conway, who has carried through the tedious and exacting work of plotting line profiles; and to Mr H. Schneider, of the Royal Observatory staff, for his analysis of the line-width measures. The part accomplished at Sherborne was made possible by the assistance of the Government Grant Committee of the Royal Society.

Royal Observatory,
Edinburgh:
1948 *December* 7.

References

(1) H. W. Newton, *M.N.*, **99**, 463, 1939.
(2) R. G. Giovanelli, *Ap. J.*, **91**, 334, 1940.
(3) H. W. Newton, *The Observatory*, **68**, 29, 1948.
(4) H. W. Newton, *M.N.*, **103**, 244, 1943; *Geophys. Suppl.*, **5**, 159, 1948, and **5**, 200, 1948.
(5) E. V. Appleton and J. S. Hey, *Phil. Mag.*, **37**, 73, 1946. J. S. Hey, *The Observatory*, **66**, 360, 1946, and **68**, 193, 1948. J. S. Hey, S. J. Parsons and J. W. Phillips, *M.N.*, **108**, 354, 1948.
(6) J. A. Ratcliffe, *Sixième Rapport de la Commission pour l'Étude des Relations entre les Phénomènes Solaires et Terrestres*, p. 87, 1948. R. N. Bracewell and T. W. Straker *M.N.*, **109**, 28, 1949.
(7) M. A. Ellison, *M.N.*, **103**, 3, 1943.
(8) M. A. Ellison, *M.N.*, **106**, 500, 1946.
(9) M. A. Ellison, *M.N.*, **104**, 22, 1944.
(10) A. Hunter, *J.B.A.A.*, **57**, 218, 1947.
(11) R. G. Giovanelli, *M.N.*, **108**, 163, 1948.
(12) H. W. Newton, *J.B.A.A.*, **57**, 54, 1947.
(13) M. A. Ellison, *The Observatory*, **67**, 206, 1947, and **68**, 69, 1948.
(14) F. Ellerman, *Ap. J.*, **46**, 298, 1917.
(15) M. A. Ellison and F. Hoyle, *The Observatory*, **67**, 181, 1947.
(16) J. Evershed, *The Observatory*, **68**, 67, 1948.
(17) H. W. Newton, *M.N.*, **102**, 2, 1942.
(18) M. A. Ellison, *M.N.*, **102**, 11, 1942.
(19) R. R. McMath and O. Mohler, *The Observatory*, **68**, 110, 1948.
(20) M. A. Ellison, *The Observatory*, **64**, 300, 1942.
(21) F. D. Kahn, *M.N.*, **109**, No. 3, 1949. (In press.)
(22) R. S. Richardson and R. Minkowski, *Ap. J.*, **89**, 347, 1938.
(23) C. W. Allen, *M.N.*, **100**, 635, 1940.
(24) A. B. Partridge, *The Observatory*, **67**, 62, 1947.
(25) M. Waldmeier, *Z. f. Ap.*, **20**, 46, 1940.
(26) R. S. Richardson, *Annual Report, Mount Wilson Observatory*, 1943–44.
(27) H. A. Brück and F. Rutllant, *M.N.*, **106**, 130, 1946.
(28) M. et Mme L. d'Azambuja, *Bulletin Astronomique, tome XI, fasc.* 7.
(29) R. v. d. R. Woolley and H. W. Newton, *M.N.*, **96**, 5, 1935.

THE STUDY OF SOLAR FLARES BY MEANS OF VERY LONG RADIO WAVES

R. N. Bracewell and T. W. Straker

(Communicated by R. O. Redman, F.R.S.)

(Received 1949 January 22)

Summary

The phase of very long radio waves reflected from the ionosphere is very sensitive to the occurrence of solar flares. The course of the ionospheric disturbance can be followed in detail and a measure of the maximum disturbance given. A method is outlined which may lead to the identification of the radiation which disturbs the ionosphere. Continuous automatic records provide abundant data of great value to the study of solar-terrestrial relations.

1. *Introduction.*—Among the terrestrial effects of solar flares there is a phenomenon, little studied hitherto, though discovered at the Cavendish Laboratory in 1936*, which may prove to be of great value in supplementing the visual observations of flares. It is the anomaly sometimes observed in the phase of a radio wave which has been reflected from the ionosphere after emission from a nearby very-long-wave transmitter. This paper first describes how the phase anomalies are observed and how they are related to the better-known radio effects. Then it deals with their relation to solar flares and shows what information about them the observations can yield. Detailed statistical evidence based on the observation of over three hundred phase anomalies is given in Sections 3 and 4 to show that the observation of a radio phase anomaly is very closely related to the occurrence of a solar flare, and provides a considerably better index of such an occurrence than other ionospheric phenomena. Since radio observations are not interfered with by cloud, a continuous record of phase anomalies taken on a very-long-wave radio transmission would prove very useful to those searching for correlations of geophysical phenomena with the occurrence of solar flares.

In Section 5 the detailed characteristics of the observed phase anomalies are compared with what is known of the detailed characteristics of flares, and the comparison suggests that further knowledge of flares can be obtained by continued studies of phase anomalies. The present position is summarized in Section 6.

2. *Sudden Phase Anomalies.*—Experimental studies of the propagation of very long waves were resumed at Cambridge in 1946. In a typical experiment, the field of the Post Office morse transmitter GBR at Rugby is observed 90 kilometres away at Cambridge. The transmitter radiates 350 kilowatts from a horizontal wire supported on twelve 800-foot steel masts. The frequency is 16,000 cycles per second and the wave-length 18·74 kilometres. At Cambridge a special apparatus fundamentally similar to that described by Budden, Ratcliffe and Wilkes, is used to measure the difference of phase between the ionospheric wave and the ground wave. The normal daily behaviour of the phase of the ionospheric wave is shown in Fig. 1 (*a*). If we assume that mirror-like reflection occurs, then Fig. 1 (*a*)

* K. G. Budden and J. A. Ratcliffe, *Nature*, **140**, 1060, 1937. K. G. Budden, J. A. Ratcliffe and M. V. Wilkes, *Proc. Roy. Soc.*, **171** A, 188, 1939.

shows that the effective height of reflection falls and rises regularly through about 15 kilometres during the day, giving rise to a corresponding variation of 500 degrees in the phase of arrival. The phase-time curve is usually free from fluctuations of more than about 10 degrees during the day, and usually repeats from one day to the next within about 20 degrees. Such steadiness is unusual for waves which have entered the ionosphere, but the irregular variations which set in at night are more reminiscent of the behaviour on less extreme wave-lengths.

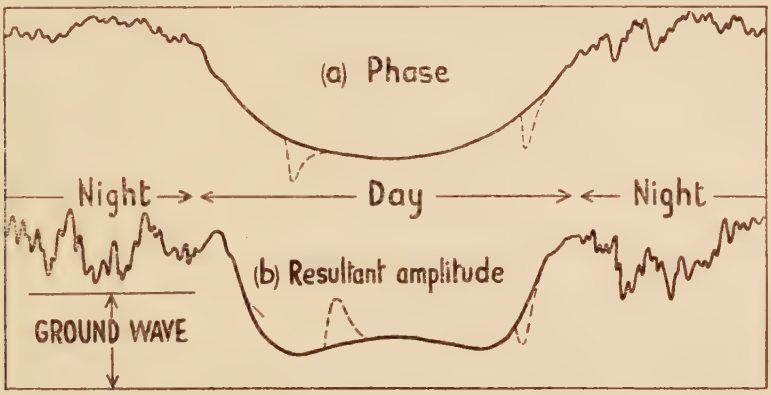

FIG. 1.—*Diurnal behaviour near a very-long-wave transmitter. Phase anomalies are shown in broken outline.*

The anomaly which often accompanies reports of flares is a fall of the effective height of reflection, through, say, three kilometres, over a time of several minutes, followed by a slower recovery taking about three times as long. Unlike short waves, which on these occasions are often completely absorbed, the very long waves scarcely alter in amplitude. Fig. 1 (*a*) shows in broken outline how two typical anomalies might appear on the phase-time curve.

There is a simpler experiment which reveals the occurrence of phase anomalies, and which does not require the special phase-measuring apparatus mentioned above. The e.m.f. induced in a vertical-wire, or loop aerial, is amplified and applied to the plates of a cathode-ray oscilloscope, or peak-rectified and applied to a recording milliammeter. The quantity thus observed is the resultant amplitude of the constant ground wave and the ionospheric wave, which, as it varies in *phase* with respect to the ground wave, produces variation in the resultant *amplitude*. The daily record might appear as in Fig. 1 (*b*), and phase anomalies would appear as in the dotted examples. From such a record one may obtain the times of start, maximum and finish. Favourable records are obtained at distances about 200 kilometres from a transmitter such as that at Rugby.

As the ionospheric wave varies in phase, it generally changes somewhat in amplitude also. As a result, the times of maximum and finish of the phase anomaly, as judged from a record of resultant amplitude, can be in error by a few minutes. Furthermore, only a coarse estimate of total amount of phase change can be made.

The records taken daily at Cambridge are of the phase and amplitude of the ionospheric wave. These records give not only the times of start, maximum and finish, but also the "size" of a phase anomaly, i. e. the total fall of effective height of reflection and the "shape", which is obtained by subtracting from the phase-time record, the values the phase would have assumed had no anomaly occurred.

This can be done either by examining the trends before and after the anomaly or by comparison with other days. The shapes of about thirty phase anomalies are shown in Fig. 2, all drawn to the same scale, and Table I gives their times of occurrence.

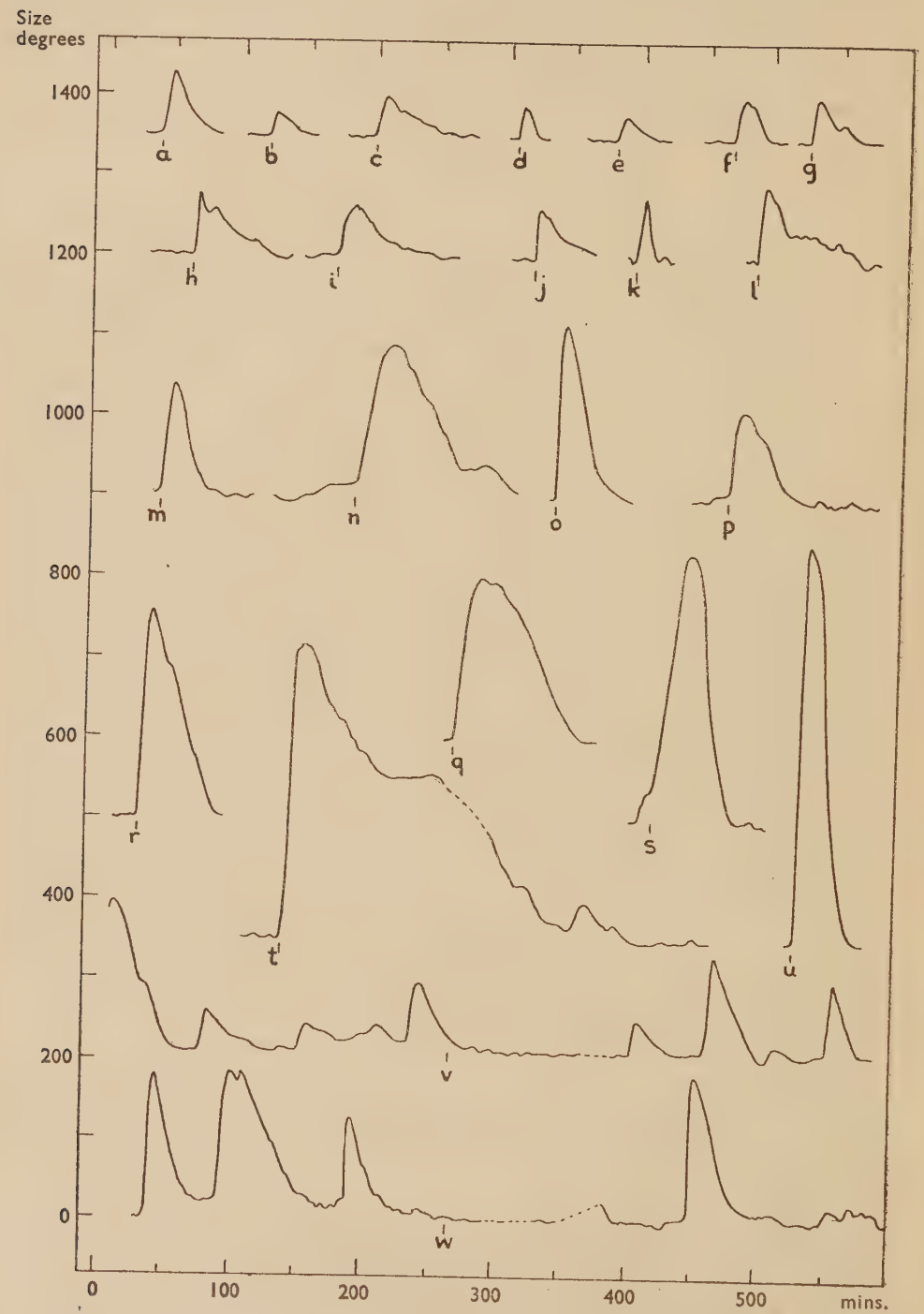

FIG. 2.—*Examples of phase anomalies. Table I gives dates and times.*

TABLE I

	Date 1948	U.T.		Date 1948	U.T.
		h m			h m
a	Aug. 8	08 09	m	Apr. 27	12 43
b	Aug. 3	07 59	n	June 8	11 06
c	May 10	14 18	o	Aug. 1	16 12
d	Aug. 5	11 06	p	May 11	10 50
e	July 23	14 51	q	Aug. 17	10 56
f	Apr. 30	15 19	r	June 9	05 00
g	Aug. 20	11 46	s	Oct. 2	05 57
h	July 1	14 02	t	May 21	11 17
i	Aug. 30	10 23	u	Dec. 9	11 47
j	Aug. 29	14 51	v	Aug. 4	14 00
k	June 8	04 38	w	May 7	12 00
l	May 20	08 38			

3. *The Relation between Sudden Phase Anomalies and other Ionospheric Phenomena.*—We have seen what is observed when a phase anomaly occurs and how the observation is made, and now show the measure of agreement with two other important radio effects associated with flares, namely the sudden fadeout of short waves and the sudden enhancement of atmospherics.

The sudden fadeout, whose main features were ascertained by H. Mögel* between 1927 and 1930, and to which attention was redirected by J. H. Dellinger† in 1935, has been studied in relation to solar flares by Newton and Barton‡, Waldmeier§, and Giovanelli and Higgs‖. Sudden enhancements of atmospherics have been recorded continuously since about 1929 and were reported by Bureau¶ in 1936. He showed in 1944**, from fourteen years of records, that their frequency agreed with the eleven-year cyclic variation as revealed by the published areas of calcium flocculi. The phenomenon is discussed at length in a later paper††, but not particularly in relation to solar data. It is closely associated with the sudden increases found by Budden, Ratcliffe and Wilkes in the field of a distant very-long-wave transmitter.

Fig. 3 shows simultaneous records of short-wave field strength, atmospherics on 27 kilocycles per second, and phase of the ionospheric wave from GBR Rugby received at Cambridge on 1948 May 5. For permission to reproduce the first two we are indebted to Dr Bureau. At $11^h 29^m$ a big phase anomaly is shown commencing. The enhancement of atmospherics (shown inverted) can be seen setting in at the same time, and is reported in the *Bulletin d'Information du Laboratoire National de Radioélectricité* as starting at $11^h 30^m$, having its maximum at $11^h 50^m$, and ending at $12^h 35^m$. The diminution of short-wave field strength

* H. Mögel, *Telefunken-Zeitung*, **11**, 14, 1930; see also a note by E. V. Appleton, *Terr. Magn.*, **43**, 487, 1938.

† J. H. Dellinger, *Science*, **82**, 351 and 458, 1935.

‡ H. W. Newton and H. Barton, *M.N.*, **97**, 594, 1937.

§ M. Waldmeier, *Z. für Astrophysik*, **14**, 229, 1937.

‖ R. G. Giovanelli and A. J. Higgs, *Terr. Magn.*, **44**, 181, 1939.

¶ R. Bureau, *Transactions of the Edinburgh Meeting* (1936 *September*) *of the Association of Terrestrial Magnetism and Electricity*, Copenhagen, 1937; *Nature*, **139**, 110, 1937.

** R. Bureau, *Comptes Rendus*, **219**, 461, 1944.

†† R. Bureau, *L'Onde Electrique*, No. 239, 1947 February.

completely disrupted communication, a "particularly severe" fadeout from $11^h 33^m$ to $12^h 40^m$ being reported by Cable and Wireless Ltd., a "total fadeout" from $11^h 35^m$ to $12^h 15^m$ by the receiving centre at Noiseau, and from $11^h 35^m$ to $12^h 25^m$ by Villecresnes. Two further phase anomalies followed, but there were no reports of fadeouts or enhancements of atmospherics.

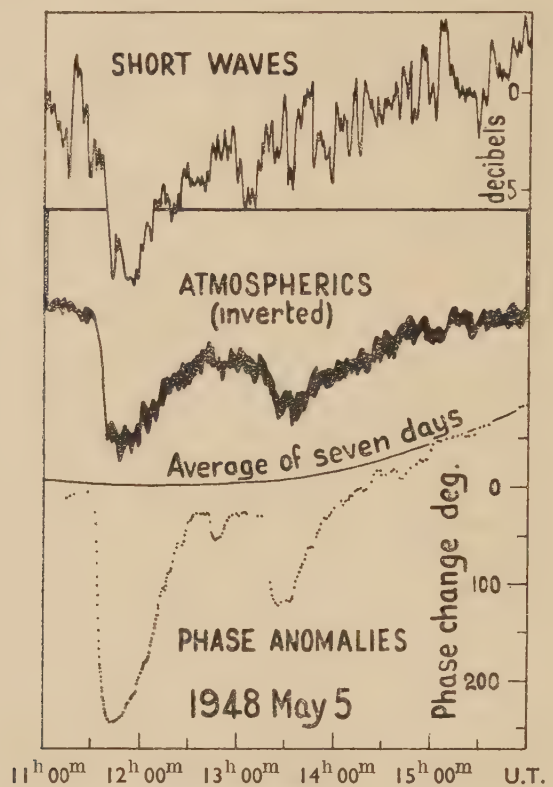

FIG. 3.—*Sudden ionospheric disturbances on simultaneous records of short-wave field strength (Leipzig 9732 kc./s. observed at Bagneux), numbers of atmospherics on 27 kc./s. recorded at Poitiers, and the phase of the ionospheric wave from GBR Rugby 16 kc./s. observed at Cambridge.*

Budden* has shown that the times of start often agree within a few minutes and that the durations also often agree, though not so accurately. This experience and the particular example given in Fig. 3 show that the phase anomaly is a phenomenon closely related to the short-wave fadeout and the enhancement of atmospherics.

In spite of the close agreement which is often noted, there is a large discrepancy in the total numbers of these phenomena. For example, in the sixty-six days from 1947 February 7 to April 13, and during the part of the day between one hour after sunrise and one hour before sunset, there occurred 122 phase anomalies. During the same period only 40 fadeouts were contained in the combined reports of Cable and Wireless Ltd., Villecresnes and Noiseau, and only 79 enhancements of atmospherics were reported by Bureau. Moreover, a virtually continuous watch is kept on fadeouts and atmospherics, whereas gaps in transmission were interrupting the long-wave observations for about one quarter of the time.

* K. G. Budden, Ph.D. thesis, Cambridge, 1939.

The bulk of this disagreement can be explained as follows. In the absence of a flare on the Sun, the three quantities, short-wave field strength, numbers of atmospherics and long-wave phase, are subject to fluctuation; the first because of interference between rays arriving at the receiver by different paths via a changing ionosphere, the second because of the varying strengths and positions of the tropical and local sources of atmospherics, and the last because of irregularity in the ionosphere. When a flare occurs, it will give rise to a report of any of the three phenomena only if it is intense enough to produce an effect which exceeds the threshold of recognition set by the fluctuations at the time. In proportion to the effect produced by a given flare, the fluctuation is found statistically to be greatest for fadeouts and least for phase anomalies. Individual records such as those of Fig. 3 also show that fluctuations are relatively least important for phase anomalies.

The statistical evidence is based on the use of the size of the phase anomaly as a measure of the intensity of the ionospheric disturbance. In Fig. 4, 196 phase anomalies are arranged in order of size, each represented by a vertical strip of length proportional to size. These are all the anomalies measured in 150 days during the period 1948 March 11 to August 31, by observing GBR Rugby at Cambridge. The strip is black if a fadeout was reported at the same time, otherwise it is white. We see at once a striking clustering of the black strips at the tall end. There is a threshold size of 150 to 200 degrees which is exceeded by the bulk of phase anomalies accompanied by reports of fadeouts. Few of the phase anomalies falling below this threshold were accompanied by reports of fadeouts, and few of those above it were unaccompanied.

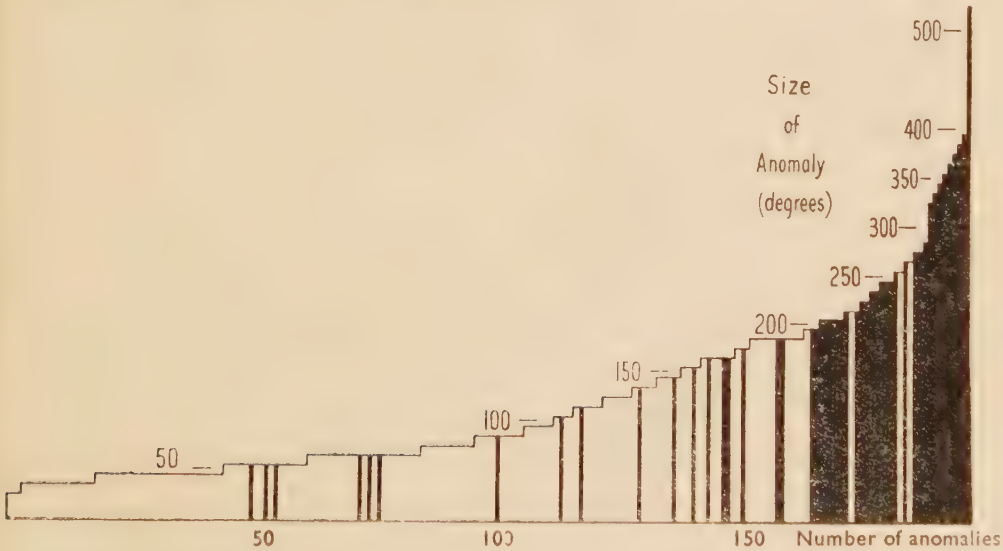

FIG. 4.—*The relation between fadeouts and the size of phase anomalies. One hundred and ninety-six phase anomalies are represented by vertical strips which are coloured black if a fadeout occurred. The boundaries between contiguous strips of the same colour are not shown.*

Now the fact that a threshold, by its own nature variable, can be put in evidence with a precision of some 25 per cent by reference to a quantity θ, the size of a phase anomaly, shows that θ is a reliable measure of the intensity of the ionospheric disturbance to that accuracy. The bulk of phase anomalies are comprised within

a range of θ of ten to one, and therefore we can expect that at least ten different sizes of disturbance can be reliably distinguished.

The possibility that the diurnal, seasonal and all other disturbing influences on θ may be so limited that it is still possible to classify the flare itself, is worthy of consideration, for international observation in hydrogen light at present permits a coarse division of flares into only three strengths. This matter is taken up in the following sections where the application of the present technique to solar research is discussed.

The two further features which distinguish the long-wave observations, viz. high efficiency of detection and ability to follow the ionospheric disturbance in detail, are also considered later, but results relating to the ionosphere, the fadeout and the enhancement of atmospherics will not be pursued here.

4. *The Relation between Sudden Phase Anomalies and Flares.*—It is known that with flares, as with phase anomalies, there is a threshold which must ordinarily be exceeded before fadeouts are reported (Giovanelli and Higgs*, and Newton†). It is of interest to study the relative abundance of phase anomalies and flares which are too weak to be associated with fadeouts. Are there flares which are too weak to cause phase anomalies? The impression gained from day-to-day reports of flares from British observatories is that there is always an accompanying phase anomaly if the transmitter is on.

Comparison by counting.—There are, however, occasions when a flare is seen and no phase anomaly is recorded. The analysis of these occasions is instructive and has been carried out for two series of observations. The first covers the 66 days from 1947 February 7 to April 13, and international flare lists are available; the second covers 150 days from 1948 March 11 to August 31, and British flare reports are to hand. During the first period there were 122 phase anomalies and 70 flares. In Fig. 5 (*a*) these numbers are represented by circles of proportionate

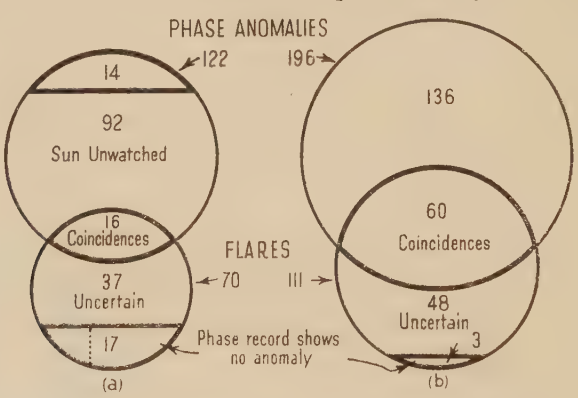

FIG. 5.—*Coincidences of phase anomalies and flares.*

area. The amount of overlap is in proportion to the 16 coincidences. Of the 54 flares unaccompanied by phase anomalies, in only seventeen cases is there a record to show that an anomaly was absent. In 37 cases there is uncertainty. For about half of them the transmitter was off, and the rest are accounted for by accidental gaps in the observations, insufficiently high rate of reading (in the case of visual observations), and other reasons. Among the cases of

* *Loc. cit.*

† H. W. Newton, *M.N.*, **104**, 4, 1944.

uncertainty many probable phase anomalies were revealed, for example by their recoveries when transmission was resumed after interruption, but the records were considered inadequate to establish the occurrence of a phase anomaly independently of the reports of flares. The 17 unaccompanied flares prove to be significantly distributed among the various observatories. No fewer than 11 were reported from spectroheliograms taken at the McMath-Hulbert Observatory, whilst all other observatories contributed six. (Of the 16 coincidences, 1 was reported by McMath.) It is known that different observers have different criteria for deciding when a patch of bright hydrogen shall be called a flare, and by singling out these reported flares which produced no phase anomaly, we have put this variable criterion strongly in evidence. This consideration suggests that the feeble flare-like brightenings and "points brillants" which distend the lists of flares may be responsible for the bulk of failures to produce phase anomalies. The second series of observations represented in Fig. 5 (*b*) supports this. The area of uncertainty has been considerably reduced by improved instrumentation, with the result that the number of coincidences has swollen. There is, however, no corresponding increase in the flares which produce no anomaly. In fact, they have become very few.

It remains undecided whether there are occasional flares abnormally weak, or deficient, in radiation capable of disturbing the ionosphere. Among the first series, Zürich observatory reports a flare (1947 March 9, **16^h 11^m–16^h 25^m**, max. 16^h 15^m, 8° E. 23° S.)* of Class 2 though spent in 14 minutes, during which the phase did not falter. The Bagneux atmospherics record on 30 kilocycles per second is equally unaffected. The three unaccompanied flares of the second series occurred as follows: 1948 July 26, 16^h 15^m–**16^h 25^m**, 38° W. 27° S., August 18, 08^h 40^m–**08^h 51^m**, 2° E. 14° N. (Greenwich); June 17, 18^h 39^m–**18^h 50^m**, 31° W. 11° N. (Edinburgh). They are all of Class 1.

The converse possibility, that some phase anomalies may not be caused by flares as ordinarily seen in hydrogen light, is suggested by the upper part of Fig. 5 (*a*). Of the 106 phase anomalies which were not accompanied by reports of flares, Table II gives fourteen which occurred at times when the graph of "Heures effectives d'observations" published in the *Quarterly Bulletin on Solar Activity* shows that the Sun was under observation. Whether this is evidence that no flare occurred is uncertain. The graph is compiled from the statements of different observers with different practices, who may at times quickly search the Sun's disk every fifteen minutes, and at other times attend continuously, but to a limited part of the disk. The question will be settled if spectroheliograms showing no flare are taken at times when a phase anomaly is near its maximum.

The distribution on the Sun's disk of 60 flares associated with phase anomalies shows no significant deviation from uniform distribution with distance from the central meridian.

Comparison by timing.—We now focus attention on the nature of the coincidences which are found between phase anomalies and flares. We could start by comparing the times of start, maximum and finish. It is not very fruitful. Perhaps three out of four flares are already in progress when first seen and no time of start can be given. The maximum must be seen more often than the start, but for the first half of 1947, fewer times of maximum are quoted than times of observed start, no doubt because of the difficulty of judging, without photometric

* Bold type indicates the beginning or end of the flare, not of observation.

TABLE II

Phase Anomalies when the Sun was under Observation but no Flare was Reported

Subscript numerals indicate precision in minutes. A change of phase of 100 degrees would be produced by a change of effective height of reflection of 4·7 kilometres.

1947	Start U.T.	Maximum U.T.	Finish U.T.	Size (degrees)
	h m	h m	h m	
Mar. 2	$10\ 31_1$	$10\ 42_2$	$12\ 30_{10}$	180
6	$13\ 46_1$	$13\ 48_1$	$14\ 09_3$	30
7	$11\ 21_2$	$11\ 35_2$	$12\ 03_3$	90
30	$09\ 26_3$	$09\ 32_3$	$10\ 54_3$	180
Apr. 3	$12\ 42_1$	$12\ 52_1$	$13\ 40_{10}$	90
3	$14\ 38_1$	$14\ 46_1$	$15\ 03_3$	50
8	$14\ 49_1$	$14\ 58_2$	$15\ 30_5$	100
11	$12\ 52_2$	$13\ 10_2$	$13\ 43_9$	70
11	$15\ 15_1$	$15\ 23_3$	$15\ 55_5$	50
11	$16\ 26_1$	$16\ 42_2$	$17\ 38_8$	40
12	$12\ 00_1$	$12\ 04_1$	$12\ 25_{10}$	35
12	$13\ 15_2$		$14\ 08_5$	>75
12	$14\ 03_1$	$14\ 05_1$	$14\ 20_3$	15
12	$16\ 48_1$	$16\ 52_2$		35

aid, when the maximum occurs. The time of finish is difficult to estimate, and is quite unsuitable for comparison with phase anomalies. It was only recorded for one flare in three. Fig. 6 shows all the phase anomalies between 1948 March 11 and August 31 which lasted less than 45 minutes, and were accompanied by reports of flares. Each is represented by a thin horizontal line proportional to its

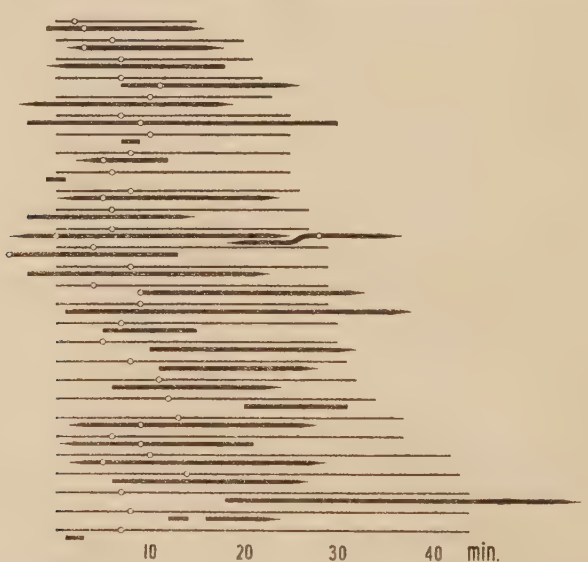

FIG. 6.—*Temporal association of phase anomalies and flares. The phase anomalies are represented by thin lines and arranged in order of duration. Flares are represented immediately below by thick lines, which are pointed if the beginning or end of the flare was observed. The times of maximum are shown by eyes.*

duration, and the lines are arranged in order of increasing length. The time of maximum is represented by a small circle. The accompanying flare is represented by a thick line just below. If the start or finish was seen, the line tapers to a point; otherwise it is left blunt. A small circle marks the maximum, when reported. This figure shows the various relationships which were counted above as coincidences. It can be seen that when the times of start and maximum of the flare are given, the agreement with the phase anomaly is often close. We have now, however, a means of making such comparisons with a much higher precision.

Detailed comparison.—If the width of the *Hα* line is measured throughout the course of a flare, it is found to vary in a characteristic way and to bear a close relation to the intensity of the flare. Thanks to the cooperation of Dr M. A. Ellison in Edinburgh, we have been able on one occasion to compare the course of a phase anomaly with the width of the *Hα* line measured simultaneously. The result is shown in Fig. 7. A zero level of 1·5 A. has been taken for quiescent

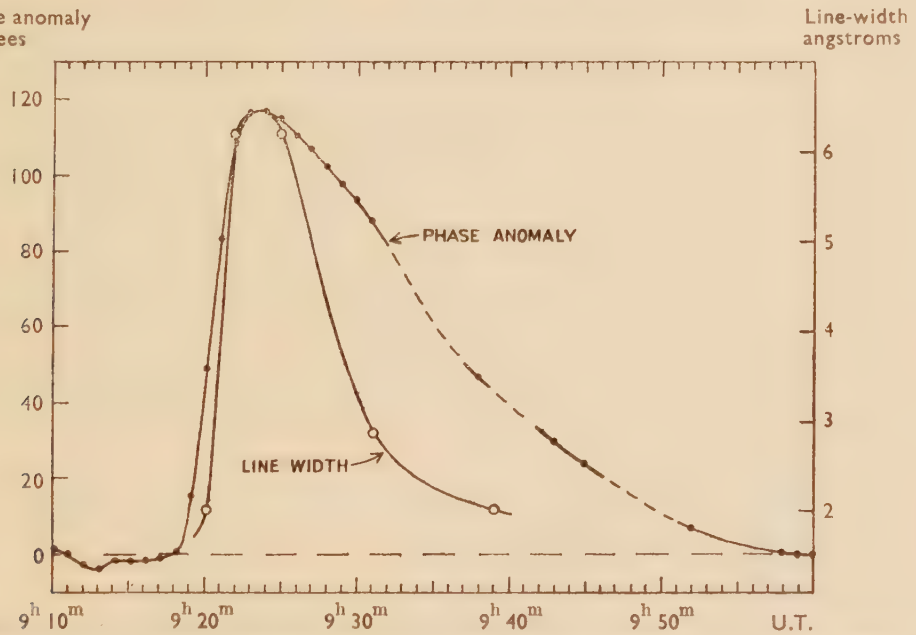

FIG. 7.—*A phase anomaly compared with the line-width of the Hα emitted from the associated flare* (1948 *June* 7).

bright hydrogen, and the ordinate scales have been adjusted to give equal maxima. There is good agreement in the times of start and maximum. The recoveries can be brought into agreement by selecting an empirical functional relation between phase and line-width. There are not sufficient observations to check this function by a redetermination between the start and maximum, and on the present data it is best to draw no conclusion. The beginning and end of the same flare were observed elsewhere as follows: Kanzelhöhe **09h 18m–09h 40m**, max. 09h 25m, 61° E. 14° S., Class 1 (kindly supplied by Professor d'Azambuja). Greenwich **09h 18m–09h 36m**, max. 09h 27m, 70° E. 13° S., Class 2. The Edinburgh report was **09h 20m–09h 39m**, max. 09h 22m, 68° E. 14° S., Class 2. The reports agree in placing the end of the flare within a few minutes of 09h 40m, but although the rate of decay had fallen to a low value by this time, there is nothing to show

that the enhanced flare emission ceased before the end of the phase anomaly. Thus one cannot conclude that the ionosphere continued disturbed after the visible flare had ended. Indeed the line-width measurements suggest that observers may judge a flare to have ended, not when it has recovered to its initial brightness, but when the rate of change of brightness has become so small that the brightness appears stationary to the eye.

Curves showing the behaviour of line-width during flares have been published by Waldmeier* and Ellison† and they show great similarity to the phase curves of Fig. 2. The observations are made by turning the line-shifter of the spectro-helioscope to each side until the flare is no brighter than its surroundings. A few such comparisons can soon tell as much about the simultaneity of flares and sudden ionospheric disturbances as years of statistics. As yet only one comparison has been made, and it is not known to what extent the features seen in it will be reproduced in future.

The rate at which the ionospheric disturbance would abate, if the disturbing radiation were suddenly removed, is not known and might delay the recovery of a phase anomaly. The occurrence of brief but intense anomalies such as that of Fig. 2 (*u*) shows that a rate of recovery of 10 degrees per minute is possible when the amount of the anomaly is as little as 50 degrees. If the flare and the anomaly contribute equally to this rate, the "time-constant" for the recovery of the ionosphere cannot exceed $2\frac{1}{2}$ minutes. This is small enough to allow the phase anomaly to follow the recovery of flares of ordinary strength and duration quite closely.

Attempts to follow the course of flares photometrically were made by Richardson‡, but the irregularity of the curves which his data yield reveal the difficulties of the technique. Barton § has recently succeeded at Greenwich in getting ten photometer measurements during the recovery of the brilliant flare of 1948 May 21. His curve is shown in Fig. 8. The reports of this flare are as follows :

Greenwich	**11h 20m–12h 05m**,	max. 11h 26m,	70° W. 13° S., Class 3+
Muswell Hill	11h 19m–12h 00m,		68° W. 10° S., Class 3
Edinburgh	11h 59m–**12h 15m**,		70° W. 12° S.

At 11h 20m a phase anomaly was noticed to be in progress and the measurements up to 12h 00m are shown in Fig. 8. The subsequent history of this anomaly can be seen at *t* in Fig. 2. The close agreement in the times of start leaves no doubt that the flare caused the anomaly, but there is striking disagreement in the recoveries. The reports show that the flare ceased to emit *Hα* by 12h 15m at the latest, whereas the phase anomaly continued for another two or three hours. There is a chance that further flares, which were not seen, complicated the phase anomaly. The humps shown in Fig. 2 *t* strongly suggest this, and one of them, at 15h 00m, was accompanied by a reported flare. But the simple behaviour of the anomaly from 11h 20m to 12h 00m argues a unique source, in which case the disturbing agency must have continued to impinge on the ionosphere after the flare visible in *Hα* had ceased.

* M. Waldmeier, *Z. für Astrophys.*, **20**, 46, 1940.
† M. A. Ellison, *M.N.*, **103**, 3, 1943.
‡ R. S. Richardson, *Ap. J.*, **90**, 368, 1939.
§ H. Barton, *The Observatory*, **68**, 191, 1948.

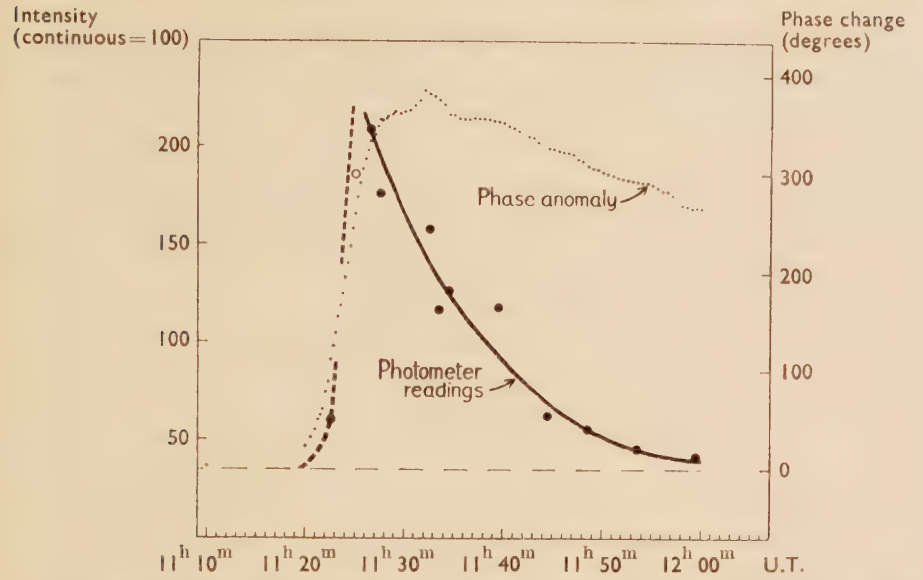

FIG. 8.—*A phase anomaly compared with photometric intensity measures of Hα emission from the associated flare* (1948 *May* 21).

Comparison of size with class.—For the majority of flares no measurements of line-width or area are available and it is thus interesting to compare the size of phase anomalies with the "importance" (Class 1, 2 or 3) of the flares which caused them. In Fig. 9, 43 phase anomalies are represented by vertical strips proportional

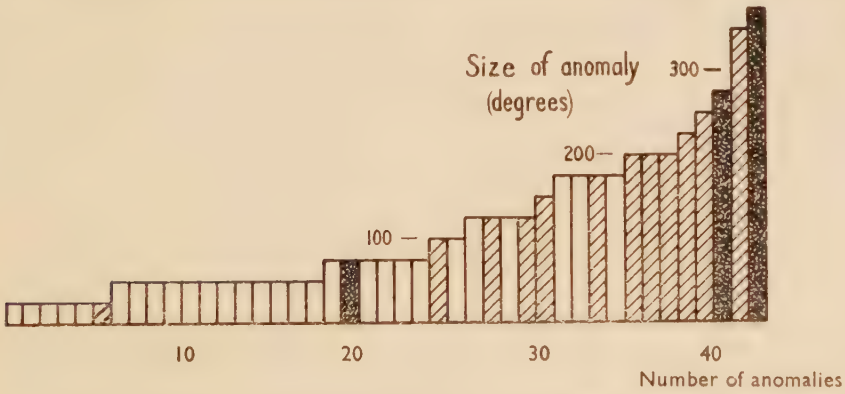

FIG. 9.—*The relation between the class of flares and the size of phase anomalies. The strip representing each anomaly is white for flares of Class* 1, *hatched for Class* 2 *and black for Class* 3.

in length to the size of each anomaly. The strip is white for flares of Class 1 (and 1+), hatched for Class 2 (and 2+) and black for Class 3. There is a distinct tendency for the grey and black strips to be grouped towards the tall end. No better marked division could be expected because of the uncertainty in the class of a flare when a number of observers compile the data. Recent issues of the *Quarterly Bulletin* show that, in cases where a flare was seen by more than one observer, the estimates of class differed as often as they agreed. Flares which are classed as 1 by one observer and 2 by another, are more numerous than those which are classed as 2 by two observers, and flares classed 3–2 and 3–1 are both more numerous than those classed 3–3.

It appears from the above that combined observations of phase anomalies and flares will be more profitable where special measurements of line-width, area and brightness are obtained at brief intervals on individual flares, than where extended series of coarser data are used. The next section deals with knowledge about flares which may be gained from phase anomalies independently of optical observations. Although it will be shown circumstantially that many of the following results are probably true for $H\alpha$ emission, the full story of the connection between $H\alpha$ and the radiation which disturbs the ionosphere awaits the appearance of more comparisons such as that shown in Fig. 7.

5. *Results obtained from Sudden Phase Anomalies.*—The course of a typical phase anomaly comprises a rapid onset and a slower recovery. The rise to maximum is not linear, and the rate of growth seems to decrease from the beginning, so that, as far as the maximum, the development curve is often not unlike a parabola with axis vertical. The recovery consists of a part which continues for a time to be convex; then there is an inflexion, after which the curve is quasi-exponential. The inflexion occurs at levels varying between 0·2 and 0·9 of the maximum. If the beginning is examined on an expanded time-scale, a small fillet preceding the rapid rise can generally be discerned, and there is therefore an inflexion during the onset. This inflexion rarely climbs above 0·2 of the maximum. The anomaly thus attains its maximum rate of growth when it is still quite small, but the time taken may be quite large, as the fillet can often be traced backwards for several minutes.

The size of phase anomalies varies from about 30 to over 500 degrees, for GBR observed at Cambridge, which corresponds to a change of effective height of reflection from 0·9 to 15 kilometres. Although, for a given change in effective height, the size in degrees depends on both the distance of the transmitter and its wave-length, and to a small extent on the time of day, degrees will be used in this paper, and it need only be remembered that the conversion to changes of effective height is at the rate of 3 kilometres to 100 degrees, save only in Tables II and III. Fig. 10 (*a*) shows the size distribution over the period 1948 March 11 to August 31.

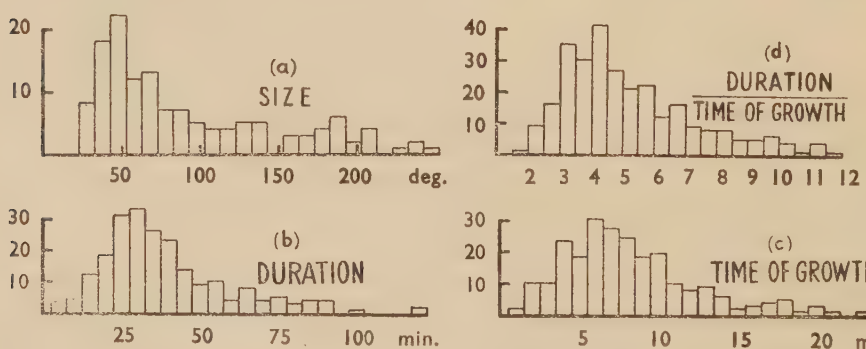

FIG. 10.—*Distribution of size, duration, time of growth, and duration/time of growth, for phase anomalies.*

It is very skew. The median is 70 degrees and the mode 45 degrees. One interpretation is that there is a minimum strength to which the ionosphere-disturbing radiation always grows. On the other hand it is probable, from the discussion of the overlap diagrams of Fig. 5, that there exist numerous small flares which do not produce recognizable phase anomalies. A better interpretation is,

therefore, that 20 to 40 degrees is the threshold of recognition for anomalies in present records of long-wave phase, and that smaller anomalies are present but not detected. It will be recalled that the threshold for fadeouts is from 150 to 200 degrees.

Fig. 10(*b*) shows the distribution of durations of phase anomalies. The duration is measured from the earliest sign of disturbance to the time when only 5 per cent of the maximum phase change remains. The mode is 30 minutes, the median 33 minutes, the quartiles are 26 and 48 minutes and the extreme range is from 5 to 250 minutes. This is quite different from the result given by Waldmeier for flares, viz. a mode of 10 and a median of 21 minutes. A sample of 130 flares, whose beginning and end were reported in the *Quarterly Bulletin*, is in accord with his result.

Fig. 10(*c*) gives the distribution of time of growth. The mode is 6 minutes, the median $7\frac{1}{2}$ minutes, the quartiles $5\frac{1}{2}$ and $10\frac{1}{2}$ and the extremes 2 and 70 minutes. Giovanelli found a mean of 7 and a median of 4 minutes from 24 flares, but a sample of 90 flares whose beginning and maximum are recorded in the *Quarterly Bulletin* has a mode and median of 6, quartiles $3\frac{1}{2}$ and $10\frac{1}{2}$ and extremes of 1 and 32 minutes. This agreement is good; the only difference lies in the higher number of flares with times of growth of one and two minutes.

Various authors have commented on the value to which the ratio of duration to time of growth of a flare tends. For example, Waldmeier (1940) says that the time of growth amounts to only about one-fifth of the duration and Giovanelli gives the average times of growth and *decay* as 4 and 17 minutes for Class 1, and 11 and 27 minutes for Class 2. The tendency is shown for 281 phase anomalies in Fig. 10(*d*). The mode is at 4 and the interquartile range is from $3\frac{1}{2}$ to $6\frac{1}{2}$. The ratio rarely falls below 2 but may be as high as 20, though in such a case it may be suspected that further flares are prolonging the anomaly.

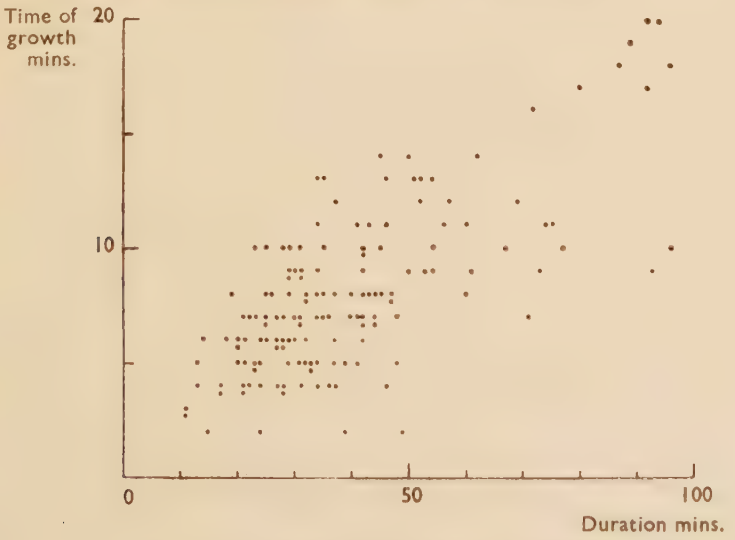

Fig. 11.—*Duration and time of growth of phase anomalies.*

Fig. 11 represents a synthesis of the foregoing remarks on the distribution of duration and time of growth and their ratio. There is no obvious tendency for the ratio to depend on duration. The trend suggested by Giovanelli's figures,

that the duration is less in proportion to the time of growth for stronger flares, is not seen here.

Returning to the disagreement in the distribution of durations of phase anomalies and flares, we may note that only those flares were selected whose beginning and end were seen. As flares of short duration are more likely to be followed until they end, the data are biassed towards short durations However, a study of the data not utilized shows that the disagreement cannot be accounted for wholly in this way. The flares which produce no phase anomalies are not numerous enough to account for the discrepancy. The remaining difference must be due to some systematic tendency for phase anomalies to continue after the reported end of the associated flares. This suggests a sustained arrival of the disturbing agency at the ionosphere after the $H\alpha$ has ceased, but might be due, as pointed out in connection with Fig. 7, to inability to judge by eye whether a small excess intensity still remains. It follows that the distribution of duration/time of growth will be different in the two cases, but the distribution for flares has not been given. A selection of 110 flares from the *Quarterly Bulletin* showed a mode at $2\frac{1}{2}:1$.

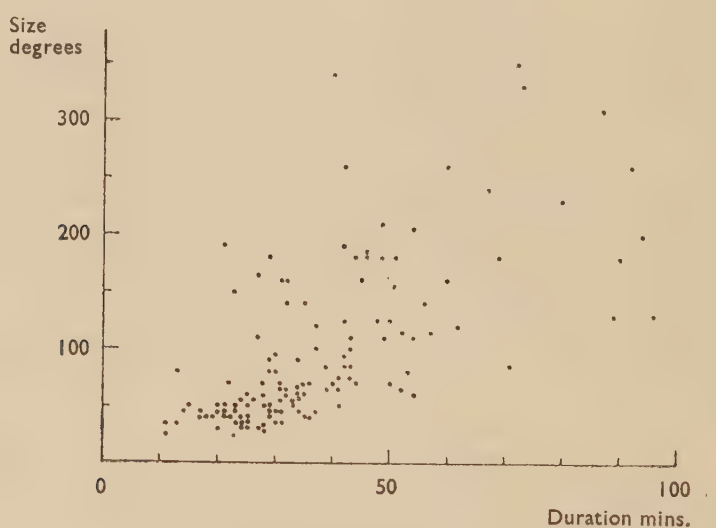

FIG. 12.—*Duration and size of phase anomalies.*

Fig. 12 is the scatter diagram for duration and size of phase anomalies. There is a clear tendency for the size of anomalies to increase with increasing duration. However, there can be brief anomalies which are large, and long-lived anomalies which are small. The tendency revealed betokens a much sharper relation intrinsic in the flares, for the data are subject to several known derangements. The size of a phase anomaly is subject to terrestrial influences and many of the long-lived anomalies are believed to be associated with more than one flare. The size of the phase anomaly produced by a given flare is believed to depend on the Sun's zenith distance. In the present paper no correction has been made for this, as the amount of the correction is not known. The data can, however, be improved by confining attention to the middle hours of the day. When international flare reports are available it will also be possible to eliminate many composite anomalies, to the further improvement of the data. It is expected that the dots will then tend to a more definite relation.

6. *Conclusion.*—Research on the propagation of very long waves has revealed anomalies whose study can add greatly to the knowledge of solar flares. Neither the agency which causes the anomalies, nor the reaction by which it is absorbed in the lowest part of the ionosphere, is known. Because of the agreement with flares in time of occurrence, one may tentatively picture it to be electromagnetic radiation originating in the visible flare.

Much remains to be done in establishing the extent to which the radiation which disturbs the ionosphere is linked with the emission of visible hydrogen light from the flare, but a method has been outlined for doing this. It may be possible, from a comparison of phase anomalies with curves showing the width of the $H\alpha$ line, to decide whether or not the radiation which disturbs the ionosphere comes from the hydrogen atoms which are seen glowing in the spectrohelioscope. If the Lyman α ultra-violet line at 1215 A. proves to be responsible, as has been suggested by Martyn, Munro, Higgs and Williams*, the close agreement already established between phase anomalies and $H\alpha$ emission will be strengthened in the future. If, on the other hand, discrepancies between phase anomalies and curves showing the width of the $H\alpha$ line are found which can eliminate the hydrogen atom as the sole source of the radiation, then the evidence for the existence of flares which disturb the ionosphere but emit no $H\alpha$, and strong $H\alpha$ flares which do not disturb the ionosphere, will gain added significance. In this event it should prove possible to identify the atom responsible by comparing the phase anomaly with series of flare spectra.

Many researches into solar and terrestrial phenomena, such, for example, as corpuscular streams from the Sun, magnetic crochets, magnetic storms, ionospheric storms, sudden ionospheric disturbances and solar radio noise, require the solar flare data compiled by the I.A.U. from international observations. Often the information required is simply whether or not a flare began or was in progress at a stated time. Now the enhanced emission of visible hydrogen light follows a similar course to the radiation which disturbs the ionosphere, and a record of a phase anomaly is practically equivalent to a report of a flare having been seen. Continuous automatic records of phase anomalies are being made, and a single apparatus is yielding lists of flares as long as the combined reports of many observatories. The data have two advantages for the researches mentioned, which are not possessed by flare data. The times of start and maximum, which are easily missed at the spectrohelioscope, are almost always recorded, and a consistent measure of intensity can be given which does not suffer from the variations introduced by numerous observers. A third attainable advantage, not realized at present, is continuity of observation. Table III gives a list of anomalies compiled from manual observations and simple automatic records of resultant amplitude. They were obtained during experiments involving GBZ Criggion, 15,200 cycles per second, a station 220 kilometres from Cambridge. The period falls near the time of maximum sunspot number in 1947 and embraces three appearances of a great active spot group. The subscript numerals indicate the precision, in minutes, with which times could be established from the records. These early records are subject further to occasional zero errors of one or two minutes.

It is a disadvantage of the present method that it involves a very-long-wave transmitter. There are only a small number of them in the world and it is necessary

* D. F. Martyn, G. H. Munro, A. J. Higgs and S. E. Williams, *Nature*, **140**, 603, 1937.

to observe within a few hundred kilometres in order to measure phase. Their primary function is communication, and they have frequent sporadic gaps, and daily breaks for maintenance, and from time to time have slack periods or close down completely. In recent months GBR Rugby has transmitted about two-thirds of the time. Even this fraction is greater than the world-wide cooperation with spectrohelioscope observations has been able to achieve, and if recording, similar to that at Cambridge, were commenced near two or three further transmitters, a virtually continuous watch on the Sun could be kept. How

TABLE III

Sudden Phase Anomalies observed at Cambridge

Subscript numerals indicate precision in minutes. Parentheses indicate the beginning or end of transmission. The finish is defined as the time of recovery to 5 per cent of the maximum disturbance. A phase change of 100 degrees would be produced by a change of effective height of reflection of 4·7 kilometres.

Date 1947	Start U.T.	Max. U.T.	Finish U.T.	Size degrees	Date 1947	Start U.T.	Max. U.T.	Finish U.T.	Size degrees
	h m	h m	h m			h m	h m	h m	
Feb. 7	10 01_4	10 22_4	11 08_7	100	Mar. 9	10 32_2	10 44_2	10 57_3	20
7	11 04_3	11 15_4	11 45_{10}	30	9	(12 00)		12 40_{10}	>50
7	12 00_3	12 14_4	12 30_{10}	60	9	15 03_2	15 08_2	15 30_5	50
8	09 46_3	10 08_3	11 05_{10}	190	11	12 13_1	12 17_1	13 25_{10}	90
8	10 59_1	11 08_2			11	12 38_1			
8	11 16_1	11 20_1			11	13 33_{18}		14 12_3	>20
8	11 25_1	11 27_2			12	13 40_5	13 57_3	15 06_{10}	180
8	12 00_3	12 10_2	13 00_6	140	13	10 24_1	10 48_2	(11 45)	160
8	14 04_1	14 18_2	15 03_3	160	13	11 21_3	11 34_2	12 12_4	50
10	12 57_3	13 21_3	14 00_{15}	90	13	12 36_4	13 46_2	16 45_5	150
13	14 00_1	14 12_2	14 30_3	30	14	13 15_2	13 54_4	15 20_7	100
13	14 50_1	14 54_1	15 12_3	10	16	07 21_2	07 30_2	07 53_3	20
14	13 51_1	13 58_2	14 20_4		16	13 34_2	13 40_3	15 00_{10}	40
15	10 19_1	10 24_2	10 45_3		16	15 16_2	15 23_3	16 06_3	60
15	13 14_1	13 20_2	13 32_5	40	17	08 03_2	08 15_2	08 38_2	120
16	11 32_1	11 49_2	12 52_5	110	17	13 00_2	13 06_2	13 54_{18}	40
16	14 49_1	14 56_1	15 12_2	140	17	14 53_1	15 02_1	15 16_2	25
16	16 12_1	16 18_1	16 38_5	50	18	14 32_1	14 50_2	15 36_3	60
17	11 31_1	11 51_2	12 30_4	90	21	11 03_1	11 12_2	11 42_3	30
17	12 42_1	12 48_2	13 06_3	30	21	13 47_2	13 53_2	14 06_2	60
18	12 25_1	12 42_2	13 00_3	110	29	12 11_1	12 22_1	13 55_5	
20	14 30				30	09 26_3	09 32_3	10 54_3	180
20	14 45				30	10 56_1	10 59_1	11 20_2	15
20	15 06				30	11 31_2	11 48_2		40
22	12 16_1	12 20_1	12 51_2	70	30	12 04_1	12 14_2	(13 00)	45
23	12 33_5	12 43_5		70	30	12 52_1	13 00_2	13 48_2	60
26	(11 54)		12 30_5	>60	30	14 06_1	14 08_1	14 34_2	60
27	12 10_1	12 15_1	12 35_3	20	30	14 55_1	14 57_1	15 02_1	15
27	14 45_1	14 50_2	15 12_5	70	31	12 54_1	12 58_2	13 04_2	15
28	12 20_1	12 38_2	13 34_4	135	31	17 07_1	17 10_1	17 32_{10}	50
28	14 03_1	14 09_1	14 28_3	90	Apr. 1	07 05_1	07 15_3	07 25_1	25
Mar. 2	10 32_1	10 42_2	12 30_{10}	180	1	09 45_1	09 48_1	09 59_2	70
5	07 29_3	07 42_4	08 39_3	70	2	12 09_1	12 14_2	12 42_2	40
5	09 30_5	09 45_5	11 45_{15}	130	2	14 30_1	14 38_2	15 04_1	45
5	15 30_1	15 45_5	16 48_8	60	2	16 30_1	16 36_1	17 00_{10}	25
6	13 46_1	13 48_1	14 09_3	50	3	06 50_2	06 56_2	07 25_{10}	210
7	11 21_2	11 35_2	12 03_3	90	3	12 42_1	12 52_1	13 40_{10}	90
7	15 07_1	15 11_2	15 39_3	40	3	14 09_1	14 14_1	14 27_2	45
8	12 50_1	12 53_1	13 30_5	80	3	14 38_1	14 46_1	15 03_3	50

TABLE III.—*continued.*

Date 1947	Start U.T.	Max. U.T.	Finish U.T.	Size degrees	Date 1947	Start U.T.	Max. U.T.	Finish U.T.	Size degrees
	h m	h m	h m			h m	h m	h m	
Apr. 3	(15 48)	$15\ 52_1$	$15\ 58_1$		Apr. 10	$10\ 26_1$	$10\ 34_2$	$11\ 10_{10}$	105
4	$12\ 20_1$	$12\ 31_3$	$14\ 00_{10}$	110	10	$11\ 20_{20}$	$11\ 42_3$		70
4	$15\ 05_1$	$15\ 10_1$	$15\ 25_2$	90	10	$11\ 51_2$	$12\ 14_2$	$13\ 30_{10}$	65
4	$15\ 44_1$	$15\ 49_1$	$16\ 01_1$	110	10	$13\ 50_2$	$14\ 05_1$		40
5	(09 36)	.	$10\ 45_5$		10	$14\ 28_1$	$14\ 38_2$	$15\ 30_{10}$	60
5	$11\ 05_5$	$11\ 12_3$		70	10	$14\ 41_1$	$14\ 44_1$		10
5	$11\ 45_5$				11	$12\ 52_2$	$13\ 10_2$	$13\ 43_9$	70
5	$12\ 29_1$	$12\ 32_1$	$13\ 00_{10}$	35	11	$15\ 15_1$	$15\ 23_3$	$15\ 55_5$	50
5	$13\ 32_1$	$13\ 35_1$	$14\ 10_5$	60	11	$16\ 26_1$	$16\ 42_2$	$17\ 38_8$	40
5	$14\ 14_1$	$14\ 16_1$	$14\ 30_2$	35	12	$10\ 39_1$			>50
5	$14\ 30_1$	$14\ 37_5$	$15\ 30_{10}$	130	12	(11 48)		$12\ 01_5$	>30
6	$11\ 52_2$		$15\ 15_{15}$	80	12	$12\ 00_1$	$12\ 04_1$	$12\ 25_{10}$	35
6	$14\ 09_1$	$14\ 15_2$	$14\ 24_3$	15	12	$12\ 34_1$	$12\ 40_2$	$13\ 15_5$	35
6	$14\ 32_1$	$14\ 34_1$	$14\ 38_3$	15	12	$13\ 15_2$		(14 03)	>75
6	$15\ 50_2$	$15\ 53_1$	$16\ 22_2$	40	12	$14\ 03_1$	$14\ 05_1$	$14\ 20_3$	15
7	$12\ 04_1$	$12\ 15_3$	$12\ 52_3$	40	12	$14\ 19_1$	$14\ 20_1$	$14\ 30_5$	5
7	$14\ 08_1$	$14\ 16_1$		50	12	$14\ 35_1$	$14\ 36_1$	$14\ 40_1$	5
7	$14\ 29_1$	$14\ 36_2$	$15\ 20_{10}$	60	12	$16\ 48_1$	$16\ 52_2$		35
8	$08\ 12_1$	$08\ 18_2$		40	13		$11\ 50_{10}$	$12\ 15_5$	
8	$14\ 49_1$	$14\ 58_2$	$15\ 30_5$	100	13	$12\ 36_1$	$12\ 44_1$	$13\ 48_5$	105
9	$12\ 15_1$	$12\ 17_1$	$12\ 31_1$	15	13	$14\ 24_1$	$14\ 27_1$	(15 04)	90
9	$13\ 20_1$	$13\ 32_2$	$13\ 57_2$	40	13	$14\ 47_1$	$14\ 55_1$	$15\ 45_{10}$	80

valuable it would be, as the present solar cycle falls to a minimum, to record the complete history of the flare occurrences associated with a single spot as it moved alone across the disk of the Sun.

7. *Acknowledgments.*—This work was carried out in the Radio Group of the Cavendish Laboratory under the direction of Mr J. A. Ratcliffe, whom the authors wish to thank for advice and assistance. Cordial thanks for their essential cooperation are due to the British solar observers, particularly Dr M. A. Ellison and Mr H. W. Newton; to Dr R. Bureau for copies of atmospheric records; and to Professors L. d'Azambuja and M. Waldmeier for discussions with one of the authors.

The work was assisted by a grant from the Department of Scientific and Industrial Research. On some occasions use was made of a special frequency-dividing circuit designed and constructed by Mr H. B. Law of the General Post Office research station, Dollis Hill, to whom our best thanks are due. On several occasions special transmissions were made from the Rugby transmitter GBR, through the helpful cooperation of the General Post Office (Radio Engineers' Branch). Our very best thanks are due to the Chief Engineer and all those who assisted with these arrangements.

A New Zealand Government Scholarship is held by T. W. Straker. Part of the work was carried out during the tenure of a Studentship of the Australian Council for Scientific and Industrial Research by R. N. Bracewell, who is at present seconded to the Cavendish Laboratory from the staff of the Council's Radiophysics Laboratory, Sydney.

Cavendish Laboratory,
Cambridge:
1949 *January* 20.

VARIABLE GUILLOTINE FACTOR MODELS FOR LATE TYPE MAIN SEQUENCE STARS

Ralph E. Williamson and G. F. D. Duff

(Communicated by C. A. Chant)

(Received 1948 September 8)

Summary

Five integrations of point source models for late type main sequence stars are presented, the guillotine factor varying with different powers of the density. Radiation pressure has been neglected. A method of applying the models for given luminosity, mass and radius is suggested. Certain transformations of the equations into a form convenient for numerical work are included.

---

1. *Introduction.*—With the increasing certainty of our knowledge of the chemical composition of the Sun *, it becomes of interest to have some means of estimating the hydrogen and helium contents of the late type main sequence stars, as a further step in understanding the evolutionary processes of stars. Up to the present, however, integrations adequate to explore the internal conditions of these stars have not been available ; it is the purpose of this paper to contribute a set of models toward this end.

Recent work of Schwarzschild *, Keller †, and Mrs Harrison ‡ has shown the great importance of allowing for the variation of the guillotine factor throughout the star. Any adequate discussion of the internal constitution of a star or of a class of stars can be carried out only on the basis of models which suitably represent the run of the guillotine factor as given by some definite physical theory of the opacity as a function of the density and temperature, such as that given by Strömgren § or Morse ||, or more recently by Chandrasekhar¶.

A satisfactory means of taking account of the variation of guillotine factor throughout a star has been used by Schwarzschild in a model for the Sun; it consists in representing the guillotine factor as proportional to a suitable power of the density. A preliminary application of his model to typical late type main sequence stars shows that to a fair approximation Morse's opacities can in fact be represented by assuming the guillotine factor to vary as some power of the density; the indication is that the exponent should be somewhat greater than the value of 0·25 used by Schwarzschild. Such a representation of the guillotine factor allows the use of homology-invariant models, so that one model is applicable to stars of arbitrary mass (M), luminosity (L), radius (R) and chemical composition (X, Y, μ).

* M. Schwarzschild, *Ap. J.*, **104**, 203, 1946.
† G. Keller, in press.
‡ M. H. Harrison, in press.
§ B. Strömgren, *Zs. f. Ap.*, **4**, 118, 1932.
|| P. M. Morse, *Ap. J.*, **92**, 27, 1940.
¶ S. Chandrasekhar, in press.

In view of the twofold uncertainty of the physical theory of the opacity on the one hand, and of the exact values of the stellar parameters L, M and R on the other, this simplification is much to be preferred to point-to-point integrations, which must be particularized for any given star and chemical composition.

2. *The Equations of Equilibrium for the Model.*—For a first investigation of the late type dwarfs, there seems little doubt of the suitability of a point-source model with radiative envelope and convective core. The following additional assumptions are embodied in the present models:

(1) The chemical composition and also the mean molecular weight are constant throughout the configuration.

(2) The perfect gas law is valid throughout.

(3) The effect of radiation pressure may be neglected in the hydrostatic equation, in comparison with the gas pressure.

(4) The opacity κ can be adequately represented by a generalization of Kramers' law, with the guillotine factor * τ proportional to a power of the density ρ:

$$\kappa = \frac{\kappa_0}{\tau}\rho T^{-3.5}, \qquad \text{where } T \text{ is absolute temperature,} \tag{1}$$

$$\tau = \tau_0 \rho^{\alpha}, \qquad \text{where } \tau_0 \text{ is a constant.} \tag{2}$$

It is understood that the constants κ_0 and τ_0 may be functions of the chemical composition, and further, that τ_0 may be different for stars of different L, M, and R.

In a standard notation †, the equations of equilibrium for the radiative envelope embodying the above assumptions may be written:

$$\frac{dP}{dr} = \frac{k}{\mu H}\frac{d}{dr}(\rho T) = -\frac{GM(r)}{r^2}\rho, \tag{3}$$

$$\frac{dM(r)}{dr} = +4\pi r^2 \rho, \tag{4}$$

$$\frac{dT}{dr} = \frac{-3\kappa L\rho}{16\pi a c r^2 T^3}, \tag{5}$$

where k is Boltzmann's Constant, H is the proton mass, μ the mean molecular weight, G the Constant of Gravitation, a Stefan's Constant, and $M(r)$ the mass interior to the point r. The quantity κ is as defined in equations (1) and (2). The core is defined by the Lane-Emden function ‡ of index $n = \frac{3}{2}$, and the fitting is to be accomplished in the usual way §: at the point where the effective polytropic index of any solution of the envelope equations (3), (4) and (5) drops to $\frac{3}{2}$, the dimensionless fitting-variables u and v are computed. That solution is selected whose end-point lies on the u–v curve for the Lane-Emden core function.

Schwarzschild's transformations ‖,

$$P = p\frac{GM^2}{4\pi R^4}, \qquad T = t\frac{\mu H}{k}\frac{GM}{R}, \qquad M(r) = qM, \qquad r = xR \tag{6}$$

---

* We shall use the term guillotine factor to include all deviations from Kramers' law, whether actually due to guillotine factor corrections, Gaunt factors, or others.

† S. Chandrasekhar, *An Introduction to the Study of Stellar Structure*, Chapter VI.

‡ N. Fairclough, *M.N.*, **92**, 644, 1932.

§ Chandrasekhar, *op. cit.*, p. 351 ff.

‖ Schwarzschild, *loc. cit.*

force the envelope equations into a dimensionless form:

$$\left.\begin{aligned}\frac{dp}{dx} &= -\frac{p}{t}\frac{q}{x^2},\\ \frac{dq}{dx} &= \frac{px^2}{t},\\ \frac{dt}{dx} &= -C\frac{p^{2-\alpha}}{x^2 t^{8\cdot5-\alpha}},\end{aligned}\right\} \tag{7}$$

where

$$C\equiv C(\alpha)=\frac{3}{4(4\pi)^{3-\alpha}ac}\left(\frac{k}{GH}\right)^{7\cdot5}\frac{\kappa_0}{\tau_0\mu^{7\cdot5}}\frac{1}{}\frac{LR^{0\cdot5+3\alpha}}{M^{5\cdot5+\alpha}}, \tag{8}$$

or, numerically,

$$\log C=-28\cdot5283+0\cdot3276\alpha+\log\frac{\kappa_0}{\tau_0\mu^{7\cdot5}}+\log\frac{\dfrac{L}{L_\odot}\left(\dfrac{R}{R_\odot}\right)^{0\cdot5+3\alpha}}{\left(\dfrac{M}{M_\odot}\right)^{5\cdot5+\alpha}}. \tag{8a}*$$

The mathematical problem consists of obtaining by trial and error that value for C which insures the fitting at the boundary of the convective region; the integration, starting at the exterior, is subject to the initial conditions

$$p=t=0, \qquad q=1 \quad \text{when } x=1. \tag{9}$$

3. *Forms of the Envelope Equations for Integration.*—The form of the equations (7) is inconvenient for numerical work, owing partly to the high power to which the variable t is raised. This difficulty may be obviated by the following substitutions:

$$\left.\begin{aligned}\eta &= -\log_{10}x,\\ y &= +\log p,\\ w &= -\log q,\\ l &= \log\frac{\nu}{\nu_\alpha(0)}-\log q,\end{aligned}\right\} \tag{10}$$

where $$\nu=n_{eff}+1=\frac{d\log p}{d\log t}; \qquad \nu_\alpha(0)=\frac{8\cdot5-\alpha}{2-\alpha}.$$

The quantity l is thus intimately related to the local polytropic index, n_{eff}. In terms of the new variables, the envelope equations become:

$$\left.\begin{aligned}\log_{10}\left(\frac{dy}{d\eta}\right) &= -w+\eta-\left(\frac{2-\alpha}{8\cdot5-\alpha}\right)y-\left(\frac{1}{8\cdot5-\alpha}\right)l-\left(\frac{1}{8\cdot5-\alpha}\right)\log C\nu_\alpha(0),\\ \log_{10}\left(\frac{dw}{d\eta}\right) &= \left(\frac{6\cdot5}{8\cdot5-\alpha}\right)y-\left(\frac{1}{8\cdot5-\alpha}\right)l-3\eta+w-\left(\frac{1}{8\cdot5-\alpha}\right)\log C\nu_\alpha(0),\\ \frac{dl}{d\eta} &= (2-\alpha)(10^{w-l}-1)\frac{dy}{d\eta},\end{aligned}\right\} \tag{11}$$

subject to the initial conditions

$$w=l=0, \qquad y=-\infty \quad \text{when } \eta=0. \tag{12}$$

* It should be carefully noted that since τ_0 cannot be regarded as a universal constant, this equation cannot be taken as a pure *L-M-R* relationship.

Some difficulty is experienced near the outer surface of the model from the singularity of y at that point. A transformation of independent variable which removes this difficulty was found convenient. Let

$$\pi = A + \nu_\alpha(0) \log\left(\frac{1}{x} - 1\right) = A + \nu_\alpha(0) \log_{10}(10^\eta - 1), \tag{13}$$

where

$$A = \frac{-\log C}{2-\alpha} + \left(\frac{9{\cdot}5-\alpha}{2-\alpha}\right) \log\left(\frac{2-\alpha}{8{\cdot}5-\alpha}\right). \tag{14}$$

Then the equations of the envelope become:

$$\left.\begin{aligned} \log_{10}\left(\frac{dy}{d\pi}\right) &= -\left(\frac{2-\alpha}{8{\cdot}5-\alpha}\right) y - w - \left(\frac{1}{8{\cdot}5-\alpha}\right) l + \left(\frac{2-\alpha}{8{\cdot}5-\alpha}\right) \pi, \\ \log_{10}\left(\frac{dw}{d\pi}\right) &= \left(\frac{6{\cdot}5}{8{\cdot}5-\alpha}\right) y + w - \left(\frac{1}{8{\cdot}5-\alpha}\right) l + \left(\frac{2-\alpha}{8{\cdot}5-\alpha}\right) \pi - 4\eta, \\ \frac{dl}{d\pi} &= (2-\alpha)(10^{w-l} - 1)\, \frac{dy}{d\pi}, \\ \eta &= \log_{10}(1 + 10^{(\pi - A)/\nu_\alpha(0)}). \end{aligned}\right\} \tag{15}$$

The initial conditions are now

$$w = l = 0 \qquad y \sim \pi \qquad \text{as} \quad \pi \to -\infty. \tag{16}$$

4. *Integration of the Envelope Equations.*—A set of values for α which appears to cover the necessary range is $\alpha = 0{\cdot}375$, $0{\cdot}50$, $0{\cdot}55$, $0{\cdot}60$ and $0{\cdot}625$. For any given value of α, the procedure for integrating the envelope equations is to estimate a value for the eigenvalue C, and to calculate the values for the combinations of α and C which appear in the equations.

Values of η can then be tabulated over the relevant interval which is approximately $-4 \leqslant \pi \leqslant +6$. For values near the boundary, accurate values of

$$\frac{dw}{d\eta} = \frac{dw}{d\pi}\frac{d\pi}{d\eta}$$

may be calculated from equations (13) and (15), and thus a place may be selected to begin integration, where w is one or two units in the last place to be retained.

The integrations were performed by the central-difference method, and were carried to at least four figures. All work was done with either an electric Marchant or a hand-type Monroe calculator. Steps of $0{\cdot}2$ in π were found convenient and accurate, making approximately 50 steps per integration. An average of four integrations for each value of α was required to isolate the appropriate eigenvalue and solution.

Some difficulty with equation (15) was experienced in starting, but it is not difficult to transform it for points near the boundary, so that

$$l = 2{\cdot}303(2-\alpha)10^{-(2-\alpha)\pi} \int_{-\infty}^{\pi} 10^{(2-\alpha)u} w(u)\, du.$$

As the main contribution to the integrand comes from values of u just below π, we have, very approximately,

$$l = \text{const.} \times w \qquad \pi \ll 0.$$

The accuracy of the integration is such that errors of one in the third decimal can hardly occur; this conclusion was reached by making integrations with

$\alpha=0$ and $\alpha=0{\cdot}25$, and comparing them with Cowling's * and Schwarzschild's published integrations. Comparison of five-figure integrations (when available) with four-figure ones also confirmed this accuracy.

The fit with the convective core was considered adequate when the maximum distance from end-point of envelope to core locus was 0·003 or less in the u–v plane.

5. *Results of the Integrations.*—Parameters of direct physical significance for the models are the eigenvalue (which gives, for any physical theory of opacity, such as Morse's tables, a relationship between the hydrogen and the helium content of a star), the mass and radius of the core, the central density ρ_c and temperature T_c of the model. The latter two quantities are related to certain results of the integration in the following way: if we write

$$\rho_c = Q\frac{M}{M_\odot}\left(\frac{R_\odot}{R}\right)^3, \qquad T_c = \Theta\mu\frac{M}{M_\odot}\frac{R_\odot}{R}, \tag{17}$$

then the quantities Q and Θ are related to boundary-values of the envelope variables p_f/t_f and the core-variables θ_f and ξ_f by

$$Q = \frac{p_f}{4\pi t_f \theta_f^{1\cdot5}}\frac{M_\odot}{R_\odot{}^3}; \qquad \Theta = \frac{t_f}{\theta_f}\frac{GH}{k}\frac{M_\odot}{R_\odot}, \tag{18}$$

or in the terms of the integration variables:

$$\left.\begin{aligned} \log Q &= -0{\cdot}3275 - \frac{1}{8{\cdot}5-\alpha}[l_f - 6{\cdot}5y_f + \log C\nu_\alpha(0)] - 1{\cdot}5\log\theta_f, \\ \log\Theta &= 7{\cdot}3635 + \frac{1}{8{\cdot}5-\alpha}[l_f + (2-\alpha)y_f + \log C\nu_\alpha(0)] - \log\theta_f. \end{aligned}\right\} \tag{19}$$

TABLE I

α	0·375	0·500	0·550	0·600	0·625
$-\log C$	5·189	4·744	4·510	4·229	4·066
η_f	1·0144	1·1485	1·2196	1·3046	1·3537
x_f	0·0967	0·07104	0·0603	0·0496	0·0443
l_f	0·6749	0·6980	0·7083	0·7184	0·7235
y_f	2·5271	2·9923	3·2442	3·5516	3·7317
w_f	0·9759	1·0271	1·0494	1·0720	1·0830
q_f	0·1057	0·09395	0·0892	0·0847	0·0826
u_f	2·6547	2·678	2·6822	2·6898	2·6939
v_f	0·4024	0·3779	0·3679	0·3586	0·3543
θ_f	0·8198	0·8297	0·8337	0·8374	0·8384
ξ_f	1·0858	1·0528	1·0394	1·0266	1·0205
$8{\cdot}5-\alpha$	8·125	8·0	7·95	7·90	7·875
$2-\alpha$	1·625	1·5	1·45	1·40	1·375
$\log\nu_\alpha(0)$	0·69897	0·72700	0·7390	0·7515	0·7579
$\log t_f$	0·0359	0·14618	0·2065	0·2801	0·3234
$\log\theta_f$	−0·0863	−0·0811	−0·0790	−0·0771	−0·0766
$\log Q$	2·2932	2·6404	2·8288	3·0598	3·1958
$\log\Theta$	7·4860	7·5911	7·6493	7·7210	7·7638
Cowling Model		$\alpha=0{\cdot}0$	$\log Q=1{\cdot}7177$		$\log\Theta=7{\cdot}3177$
Schwarzschild Model		$\alpha=0{\cdot}25$	$\log Q=2{\cdot}0477$		$\log\Theta=7{\cdot}4131$

* T. G. Cowling, *M.N.*, **96**, 42, 1935.

In Table I are summarized the results of the integrations for the different values of α. Certain relevant quantities reduced from Cowling's and Schwarzschild's integrations have been entered in Table I for comparison. It is to be noted that the quantities x_f and q_f are the fraction of the star's radius and mass, respectively, occupied by the convective core.

It is easy to establish the relationship between ρ/ρ_c and T/T_c and the integration variables:

$$\log \frac{T}{T_c} = \log t + \log \frac{\theta_f}{t_f},$$

$$\log \frac{\rho}{\rho_c} = \log p - \log t + \log t_f \frac{\theta_f^{1.5}}{p_f},$$

$$\log p = y,$$

$$\log t = \frac{1}{8{\cdot}5-\alpha}[l + (2-\alpha)y + \log C\nu_\alpha(0)].$$

6. *Application of the Models to any given Star and Opacity Theory.*—Suppose it is desired to investigate the internal conditions of a star of given L, M and R, on the basis of a definite assumption about the chemical composition and the theory of opacity. It is obvious that the application of equations (17) to the results summarized in Table I allows the determination of T_c/μ and ρ_c for each model, once L, M and R are known. From this, the run of T and ρ throughout the star for any given value of μ may be computed for each model from Tables II–VI.

TABLE II

$\alpha = 0{\cdot}375 \qquad -\log C = 5{\cdot}189$

π	y	w	l	$\log \frac{\rho}{\rho_c} + 10$	$\log \frac{T}{T_c} + 10$	η
−4·0	−4·00000	0·00002	0·00001	4·732	8·525	0·0871
−3·0	−3·00015	0·00016	0·00011	5·532	8·725	·1309
−2·0	−2·00109	0·00098	0·00066	6·331	8·925	·1925
−1·0	−1·00611	0·00509	0·00356	7·127	9·124	·2750
0·0	−0·02864	0·02196	0·01590	7·907	9·321	·3803
0·6	0·53456	0·04794	0·03520	8·355	9·436	·4543
1·2	1·06116	0·09723	0·07201	8·772	9·546	·5358
1·8	1·52865	0·18221	0·13543	9·138	9·648	·6242
2·4	1·91486	0·31489	0·23267	9·435	9·737	·7185
3·0	2·20748	0·50141	0·36474	9·653	9·812	·8180
3·6	2·41043	0·73849	0·52427	9·796	9·872	0·9217
4·2	2·54128	1·01494	0·69880	9·879	9·919	1·0290
π_f						
4·1192	2·52712	0·97591	0·67487	9·871	9·914	1·0144
				$\log Q$	$\log \Theta$	
				2·2932	7·4860	

$$\log \frac{\rho}{\rho_c} = 0{\cdot}80000\,y \quad -0{\cdot}12308\,l \quad -2{\cdot}06807$$

$$\log \frac{T}{T_c} = 0{\cdot}20000\,y \quad +0{\cdot}12308\,l \quad -0{\cdot}67478$$

TABLE III

$\alpha=0.500$ $-\log C=4.744$

π	y	w	l	$\log\frac{\rho}{\rho_c}+10$	$\log\frac{T}{T_c}+10$	η
−4·0	−4·0000	0·0000	0·0000	4·284	8·521	0·1134
−3·0	−3·0001	0·0001	0·0001	5·097	8·708	·1642
−2·0	−2·0009	0·0007	0·0005	5·909	8·895	·2324
−1·0	−1·0046	0·0036	0·0025	6·718	9·082	·3201
0·0	−0·0194	0·0144	0·0103	7·517	9·268	·4278
0·6	0·5561	0·0312	0·0226	7·983	9·378	·5017
1·2	1·1067	0·0634	0·0464	8·428	9·484	·5818
1·8	1·6147	0·1208	0·0890	8·835	9·584	·6675
2·4	2·0588	0·2147	0·1581	9·187	9·676	·7581
3·0	2·4201	0·3547	0·2589	9·468	9·757	·8530
3·6	2·6908	0·5444	0·3905	9·672	9·824	0·9514
4·2	2·8781	0·7791	0·5447	9·805	9·878	1·0526
4·8	2·9995	1·0480	0·7105	9·883	9·922	1·1562
π_f						
4·7554	2·9923	1·0271	0·6980	9·878	9·919	1·1485
				$\log Q$	$\log\Theta$	
				2·6404	7·5911	

$$\log\frac{\rho}{\rho_c}=0.8125\,y \quad -0.1250\,l \quad -2.4656$$

$$\log\frac{T}{T_c}=0.1875\,y \quad +0.1250\,l \quad -0.7294$$

TABLE IV

$\alpha=0.550$ $-\log C=4.510$

π	y	w	l	$\log\frac{\rho}{\rho_c}+10$	$\log\frac{T}{T_c}+10$	η
−4·0	−4·00000	0·00002	0·00000	4·047	8·510	0·1280
−3·0	−3·00010	·00011	·00005	4·865	8·693	·1824
−2·0	−2·00069	·00057	·00037	5·682	8·875	·2358
−1·0	−1·00347	·00280	·00191	6·497	9·057	·3441
0·0	−0·01560	·01151	·00814	7·304	9·238	·4532
0·6	0·56464	·02482	·01783	7·777	9·345	·5272
1·2	1·12474	·05045	·03674	8·233	9·450	·6069
1·8	1·64980	·09657	·07090	8·658	9·550	·6917
2·4	2·12018	·17362	·12771	9·035	9·643	·7810
3·0	2·51578	·29195	·21347	9·348	9·726	·8741
3·6	2·82379	·45774	·32991	9·585	9·796	0·9704
4·2	3·04517	·66973	·47209	9·748	9·855	1·0694
4·8	3·19348	0·91964	·63012	9·849	9·902	1·1705
5·4	3·28793	1·19535	0·79345	9·906	9·939	1·2734
π_f						
5·0892	3·2442	1·0494	0·7083	9·881	9·921	1·2196
				$\log Q$	$\log\Theta$	
				2·8288	7·6493	

$$\log\frac{\rho}{\rho_c}=0.81761\,y \quad -0.12579\,l \quad -2.6824$$

$$\log\frac{T}{T_c}=0.18239\,y \quad +0.12579\,l \quad -0.7600$$

TABLE V

$a=0.600$ $-\log C=4.229$

π	y	w	l	$\log\frac{\rho}{\rho_c}+10$	$\log\frac{T}{T_c}+10$	η
−4·0	−4·00001	0·00001	0·00001	3·762	8·494	0·1462
−3·0	−3·00009	·00009	·00006	4·585	8·671	·2047
−2·0	−2·00055	·00047	·00031	5·407	8·848	·2800
−1·0	−1·00280	·00219	·00150	6·228	9·025	·3732
0·0	−0·01217	·00878	·00617	7·042	9·201	·4840
0·6	0·57273	·01881	·01344	7·523	9·306	·5582
1·2	1·14216	·03816	·02765	7·989	9·408	·6376
1·8	1·68415	·07339	·05367	8·432	9·508	·7217
2·4	2·18173	·13349	·09801	8·836	9·602	·8097
3·0	2·61502	·22871	·16745	9·184	9·687	·9012
3·6	2·96726	·36735	·26612	9·461	9·762	0·9955
4·2	3·23228	·55206	·39262	9·663	9·825	1·0922
4·8	3·41733	0·77818	·53965	9·797	9·876	1·1908
5·4	3·53902	1·03577	0·69708	9·877	9·918	1·2911
π_f						
5·4803	3·55157	1·07196	0·71840	9·884	9·923	1·3046
				$\log Q$	$\log\Theta$	
				3·0598	7·7210	

$$\log\frac{\rho}{\rho_c}=0.82278\,y \quad -0.12658\,l \quad -2.9469$$

$$\log\frac{T}{T_c}=0.177215\,y \quad +0.12658\,l \quad -0.7974$$

TABLE VI

$a=0.625$ $-\log C=4.066$

π	y	w	l	$\log\frac{\rho}{\rho_c}+10$	$\log\frac{T}{T_c}+10$	η
−4·0	−4·0000	0·0000	0·0000	3·595	8·482	0·1571
−3·0	−3·0000	·0001	·0000	4·421	8·656	·2179
−2·0	−2·0005	·0004	·0003	5·246	8·831	·2954
−1·0	−1·0025	·0019	·0013	6·069	9·005	·3903
0·0	−0·0105	·0075	·0054	6·887	9·179	·5020
0·6	0·5764	·0161	·0115	7·371	9·282	·5764
1·2	1·1502	·0325	·0235	7·843	9·384	·6558
1·8	1·7003	·0625	·0457	8·294	9·483	·7395
2·4	2·2115	·1143	·0838	8·712	9·577	·8269
3·0	2·6646	·1976	·1449	9·078	9·664	0·9176
3·6	3·0416	·3215	·2335	9·378	9·741	1·0110
4·2	3·3326	·4905	·3504	9·603	9·806	1·1066
4·8	3·5410	·7022	·4903	9·757	9·861	1·2040
5·4	3·6810	0·9483	0·6430	9·853	9·904	1·3029
π_f						
5·697	3·7317	1·0830	0·7235	9·885	9·923	1·354
				$\log Q$	$\log\Theta$	
				3·1958	7·7638	

$$\log\frac{\rho}{\rho_c}=0.82540\,y \quad -0.12698\,l \quad -3.1032$$

$$\log\frac{T}{T_c}=0.17460\,y \quad +0.12698\,l \quad -0.8200$$

Next, one may take from any desired table of opacities the run of guillotine factor throughout the model. A simple graphical procedure allows one to determine the model representing the guillotine factor most satisfactorily, and the corresponding value of τ_0 for the star.

In actual fact, no simple formula for the guillotine factor can be completely accurate over the range of densities and temperatures encountered, and some judgment must be exercised about the selection of the best fit. However, the deviations are small, compared with those obtained by assuming the guillotine factor to be constant throughout the star.

The conclusions to be drawn from applying these models to several late type main sequence stars, for which the opacity is given by Morse's tables, will be discussed in a subsequent paper.

David Dunlap Observatory,
Richmond Hill,
Ontario:
1948 *September* 3.

ON THE ROLE OF THE GUILLOTINE FACTOR IN DETERMINING THE STRUCTURE OF LATE TYPE MAIN SEQUENCE STARS

Ralph E. Williamson and G. F. D. Duff

(Communicated by C. A. Chant)

(Received 1948 September 8)

Summary

It is shown that the guillotine factor plays an important role in determining the central conditions of late type main sequence stars. The standard methods of determining chemical composition in models are discussed, and possible improvements are suggested.

---

1. *Introduction.*—The problem of determining the internal constitution of a star with given mass, M, radius, R, and luminosity, L, is customarily divided into two distinct parts: first, developing the physical theories of matter at high temperatures, and second, making use of these theories to set up and solve appropriate differential equations defining the equilibrium of a star under reasonable assumptions. Under the first category are treated such matters as the correct form of the equation of state, the processes by which energy is liberated in stellar material, and the methods by which energy is carried from the high-temperature regions to the low-temperature regions. In particular, the balance between radiative and convective transfer must be enunciated, and an expression for the opacity must be furnished for regions where radiation is the principal mode of transfer.

The crux of the second problem is the correct assessment, on the basis of the physical theories, of the processes likely to be important in any given star, the crystallizing of these into equations of equilibrium, and the numerical solution of these equations. A final step, which cannot be omitted with impunity, is the use of the solutions to the equations to verify the adequacy of the original assumptions, in so far as is possible. Where the model violates in some degree one or more of its own fundamental assumptions, the work serves as an indication of the direction in which further progress should be made.

A comparison of the conclusions reached by the Cowling* model and Schwarzschild's† model for the Sun, which differ only in the approximation made for the guillotine factor in the opacity, shows that an adequate representation of the opacity is required for the determination of the internal constitution of a star.

For reasons explained in a previous paper‡, it seems inadvisable at the present time to attempt an exact solution of the equations of stellar equilibrium by making substitution for the guillotine factor as given, say, by Morse's tables§. Hence, in this investigation of the internal constitution of late type main sequence stars, we shall make use of a family of previously obtained models, each of which

* T. G. Cowling, *M.N.*, **96**, 42, 1935.

† M. Schwarzschild, *Ap. J.*, **104**, 203, 1946.

‡ R. E. Williamson and G. F. D. Duff, *M.N.*, **109**, 46, 1949; this will be referred to as Paper I.

§ P. M. Morse, *Ap. J.*, **92**, 27, 1940.

represents the guillotine factor as proportional to a different power of the density. Such representations are an obvious first step toward more refined calculations.

Specifically, the present work is an attempt to examine, for certain late type main sequence stars, the adequacy of a model which embodies the following assumptions:—

(1) The chemical composition as typified by the hydrogen content X per unit mass, and the helium content, Y, is constant throughout the star, and the heavier elements are distributed according to the "Russell Mixture"*.

(2) For all relevant regions of the star, the approximations for the mean molecular weight, and the electron density corresponding to complete ionization, are valid†.

(3) The perfect gas law is valid throughout the star, and radiation pressure is negligible in comparison with gas pressure.

(4) The opacity follows Kramers' law corrected by a guillotine factor τ varying as some power α of the density, i.e. $\tau=\tau_0\rho^\alpha$; that power is to be selected which best represents Morse's calculations over the relevant regions.

(5) The energy-production ϵ per gram follows the approximate power law given by Bethe‡ to represent the carbon cycle:

$$\epsilon \propto \rho T^{17}.$$

(6) The star has a radiative envelope and a convective core. Energy generation in the envelope is negligible.

It will be seen that this is a natural extension of the ideas embodied in Schwarzschild's model of the Sun.

2. *The Equations for Determining the Hydrogen Content and the Helium Content.*— From the foregoing assumptions, two relations can be deduced connecting X and Y with certain functions of L, M and R for any given star, as Schwarzschild has done. However, the numerical form of the relations depends on the exponent α in the expression for the guillotine factor, and we develop them in a form for arbitrary α.

From equation (16) of Morse's paper, we see that the opacity (except for electron scattering) is given by

$$\kappa=\kappa_0\rho\frac{T^{-3\cdot5}}{\tau}, \tag{1}$$

where we have written τ for his $\left(\frac{t}{\bar{g}}\right)$. Further,

$$\kappa_0=7\cdot23\times10^{24}\Gamma(1+X)(1-X-Y) \qquad \Gamma=5\cdot9480. \tag{2}$$

Our assumption consists of taking

$$\tau=\tau_0\rho^\alpha. \tag{3}$$

It is convenient to write

$$\tau_0=C_0(1+X)^\alpha. \tag{4}$$

Comparison with equations (1) and (2) of Paper I shows that κ_0 and τ are there defined consistently with the above. After the insertion of numerical values, the Mass-Luminosity-Radius relation for arbitrary α may then be written

* P. M. Morse, *loc. cit.*

† S. Chandrasekhar, *An Introduction to the Study of Stellar Structure*, p. 254.

‡ H. Bethe, *Phys. Rev.*, **55**, 434, 1939.

$$(1-\alpha)\log(1+X)+\log(1-X-Y)-7{\cdot}5\log\mu$$

$$=5{\cdot}0937+\log C_0+\log C-0{\cdot}3276\alpha-\log\frac{\dfrac{L}{L_\odot}\left(\dfrac{R}{R_\odot}\right)^{0{\cdot}5+3\alpha}}{\left(\dfrac{M}{M_\odot}\right)^{5{\cdot}5+\alpha}}, \qquad (5)$$

where
$$\frac{1}{\mu}=\tfrac{1}{2}+\tfrac{3}{2}X+\tfrac{1}{4}Y. \qquad (6)$$

This furnishes one relationship between X and Y, once C_0 has been appropriately determined.

The second relationship, on the basis of the assumptions we are investigating, comes from the energy-law for the carbon cycle. This is given in a convenient form by Schwarzschild. Adapting it for arbitrary α,

$$\frac{\dfrac{L}{L_\odot}\left(\dfrac{R}{R_\odot}\right)^{20}}{\left(\dfrac{M}{M_\odot}\right)^{19}}=\epsilon_0'\frac{M_\odot}{L_\odot}X(1-X-Y)\mu^{17}Q(\alpha)\Theta(\alpha)^{17}\frac{p_f}{t_f\theta_f^{1{\cdot}5}}\left(\frac{x_f}{\xi_f}\right)^3\int_0^{\xi_f}\theta_{1{\cdot}5}^{20}\xi^2\,d\xi.$$

The notation is fully explained in Paper I, and Table I of that paper gives all relevant quantities for the above equation. When these quantities are inserted in the energy-relation, and the definite integral evaluated from tabulated values of the Lane-Emden function for $n=\frac{3}{2}$, we find

$$\log X+\log(1-X-Y)+17\log\mu=-\log\left[Q(\alpha)\Theta(\alpha)^{17}\frac{p_f}{t_f\theta_f^{1{\cdot}5}}\left(\frac{x_f}{\xi_f}\right)^3\int_0^{\xi_f}\theta_{1{\cdot}5}^{20}\xi^2\,d\xi\right]$$
$$+123{\cdot}1390+\log\frac{L}{L_\odot}\left(\frac{R}{R_\odot}\right)^{20}\left(\frac{M_\odot}{M}\right)^{19} \qquad (7)$$

as a second relationship between X and Y.

A little consideration will show that it is not a straightforward procedure to obtain the "best" model for a star of given L, M and R. This has to do with the fact that the guillotine factor is a function of T and $\rho(1+X)$, while the integrations for the models give only T/μ and ρ. Thus, a chemical composition must be assumed in order to obtain the guillotine factors from Morse's table, and thus to derive the constant C_0 in equation (4) above. Once this has been done, equations (5) and (7) imply values for X and Y for any desired value of α, which must agree with those first assumed, for consistency. In actual practice, the procedure for obtaining a model for any given star can be broken down into the following steps :—

(1) Assume a value for X and Y.
(2) For each available value of α, compute the run of density and temperature implied by these.
(3) Make a graphical representation of the logarithm of the guillotine factor from Morse's table as a function of the logarithm of $\rho(1+X)$ for each α.
(4) From these plots, obtain the best value of C_0 for each α.
(5) Using equations (5) and (7), determine X and Y.
(6) Repeat steps (2) through (5) until satisfactory agreement is obtained.
(7) From an inspection of the plots made in step (3), select that value for α which most adequately represents the guillotine factor.
(8) Check the original assumptions, as listed in Section 1, for consistency.

3. *Results of the Iteration Procedure for Three Stars.*—Using the values of L, M and R for the three stars Kr 60A, o_2 Erid C, and Castor C_2 quoted by Chandrasekhar*, application of the iteration procedure, as detailed in Section 2, gives the following values for the chemical composition:—

α	0·375	0·500	0·550	0·600	0·625
Kr 60A					
X	0·19	0·36	0·49	0·69	0·80
Y	0·63	0·59	0·49	0·30	0·19
$1-X-Y$	0·18	0·05	0·02	0·01	0·01
μ	1·06	0·84	0·73	0·62	0·58
$\log T_c$	7·20	7·21	7·20	7·20	7·21
$\log \rho_c$	2·56	2·91	3·10	3·33	3·47
o_2 Erid C					
X	0·12	0·33	0·45	0·64	0·75
Y	0·81	0·63	0·53	0·35	0·25
$1-X-Y$	0·07	0·04	0·02	0·01	0·00
μ	1·14	0·86	0·76	0·64	0·59
$\log T_c$	7·21	7·20	7·20	7·20	7·20
$\log \rho_c$	2·70	3·05	3·24	3·47	3·61
Castor C_2					
X	0·76	$X>1$			
Y	0·23				
$1-X-Y$	0·01				
μ	0·59	$\mu<\frac{1}{2}$			
$\log T_c$	7·22				
$\log \rho_c$	2·70				

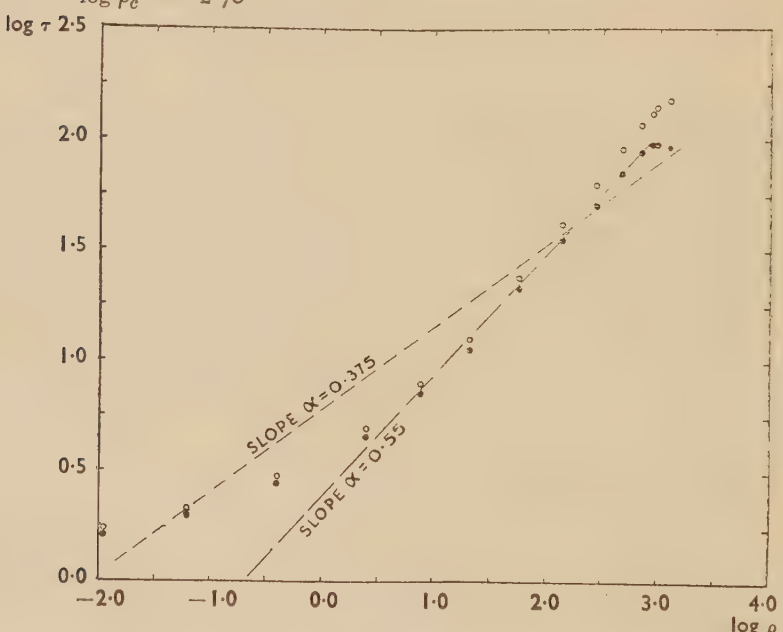

FIG. 1.—*Guillotine factors for* Kr 60A *on the basis of the model* $\alpha=0{\cdot}55$.

The upper circles represent the guillotine factor, and the lower circles show the effect of electron scattering considered as a correction to the guillotine factor. For stars with extremely high hydrogen content this correction will depress the appropriate value of α. *The two lines shown are:* (1) *a line with slope* 0·55 *which shows how the model actually represents the guillotine factor—this representation leads to a serious discrepancy in the outer regions where* $\log \rho$ *is negative; and* (2) *a line with slope* 0·375 *which gives a better overall fit. Note, however, in* (2), *the error of* 0·2 *or more in the region* $\log \rho \simeq +1$ *where a great deal more of the star's mass is present than in the outer layers.*

* S. Chandrasekhar, *An Introduction to the Study of Stellar Structure*, Appendix III.

4. *Comparison of the Models for Alternative Values of* α.—A comparison of the alternative possible models for either Kr 60A or o_2 Erid C shows that the chemical compositions and central conditions vary over a wide range, depending on the value of α. It then becomes of considerable importance to fix on the most suitable value of α, in order to have reliable estimates of the internal conditions. Consideration of Fig. 1 (which is typical of the run of $\log \tau$ with $\log \rho$ for all the models) will show that the selection of a suitable value for α is no straightforward matter. The lower limit to the density is set by the lower limit of Morse's table. Two alternative slopes are shown in the figure, one fitting the inner regions of the star most satisfactorily, the other making a compromise over the whole range of densities. The difference between the two slopes is so great as to render uncertain quantitative conclusions concerning the structure of the two stars. And it is in no sense obvious which is the better representation of the guillotine factor. One might argue that the more satisfactory procedure is to take the smaller slope, since it gives a better overall representation*. However, only an inappreciable fraction of the mass of the star (1 per cent or less) is included in the region $-2 \leqslant \log \rho \leqslant 0$. It would appear dangerous to distort the representation of the guillotine factor over the inner 99 per cent of the mass of the star, merely to obtain an approximately correct value over the less dense regions. The more so, in that the exact value of the guillotine factor for low densities is seriously influenced by the relative proportions of heavy elements, and cannot even be said to be known for densities smaller than 10^{-2} gm./cm.^{3}.

The only safe conclusion to be drawn is that even the approximation (3) for the guillotine factor is not sufficiently accurate—for these stars, at least—to allow accurate quantitative conclusions to be drawn from these models. The peculiar case of Castor C_2 also seems to bear out this conclusion.

5. *Physical Validity of the Models on Other Counts.*—It is of interest to see to what extent the conclusions reached in Section 4 could be influenced by inconsistency of the original assumptions with the results obtained for the models.

The first two assumptions will not be discussed, in the present state of the theory. Reference to Fig. 2 shows that small errors in the perfect gas law (up to perhaps 20 per cent) may be expected; of course, radiation pressure is unimportant.

Because the fraction of Russell Mixture is exceedingly low for the models with $\alpha \geqslant 0{\cdot}55$, electron scattering may contribute appreciably to the opacity. If κ_s and κ_a are the scattering and absorption opacities, respectively,

$$\frac{\kappa_s}{\kappa_a} = 0{\cdot}43 \times 10^{-26}\, T^{3{\cdot}5} \rho^{-1+\alpha} \frac{C_0(1+X)^\alpha}{(1-X-Y)}, \qquad (8)$$

where C_0 has a value of approximately 3 on the average. However, the effect of electron scattering may be considered as a correction to the guillotine factor τ. An alternative set of points in Fig. 1 illustrates for $\alpha = 0{\cdot}55$. For $\alpha = 0{\cdot}60$, the correction is more marked, and implies a somewhat smaller value of α, about 0·53. For Kr 60A, then, the high hydrogen-content models ($X = 0{\cdot}7$ or 0·8) seem definitely ruled out on the basis of electron scattering†.

If the proton-proton reaction is not forbidden, which seems unsettled at the present time, then it will provide most of the energy generation at 16×10^6 deg. K.,

* Schwarzschild has taken this point of view in his paper on the chemical composition of the Sun.

† A referee has kindly called our attention to the fact that Morse's guillotine factors, as used by us, do not contain the effect of the free-free transitions of hydrogen and helium in the stellar mixture, and, further, that the opacity from this source may be somewhat greater than that due to electron scattering for our more extreme models. While this probably does not greatly alter the above conclusions, it is an important fact, and should be borne in mind in more refined models for the late type main sequence stars.

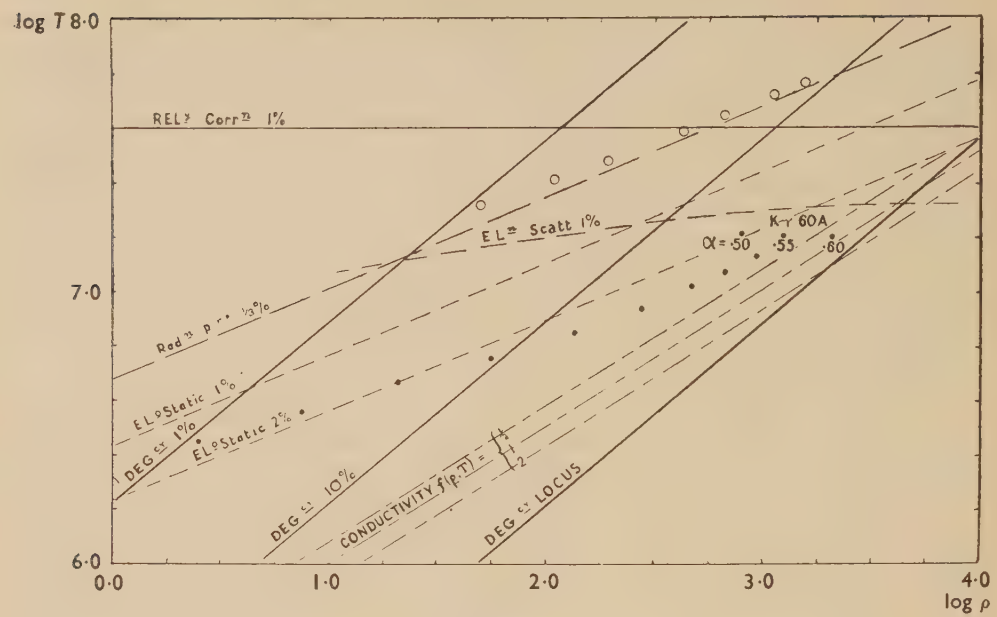

FIG. 2.

Degeneracy.

Now

$$\left(\frac{\Delta P}{P}\right)_{\text{Degcy}} = 10^{7\cdot336}\,\frac{\rho}{\mu_e T^{1\cdot5}}$$

as can be derived from the discussion in Chapter X of Chandrasekhar's monograph on Stellar Structure (in particular Formulae 252, 253, on page 399). The 1 per cent and 10 per cent levels of this correction are shown for $\mu_e=1$ together with the actual degeneracy locus as taken from Chapter XI of the same monograph. They are the three heavy sloping lines.

Electrostatic Correction.

The two medium dashed lines across the whole diagram are level curves of the electrostatic correction (R. E. Williamson, Ap. J., **103,** 139, 1946). *The expression for the percentage deviation of the pressure is*

$$\left(\frac{\Delta P}{P}\right)_{\text{e.s.c.}} = -0\cdot0140\left(\frac{\rho}{100}\right)^{\frac{1}{2}}\left(\frac{T}{10^7}\right)^{-\frac{1}{2}}.$$

(The 1 per cent and 2 per cent levels are shown.) This effect acts in the opposite way to the degeneracy correction.

Conductivity.

The three light dashed lines give the onset of conductivity. The criterion shown here is taken from F. Hund (Ergebnisse der Exakten Naturwissenschaften, **15,** 189, 1936). *It is*

$$\mu^2\frac{\lambda_{\text{cal}}}{\lambda_{\text{rad}}} = f(\rho, T).$$

Values of $f(\rho, T)$ are shown. This criterion is not necessarily accurate for partially degenerate material, and the purpose of including it here is to indicate roughly the region of log ρ and log T wherein the convective core model is suitable as a starting-point for the discussion.

Radiation Pressure.

The fractional correction to the pressure is

$$\frac{\mu a H T^3}{3k\rho}.$$

The level 0·0033 of this correction, which lies close to the locus of log Q and log Θ for the models is shown. This line runs parallel to the lines for the electrostatic correction.

The Relativity Correction for electron masses is ≅1 per cent at log T=7·6.

Electron Scattering.

Morse's expressions (Ap. J., **92,** 27, 1940) *have been used throughout. The function*

$$\frac{\kappa_s}{\kappa_a}(1-X-Y)$$

is shown at the 1 per cent level. It is the curved line extending from the right-hand side of the diagram, two-thirds of the way up. Electron scattering is to be taken into account if the content of heavier elements is of the order of three to five per cent or less.

The large open circles are the points log ρ=log Q(α), log T=log Θ(α) for each model. They are equivalent to the central densities and temperatures of the Sun, if μ is taken as unity.

The central density and temperature for Kr 60A, *according to the models α=0·50, 0·55 and 0·60, are shown, together with the "path" of the integration α=0·55 in the log ρ—log T plane.*

and the core source approximation will break down. The carbon cycle must be invoked to bring down the value of T_c (which varies as μ) to a level which will not provide too much total energy generation. Consequently, the values for log T_c quoted are the maximum permissible, and the values for X, the hydrogen content, are the minimum permissible. The actual change in X and Y for a given star (if the proton-proton reaction and others are taken into account) will be hard to estimate, particularly as the relative energy production due to various reactions depends on the chemical composition itself. In view of the present great uncertainty about X and Y, it seems desirable to postpone more detailed discussion of these matters until a model giving a better representation of the guillotine factor is available.

Assuming the carbon cycle, a numerical check of the production of energy outside the convective core indicates this to be small—at the extreme, less than 10 per cent of the total energy, and this in the layers immediately adjoining the convective core.

It is perhaps worth calling attention to the possibility (see Fig. 2) that energy transfer by conduction may occur in some of the deeper parts.

6. *Conclusions.*—It seems inescapable that the next additional refinement to the models for late type main sequence stars consists of a more sophisticated representation of the guillotine factor. Until this has been done, we are hardly in a position to make definite pronouncements about physical conditions and chemical composition in these stars, beyond the following: (*a*) the hydrogen and helium contents are probably not extreme, and (*b*) degeneracy and conductivity can conceivably play some part in determining the structure of the deep interior.

At the present time it seems possible that representation of the guillotine factor varying with two different powers of the density of different regions of the star* will clarify the issue. These matters are under investigation by the authors, and will be reported on in the near future.

The authors are much indebted to the University of Toronto Committee for Scientific Research for a grant toward defraying the cost of the research.

David Dunlap Observatory,
Richmond Hill,
Ontario:
1948 *September* 3.

* L. Henrich, *Ap. J.*, **96**, 106, 1942.

THE INTEGRATION OF THE EQUATIONS OF STELLAR STRUCTURE

C. M. Bondi and H. Bondi

(Revised version received 1948 December 8 *)

Summary

A new method of integration of the equations of stellar structure is given. This method can be used in almost all cases, whatever the particular model considered. It is claimed that the system is very quick to apply and that it avoids the instabilities met with in other methods. A few illustrations of its use are given. Graphs that enable the method to be used generally will be supplied on request.

---

1. *Introduction.*—The integration of the equations of stellar structure has been an awkward mathematical problem ever since the equations were first formulated. The increase in our knowledge of the various possible forms these equations can take has made the need for a simple method of integration only greater. For while Cowling (**1**) and later Hoyle and Lyttleton (**2**) have, with great effort, integrated one particularly important model, and others have since published some other integrations, the large range of possible stellar structures makes it imperative to have not merely a few isolated integrations but a method of dealing with the equations sufficiently simple for the mathematical consequences of any particular physical assumptions to be seen at a glance qualitatively, and worked out with little effort quantitatively. The present paper goes a good way towards satisfying this demand. It is true that we have found it necessary to transform the simple physical variables with which every worker in the field is so well acquainted to certain new variables, and the problem becomes simple only in these new variables. However, our own experience gives us reasonable hope that a little practice in working with the new variables soon leads to great familiarity with them, and it then becomes easy to visualize their physical meaning.

The peculiar nature of the equations, with their hidden instabilities which have proved so great an obstacle in the past, is of course due to the artificial assumption of a steady state. The complete equations with the time derivatives are quite stable and they are the equations which in fact determine the structure of the star. A small deviation from the steady state solution produces in a star only a small, usually heavily damped, oscillation. In the steady state equations, however, it leads to violent infinities. The simplification of omitting the time derivative is very great, but it has to be purchased at the price of introducing these instabilities.

Our method of attack is to make use of the existence of a homology relation to reduce the order of the problem by one. From the start, homology-invariant variables are introduced and made non-dimensional by the use of the appropriate physical constants, rather than of standard values of the variables, thereby avoiding the awkward and cumbersome "fitting", so familiar from other methods of integration. The homology-invariant variables chosen depend only on the universally valid equations of conservation of mass and of hydrostatic support, not on the energy transport equation which can take so many different forms.

* Originally submitted 1948 July 19.

This enables us also to give mathematical expression to the great differences in the physical importance of these equations.

Another advantage of the use of these homology-invariant variables is the transfer of an appreciable part of the instabilities from the difficult differential equations to the simple quadrature connecting our variables with the physical ones.

Finally we wish to stress that the reduction in the order of the problem enables one to spot the run of the solutions and the onset of instabilities very easily. By appropriate choice of the direction of working one can eliminate all the inconvenient effects of these instabilities. This, in turn, allows one to dispense with the extreme accuracy in the integrations hitherto necessitated by the instabilities, and work with only such accuracy as is appropriate to the character of the problem. This permits the use of graphical methods.

In our view the great advantage of graphical methods is that their use aids the acquisition of the instinctive sense of how the solutions run and what the effects of varying the physical assumptions are. It is this "feeling" for the subject which is so sorely needed rather than high accuracy in a few special models.

It is our claim that with the aid of the graphs, which can be obtained from the Assistant Secretary, Royal Astronomical Society, on request, any model of arbitrary composition can be integrated by one person in one or at most two days. A sketch of one of these graphs is given in this paper as an illustration. It has been our main purpose to present a method of integration, not individual integrations, and the examples given should be considered as illustrations of the working of the method and not as indicating any limitation in its applicability. There does not seem to be any reason to suppose that the method cannot be applied with great advantage to every spherically symmetrical steady or quasi-steady model.

The paper is divided into two parts: Part I is purely descriptive and contains all that is needed for the use of the method, while Part II gives the proofs and the considerations which led to the development of the method.

PART I

1. The conditions in stellar interiors are described in the first place in terms of the usual physical variables (p-variables) defined as follows:—

r = distance from centre of star;
$M = M(r)$ = mass contained within a radius r from the centre of star;
$\rho = \rho(r)$ = density at distance r from centre;
$P = P(r)$ = total pressure at distance r from centre.

The suffix s will be used for surface values, and c for central values.

Then the hydrostatic equation is

$$\frac{dP}{dr} = -\frac{GM\rho}{r^2}, \tag{1}$$

where G is the constant of gravitation.

The conservation of mass is expressed by

$$\frac{dM}{dr} = 4\pi r^2 \rho. \tag{2}$$

We now introduce the following variables, which are homology-invariant (h-variables):

$$S = 4\pi \frac{Pr^4}{GM^2}, \qquad Q = \frac{Pr}{GM\rho}, \qquad N = 1 - \frac{d\log\rho}{d\log P}. \tag{3}$$

As a consequence of equations (1) and (2), S, Q, N satisfy throughout a star the equation

$$\frac{S}{Q}\frac{dQ}{dS} = \frac{S+N-Q}{1+2S-4Q}, \tag{4}$$

and r is given in terms of the h-variables by

$$\log r/r_s = -\int_0^S \frac{Q\,dS}{S(1+2S-4Q)} = -\int_0^Q \frac{dQ}{S+N-Q}. \tag{5}$$

We shall use S as independent variable, so that $Q=Q(S)$, $N=N(S)$.

A particular solution of equation (4) for N constant (Emden's equation) when expressed in terms of the usual standard variables is known as Emden's function. To each value of N there corresponds such a function which, when expressed in the present variables, we denote by $Q_E(S\,;\,N)$. This is the only solution for constant N such that $Q\sim S/3$ for large S, that is, at the centre. The connection between S, Q, N and the Emden variables will be found in the appendix to Part I.

The surface of a star corresponds to the point $S=Q=0$, while the centre corresponds to S and Q infinite. The central boundary conditions are that $Q\sim S/3$ as S tends to infinity, and that N tends to a limit N_c. N also tends to a limit, N_s say, at the surface, and the surface boundary condition is that Q is proportional to S^{N_s} as S tends to 0.

At a boundary between any two regions in a star, the conditions that must be satisfied are that S, μQ and $L(r)$ should be continuous, where μ is the molecular weight and $L(r)$ the total energy crossing the boundary in unit time. The continuity condition for N follows from that for $L(r)$.

In order to find a solution $Q=Q(S)$, $N=N(S)$ for any particular region in a star, a second equation is required in addition to equation (4). This second equation is obtained by expressing the dependence of the energy transport on the temperature gradient, and may differ from one region to another.

A list of the relevant formulae will be found in the appendix to Part I.

2. In order to aid the graphical solution of the problems likely to arise, curves are available* of solutions of equation (4) for constant N, that is, of Emden's equation in h-variables. They are given for a series of values of N. The method of integration depends on the fact that N is slowly varying, and that the hydrostatic equation (1) is of primary importance even when N is not constant, while the energy transport equation is always subsidiary to it.

When the physical character of each zone of a star is defined, the scheme is described as a stellar model. A knowledge of the mass, luminosity, etc. is not required in performing the complete integration of such a stellar model. The values and significance of these constants are examined only when a complete solution in terms of S, Q and N has been found.

It has been found in almost all theoretical instances of stellar regions so far considered, that the energy transport equation may be expressed in terms of h-variables by a first order equation of the type

$$\frac{S}{Z}\frac{dZ}{dS} = \frac{f(S,Q,Z)}{1+2S-4Q}, \tag{6}$$

where Z is an h-variable functionally dependent on N (frequently $Z=N$) and slowly varying. The functional relation between Z and N depends on the

* See Introduction.

mechanism of energy transport and is given in its various forms in the appendix to Part I. The problem of the determination of Q and N as functions of S is therefore a second order one.

Since Z is slowly varying, equations (4) and (6) are in effect uncoupled for any small range of S, and equation (4) can be solved as though $N =$ constant in such a range. Any small error in equation (4) produces a minute error in equation (6) and vice versa. Thus the assumption $N =$ constant in a small range of S, which implies in fact a small error in equation (6), leads to a negligible error in the hydrostatic equation.

The system of equations is therefore suitable for the application of a semi-graphical method of integration, such as is described below:

Step I. Suppose it is known that in some solution, when $S = S'$, then $Q = Q'$, $Z = Z'$ corresponding to $N = N'$, without considering for the moment how such a point may be found. We now show how to find the values of Q, Z and N at a near point $S = S''$ in this solution, where $S'' - S'$ is small and positive.

Consider the set of graphs of solutions of equation (4) drawn for the nearest constant N value below N'. Pick out the point (S', Q') on that diagram, and by interpolation between the two adjacent curves, find the point Q''_a at which $S = S''$.

Next repeat this procedure on the diagram drawn for the nearest constant N value above N', arriving at the point (S'', Q''_b).

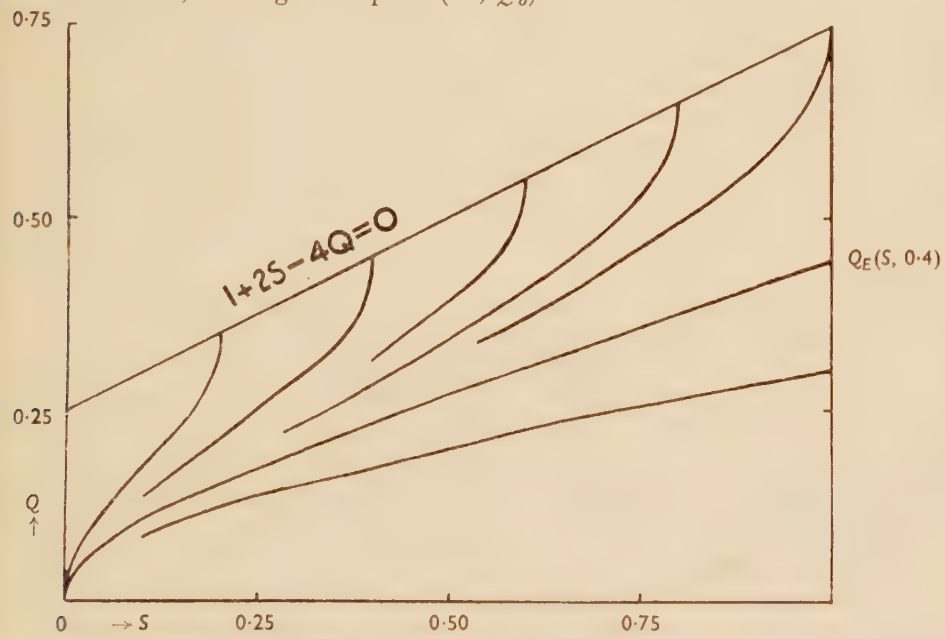

FIG. 1.—*Sketch of the solutions of Emden's equation for $N = 0{\cdot}4$ in the region $0 \leqslant S \leqslant 1$, $0 \leqslant Q \leqslant (1+2S)/4$. For lower values of N the curves rise more steeply from $S = Q = 0$, but afterwards run slightly less steeply than these.*

The first approximation to Q'' corresponding to S'' is then found by linear interpolation between these two values of N.

It is now possible to make a first approximation to the value of dZ corresponding to $dS = S'' - S'$, using the values $S = S'$, $Q = Q'$, $Z = Z'$.

N'' is then found from the functional relation between N and Z.

Q'' is then reinterpolated between Q''_a and Q''_b but now for the point $\frac{1}{2}(N'+N'')$ instead of at N'.

This recalculation of Q'' has generally been found unnecessary, the first approximation being sufficient. It is, in fact, usually possible to give a rough estimate of dN by inspection before Q'' is found, and this value can be used to give a mean value to N in the interval.

The value of dZ is then found, using the values S'', Q'' and the first approximation to Z''. The value of dZ is taken to be the mean between this and the value previously found.

It is unnecessary to recalculate Q'' with the final value of $\frac{1}{2}(N'+N'')$, since, as has been pointed out above, it is usually unnecessary to proceed beyond the first approximation to Q''.

The procedure of obtaining a new point of the solution from the previous one can then be continued indefinitely.

Step II. We have so far assumed that a first point, from which the integration of a solution may be continued, has already been found. To deal with this, consider first the case of a region running right to the surface of a star. The surface point (0, 0, N_s) is itself of no use in this connection, since it is a singular point, from which an infinity of solutions start.

However, it is possible to find series expansions for N and Q in terms of S in the neighbourhood of the point (0, 0, N_s). Each one of the solutions starting from (0, 0, N_s) is characterized by some value of the parameter A, such that $Q = AS^{N_s}$ in the immediate neighbourhood of the surface. The coefficients of the higher terms in the series expansions for N and Q depend on A.

The value of S, up to which Q and N are represented with sufficient accuracy (say $\frac{1}{2}$ per cent) by the first few terms of the series, depends greatly on the opacity law assumed to hold near the surface. For most laws N, and for some laws (e.g. electron opacity) Q, can be found sufficiently accurately up to values of S beyond which the ordinary method of integration, as given in Step I, can be employed (say $S = 0{\cdot}1$).

The gap (if any) in the range of S where neither the series nor the ordinary method can be used is closed by integrating (4) in the form

$$\frac{d \log Q}{d \log S} = \frac{S+N-Q}{1+2S-4Q} \tag{4'}$$

by step-by-step integration or graphically on log-log paper. If N is known with sufficient accuracy from the series, the values so obtained can be used in integrating (4'). Otherwise equation (6) must be used.

Thus for any region running to the surface, the solutions can be found, since we can now proceed from $S = 0{\cdot}1$ in suitable steps as above. If the region does not run to the surface the outer regions must be integrated first, and the continuity conditions used to obtain a set of starting values for the next region.

For any complete stellar model, out of the simple infinity of solutions corresponding to the simple infinity of possible A values, only that which leads to the correct central conditions $Q \sim S/3$, N tends to a limit at the centre, can give a model of physical significance.

An alternative method of getting a first point from which the integration can be continued is by starting from the centre. As has been said before, near the centre the solution is either $Q_E(S; N_c)$ or is asymptotically equal to it. The

solution here is therefore known more definitely than at the surface, but a free parameter is introduced either through lack of knowledge of N_c or through lack of knowledge of S at the first interface. Which direction of integration, inward or outward, is desirable depends on the circumstances of the case.

The following lemma is of use when constructing the solution in h-variables.

Lemma. Suppose that (i) $1+2S-4Q>0$.

(ii) N is an increasing function of S.

(iii) At $S=S_1$, $N=N_1$, $Q=Q_1\geqslant Q_E(S;N_1)$.

Then for $S>S_1$, it follows that $Q>Q_E(S;N_1)>Q_E(S;N)$.

Step III. When the solution in terms of h-variables has been obtained, the solution in terms of p-variables is constructed as follows: r/r_s is found as a function of S by a quadrature using (5).

To find M/M_s, ρ/ρ_c, P/P_c and T/T_c, we have the two definitive relations for S, Q, that is,

$$S=4\pi\frac{Pr^4}{GM^2} \qquad \text{and} \qquad Q=\frac{Pr}{GM\rho}$$

together with the relation between P, ρ, T which defines the pressure in terms of the other p-variables, and a fourth relation that depends on the form of the energy transport equation, and usually finds expression as a functional relation between N and the p-variables. This relation is also given for each region in the appendix.

These four relations determine M/M_s, ρ/ρ_c, T/T_c and P/P_c as functions of S and hence as functions of r/r_s as required.

The scale constants r_s, M_s, ρ_c, P_c (T_c being determined by P_c and ρ_c) are not independent. Two relations between them are

$$\log\frac{4\pi r_s^3\rho_c}{3M_s}=\int_0^\infty\frac{3Q-S}{S(1+2S-4Q)}\,dS \tag{7}$$

and

$$\log\frac{P_c r_s}{\rho_c GM_s}=\log Q_1+\int_0^{S_1}\frac{(Q-S)\,dS}{S(1+2S-4Q)}+\int_{S_1}^\infty\frac{N\,dS}{S(1+2S-4Q)}, \tag{8}$$

where Q_1 is the value of Q at S_1, which is an arbitrary value of S.

The equation of radiative transfer applied near the surface leads to a connection between L_s, M_s and r_s (the mass-luminosity-radius relation). A further limitation on the scale parameters arises if Bethe's law is assumed to govern the energy production. Then, by integrating Bethe's law throughout the energy producing region, L_s can be found as a function of T_c, ρ_c and r_s, and by equating these two expressions for L_s we find another relation between the scale constants, leaving only one parameter free.

If some additional assumption (such as the ratio of gas pressure to radiation pressure at the centre of a star) is made, which imposes another restriction on the parameters, then only one star corresponds to a given solution in h-variables.

3. As an example, let us consider a star of uniform composition with a convective core with ratio of specific heats $\frac{5}{3}$ and a radiative atmosphere with opacity due only to electron scattering. We assume that radiation pressure is negligible.

Throughout the star

$$\frac{S}{Q}\frac{dQ}{dS}=\frac{S+N-Q}{1+2S-4Q}.$$

In the convective core, we have in addition $N=0{\cdot}4$, while in the radiative envelope

$$\frac{S}{N}\frac{dN}{dS}=\frac{1+S-4N}{1+2S-4Q}. \tag{9}$$

Thus, at the surface, $N=\frac{1}{4}$ and $Q=AS^{\frac{1}{4}}$.

Note that in both regions in this model, $Z=N$.

The solution for the core is well known, being the ordinary Emden solution, with polytropic index 1·5. That is, in our notation, $Q=Q_E(S;0{\cdot}4)$.

The problem is therefore to determine the value of A that ensures that the solution in the atmosphere is continuous with $Q_E(S;0{\cdot}4)$ in the core. This implies that, as we work inwards, $Q(S)$ lies on $Q_E(S;0{\cdot}4)$ when N has reached the value 0·4.

The series expansions of the solutions in the neighbourhood of the origin are

$$\left.\begin{aligned} Q&=AS^{1/4}+\tfrac{5}{8}AS^{5/4}+\tfrac{98}{45}A^2S^{6/4}+\tfrac{68}{9}A^3S^{7/4}+\ldots,\\ N&=\tfrac{1}{4}+\tfrac{1}{8}S+\tfrac{2}{9}AS^{5/4}+\tfrac{4}{9}A^2S^{6/4}+\tfrac{32}{33}A^3S^{7/4}+\ldots.\end{aligned}\right\} \tag{10}$$

Suppose we take $A=0{\cdot}225$.

Then from the graphical method ($\log Q$ against $\log S$) or from the above series, it is found that, at $S=0{\cdot}1$, $Q=0{\cdot}137$, while from the series $N=0{\cdot}2662$. A number of solutions for small S is given in Table III.

We now refer to the set of graphs for $N=0{\cdot}25$, and on it find, by interpolation between curves, the curve that passes through the point $S=0{\cdot}1$, $Q=0{\cdot}137$. The point on this curve at which $S=0{\cdot}15$ is then found. A similar process is carried out on the graph for $N=0{\cdot}3$. The point on the solution for $A=0{\cdot}225$ is then found by linear interpolation with N, it being assumed for simplicity that the mean value of N in the interval $S=0{\cdot}1$ to $S=0{\cdot}15$ is about 0·27. It is then found that for $S=0{\cdot}15$, $Q=0{\cdot}160$.

The correct value of N is found by calculating dN from equation (9) for the values of the variables at $S=0{\cdot}1$ and for $dS=0{\cdot}05$. This leads to a first approximation to the value of N at $S=0{\cdot}15$, and the process is repeated, using this value of N and the values $S=0{\cdot}15$, $Q=0{\cdot}160$ and $dS=0{\cdot}05$. The mean of the two values of dN thus found is taken to be the correct one.

In this way it is found that for $S=0{\cdot}15$, $N=0{\cdot}2737$.

This procedure is continued until the solution is found to be above the corresponding Emden solution, or until $N=0{\cdot}4$.

At $S=0{\cdot}3$, it is found that $Q=0{\cdot}222$, while $N=0{\cdot}2971$. On the other hand, by linear interpolation it can be seen that $Q_E(0{\cdot}30;0{\cdot}297)=0{\cdot}220$.

Thus, from the lemma, it is clear that this value of A is too high. A lower value of A is next taken and in fact it is found that for $A=0{\cdot}218$ the solution has not crossed the corresponding Emden solution by the time $N=0{\cdot}35$, but is extremely close to it. Since the solutions diverge, it is clear that $A=0{\cdot}218$ is sufficiently near the required solution for it to be taken as correct. At the point of meeting with $Q_E(S;0{\cdot}4)$ this solution has the same gradient as the Emden solution, and so we can sketch the rest of the radiative solution to give a first approximation. Using this completed solution, the N equation, (9), can be integrated and the value of S at which $N=0{\cdot}4$ found. The point on $Q_E(S;0{\cdot}4)$ at which S has this value is then a second approximation to the meeting point. The radiative solution can then be redrawn and a higher approximation found, if required, but in fact such a step has usually been found to be unnecessary. By the quadrature (5), r/r_s is then found and ρ/ρ_c, M/M_s, T/T_c, P/P_c are found by means of (16) and (25).

Table I shows the full solution for this model and also compares our results with those of other papers.

Similarly, Table II gives the full solution and the relevant comparisons for the case in which Kramers' absorption, neglecting the guillotine factor, is the main source of opacity in the radiative region, the other conditions being as before. The method of solution is identical with that outlined above, although the series expansions at $(0, 0, N_s)$ are rather more complicated, owing to the fact that $N_s = \frac{4}{17}$.

The subsidiary equation is now

$$\frac{S}{N}\frac{dN}{dS} = \frac{S+2-8{\cdot}5N}{1+2S-4Q}. \tag{11}$$

The series expansions in this case are

$$\left.\begin{aligned} Q &= \theta - \tfrac{1}{4}\theta^2 - \tfrac{7}{16}\theta^3 - \tfrac{65}{64}\theta^4 - \tfrac{667}{256}\theta^5 + \tfrac{31}{51}S\theta + \ldots, \\ N &= \tfrac{4}{17} + \tfrac{4}{51}S + \tfrac{16}{165}S\theta + \tfrac{1124}{9735}S\theta^2 + \ldots, \end{aligned}\right\} \tag{12}$$

where $\theta = AS^{4/17}$.

The series for Q, though still sufficiently accurate at $S = 0{\cdot}01$, is no longer very useful at $S = 0{\cdot}1$, but the series for N is accurate even at $S = 0{\cdot}1$. Using the values of N given by it, a few simple stages of step-by-step integration of $\log Q$ against $\log S$ cover the range between $S = 0{\cdot}01$ and $S = 0{\cdot}1$.

A list of solutions for small values of S is given in Table IV.

The correct value of A is found to be 0·235.

As a last example, we give a qualitative treatment of the case of a star contracting through homologous configurations under gravity, without nuclear generation of energy, in order to find the configuration of the star. Radiation pressure is neglected, and the opacity is assumed to be entirely due to electron scattering.

The rate of energy production per unit mass is known to be proportional to the temperature in such a star (**3**). Therefore, there will be no convective core but radiative equilibrium throughout the star (**4**).

The relevant N equation is not of the usual type, but is the second order equation (see end of appendix)

$$[S(1+2S-4Q)]^2\frac{d^2N}{dS^2} - [2+3S-8Q-2S^2+8SQ-4Q^2-N(11+22S-48Q)] \times S\frac{dN}{dS} + N[(1+2S-4Q)(1-4N)+(1-3N)(S+1-4N)] = 0. \tag{13}$$

It is physically evident that near the surface the star is like any other star with opacity due to electron scattering. At the centre we have the usual boundary condition $Q \sim S/3$, but the radiative equation (13) will continue to be valid. Accordingly we must have:

$$\text{as} \quad S \to 0, \quad Q \sim AS^{\frac{4}{17}}, \quad N \to \tfrac{1}{4};$$

$$\text{as} \quad S \to \infty, \quad N \to N_c < 0{\cdot}4, \quad Q = Q_E(S; N_c) + o(1) = \tfrac{1}{3}S + \tfrac{1}{5}(1-N_c) + o(1). \tag{14}$$

Now consider the points where $dN/dS = 0$. Since N 0, these will be maxima whenever the last square bracket in equation (13) is positive and minima whenever it is negative. Accordingly we are interested in whether the expression

$$(1+2S-4Q)(1-4N)+(1-3N)(S+1-4N) \tag{15}$$

is positive or negative.

For large values of S the leading term in (15) is

$$5-17N_c$$

by equation (14).

The expression (15) is zero for $S=0$, $Q=0$, $N=\frac{1}{4}$.

For any likely variation of Q with S, the curve given by equating (15) to zero in the (S, N) plane will rise monotonically and very slowly from $\frac{1}{4}$ at $S=0$ to a limiting value $\frac{5}{17}$ at $S=\infty$. There can be no maxima above this curve and no minima below it.

The asymptotic expansion of N at $S=\infty$ is

$$N=N_c\left[1-\frac{3}{10}\frac{5-17N_c}{S}+O\left(\frac{1}{S^2}\right)\right],$$

while near $S=0$,

$$N=\tfrac{1}{4}+\tfrac{1}{8}S+O(S^{5/4}).$$

Accordingly, if $N_c>\frac{5}{17}$, N cannot reach the value $\frac{1}{4}$ at the origin without having a maximum in the forbidden region. Similarly we can exclude the case $N_c<\frac{1}{4}$. Hence $\frac{5}{17}>N_c>\frac{1}{4}$.

The sharp rise of N near the origin indicates that N_c must be appreciably larger than 0·25. It seems likely that $N_c\doteqdot 0{\cdot}28<0{\cdot}294\doteqdot\frac{5}{17}$, and that N rises monotonically.

Therefore the variation of N is very small and slow, and the star is very nearly a polytrope of average index 2·75.

The value of A may be deduced from the following consideration. If $N=0{\cdot}25$ throughout a star the A value is that of $Q_E(S; 0{\cdot}25)$ which is 0·249. But N is an increasing function of S, starting from the value 0·25 at the surface $S=0$. Hence A must be less than 0·249, since the increase in N implies an increase in dQ/dS, and also since the Q_E function which the solution approaches as $S\to\infty$ lies below $Q_E(S; 0{\cdot}25)$. On the other hand, the increase in N is far smaller than for the electron opacity star with nuclear generation of energy (Table I) for which $A=0{\cdot}218$. Hence A will be near 0·240 and therefore a star of this type has a luminosity 40 to 50 per cent greater than a steady star of the same composition and mass with nuclear generation of energy.

Its radius is arbitrary within wide limits, but certainly greater than for a star with nuclear generation of energy governed by Bethe's law.

The conclusions reached here differ markedly from those found by Harrison (**5**). That the convective core found there does not in fact exist is an immediate corollary of Cowling's stability criterion (**4**).

APPENDIX

We aim to present in this appendix a list of all the formulae which are likely to be useful in the application of this method of integration. We first give a list of the symbols employed.

Proofs of the formulae given in this appendix will be found in Section 7 of Part II.

r = distance from centre of star.

$M=M(r)$ = mass contained within a radius r from centre of star.

$\rho=\rho(r)$ = density at distance r from centre.

$P=P(r)$ = total pressure at distance r from centre.

$T=T(r)$ = temperature at distance r from centre.

$\beta = \beta(r)$ = ratio of gas pressure to total pressure at distance r from centre.
G = constant of gravitation.
$S = 4\pi Pr^4/GM^2$.
$Q = Pr/GM\rho$.
$N = 1 - d \log \rho / d \log P$. (3)
Z = auxiliary h-variable functionally dependent on N.
x = Emden radius.
y = Emden temperature.
n = polytropic index as it occurs in Emden's equation.
$Q_E(S;N)$ = Emden function corresponding to $N = \frac{1}{n+1}$.
μ = molecular weight.
$\mathscr{R}$ = gas constant.
γ = ratio of specific heats of a gas.
κ = constant in electron opacity law.
α = factor of proportionality in Kramers' opacity law (constant when the guillotine factor is neglected).
X = proportion of hydrogen present, by mass.
Y = proportion of helium present, by mass.
a = Stefan's constant.
c = speed of light.
$L = L(r)$ = luminosity = rate of flow of energy across sphere of radius r.
$L(r_s) = L_s$ = surface luminosity.
B = modified factor of proportionality in Kramers' opacity law $= 3\alpha L(1+X)(1-X-Y)/16\pi ac$.
C = modified factor of proportionality in electron opacity law $= 3\kappa(1+X)L/16\pi ac$.
The suffix s is used for surface values and c for central values.

I. *Formulae valid at all points of a star.*

S, Q, N satisfy the equation

$$\frac{S}{Q}\frac{dQ}{dS} = \frac{S+N-Q}{1+2S-4Q}. \tag{4}$$

The following relations are frequently useful:

$$\left.\begin{aligned} S/Q &= 4\pi r^3\rho/M, \\ S/Q^2 &= 4\pi G r^2\rho^2/P, \\ S/Q^4 &= 4\pi G^3 M^2 \rho^4/P^3. \end{aligned}\right\} \tag{16}$$

r is determined by the equation

$$\frac{S}{r}\frac{dr}{dS} = -\frac{Q}{1+2S-4Q}$$

and therefore

$$\log\frac{r_s}{r} = \int_0^S \frac{Q\,dS}{S(1+2S-4Q)} = \int_0^Q \frac{dQ}{S+N-Q}.$$

$Q_E(S;N)$ has the asymptotic expansion

$$Q_E(S;N) = \tfrac{1}{3}S + \frac{1-N}{5} + O\left(\frac{1}{S}\right).$$

The connection between $Q_E(S;N)$ and the usual Emden variables x, y is given by:

(i) If n is finite

$$n+1=1/N, \quad S=Ny^{n+1}(y')^{-2}, \quad Q_E(S;N)=Ny(-xy')^{-1}$$

and

$$\log[x(Q/3N)^{\frac{1}{2}}]=\int_Q^\infty dQ\left[\frac{1}{S+N-Q}-\frac{1}{2Q}\right].$$

(ii) In the isothermal case (n infinite)

$$N=0, \quad S=(y')^{-2}\exp y, \quad Q_E(S;0)=(-xy')^{-1}$$

and

$$\log[x(Q/3)^{\frac{1}{2}}]=\int_Q^\infty dQ\left[\frac{1}{S-Q}-\frac{1}{2Q}\right].$$

In II and III we give the equations dependent on the particular form of the heat transport equation. In each subsection we give first the form of this equation in p-variables, then its form in h-variables, this equation being displayed in bold type, and lastly the relations that enable the p-variables to be calculated when the solution in h-variables is known. In every case r is calculated by a quadrature from (5).

II. *Formulae applicable in zones of a star in a steady state.*

Throughout this section we shall assume that there is no energy generation in a zone in radiative equilibrium, so that the energy flow $L(r)$ can be treated as constant in any such zone.

A. *Radiation pressure negligible.*—In all cases considered under this heading, $P=\mathscr{R}\rho T/\mu$, $Z=N$.

(i) Convective equilibrium.

$$P=D\rho^\gamma, \tag{17}$$

where D is a constant determined by conditions in the centre of the star.

$$\boldsymbol{N=\frac{\gamma-1}{\gamma}=\text{const.}} \tag{18}$$

When $Q(S)$ has been found, r is determined by a quadrature from (5).

$M(S)$ is found from the relation

$$\frac{Q}{S^N}=\frac{r^{1-4N}}{M^{1-2N}}\left(\frac{D}{G}\right)^{1-N}(4\pi)^{-N}. \tag{19}$$

Finally ρ and P are determined by using (16).

(ii) Isothermal state.

$$T=\text{const.}, \tag{20}$$

$$\boldsymbol{N=0}, \tag{21}$$

$$M=\mathscr{R}Tr/GQ\mu. \tag{22}$$

P and ρ are again found by (16).

(iii) Radiative equilibrium. Electron opacity only.

$$\frac{dT}{dr}=-\frac{3\kappa(1+X)L}{16\pi ac}\frac{\rho}{r^2T^3}, \tag{23}$$

$$\boldsymbol{\frac{S}{N}\frac{dN}{dS}=\frac{1+S-4N}{1+2S-4Q}}, \tag{24}$$

$$M^3=L\frac{3\kappa(1+X)}{64\pi^2ac}\left(\frac{\mathscr{R}}{\mu G}\right)^4\frac{S}{NQ^4}. \tag{25}$$

When the surface value of S/Q^4 is inserted, this equation gives the mass-luminosity relation. P, ρ are found by using (16). Series expansions valid near the surface are given in equation (10).

(iv) Radiative equilibrium. Kramers' opacity only.

Consider the generalized form

$$\frac{dT}{dr} = -B\frac{\rho^\sigma}{r^2T^\nu}, \tag{26}$$

$$\frac{S}{N}\frac{dN}{dS} = \frac{S+\sigma-(\nu+\sigma)N}{1+2S-4Q}, \tag{27}$$

$$M^{\nu+1-\sigma} = B\left(\frac{\mathscr{R}}{\mu G}\right)^{\nu+1}(4\pi)^{-\sigma}\frac{S^\sigma}{NQ^{\nu+\sigma}}r^{\nu-3\sigma}. \tag{28}$$

When the surface value of $S^\sigma Q^{-\nu-\sigma}$ is inserted, (28) gives the mass-luminosity-radius relation. In the "normal" case, $\sigma=2$, $\nu=6{\cdot}5$. For this case series expansions valid near the surface are given by equation (12).

A slight modification in which $\sigma=2$, $\nu=6$ is frequently useful.

(v) Radiative equilibrium. Kramers' opacity, with guillotine factor.

$$\frac{dT}{dr} = -\frac{B\rho^2}{r^2T^{6\cdot5}}g(\rho, T). \tag{29}$$

A simple treatment is only possible if there is a function F and a constant λ such that

$$B\left(\frac{4\pi G\mu}{\mathscr{R}}\right)^{\frac{1}{2}}\frac{\rho^{2\cdot5}}{T^8}g(\rho, T) = F\left(\frac{\rho}{T^\lambda}\right) = v, \quad \text{say.}$$

Introduce now a function $H(v)$ defined as follows :

If $v=F(u)$ then $H(v)=d\log v/d\log u$,

$$\frac{S}{N}\frac{dN}{dS} = \frac{S+H(NS^{\frac{1}{2}}Q^{-2})-\frac{1}{2}-N[(1+\lambda)H(NS^{\frac{1}{2}}Q^{-2})-2]}{1+2S-4Q}, \tag{30}$$

$$v = NS^{\frac{1}{2}}Q^{-2}, \tag{31}$$

and the relations (16) determine P, ρ, T.

(vi) Radiative equilibrium. Mixed opacities.

$$\frac{dT}{dr} = -\frac{B\rho^2}{r^2T^{6\cdot5}} - \frac{C\rho}{r^2T^3}, \tag{32}$$

$$\frac{S}{N}\frac{dN}{dS} = \frac{S-(4N-1)-\omega(4{\cdot}5N-1)}{1+2S-4Q}, \tag{33}$$

where ω is a slowly varying function of S determined by

$$\frac{\omega^6}{(1-\omega)^{11}} = \frac{\mathscr{R}B^6r_s^3}{4\pi G\mu C^{11}}\frac{SN^5}{Q^7}\left(\frac{r}{r_s}\right)^3. \tag{34}$$

The expression on the left-hand side need not be accurately known, since a large change in $\omega^6(1-\omega)^{-11}$ results only in a very small change in ω.

$$T^{2\cdot5} = \frac{\mathscr{R}B(1-\omega)S}{4\pi G\mu Cr^2\omega Q^2}. \tag{35}$$

B. *Radiation pressure not negligible.*—We are now considering cases in which

$$P=\mathscr{R}\rho T/\mu+aT^4/3. \tag{36}$$

We define

$$Z=a\mu T^3/3\mathscr{R}\rho=(1-\beta)/\beta. \tag{37}$$

In all cases

$$M^2=\frac{3\mathscr{R}^4SZ(1+Z)^3}{4\pi a\mu^4G^3Q^4}, \qquad aT^4=\frac{3ZP}{1+Z}=\frac{3ZGM^2S}{4\pi r^4(1+Z)} \tag{38}$$

determine the physical variables.

(i) Convective equilibrium.

Let Γ = ordinary ratio of the specific heats of the gas.

Let

$$F(N)=[16(\Gamma-1)Z+\Gamma\log Z]/(3\Gamma-4)+\log(Z+1). \tag{39}$$

Then

$$\boldsymbol{F(N)=\int\frac{dS}{S(1+2S-4Q)}+\text{const.},} \tag{40}$$

$$1-N=\frac{(1+Z)[1+12(\Gamma-1)Z]}{\Gamma+20(\Gamma-1)Z+16(\Gamma-1)Z^2}. \tag{41}$$

$F(N)$ depends very critically on N, so that the integration determines N very accurately. The following table was computed for $\Gamma=\frac{5}{3}$.

Z	0	0·05	0·10	0·15	0·20	0·25	0·50	1·00	2·00
N	0·4000	0·3771	0·3626	0·3524	0·3445	0·3382	0·3182	0·2987	0·2817
$F(N)$	$-\infty$	−4·411	−2·676	−1·422	−0·267	+0·579	+4·583	+11·36	+23·59
β	1	0·9524	0·9091	0·8696	0·8333	0·8000	0·6667	0·5000	0·3333

(ii) Radiative equilibrium. Electron opacity only.

$$\frac{dT}{dr}=-\frac{C\rho}{r^2T^3}, \tag{42}$$

$$N=\lambda Q^2S^{-\frac{1}{2}}(1+4Z)(1+Z)^{-\frac{1}{2}}Z^{-\frac{3}{2}}-Z, \tag{43}$$

where

$$\lambda=\left(\frac{\mu}{\mathscr{R}}\right)^2\frac{ac}{3}\left(\frac{4\pi aG}{3}\right)^{\frac{1}{2}}\doteqdot 10^{-8}\mu^2(1+X)L_s/L_\odot, \tag{44}$$

$$\boldsymbol{\frac{dZ}{dS}=\frac{Z(Z+1)}{4Z+1}\,\frac{4N-1}{S(1+2S-4Q)}.} \tag{45}$$

Near the surface

$$\left.\begin{aligned} N&=\tfrac{1}{4}+S(1+4Z_s)/8+\ldots,\\ Z&=Z_s+Z_s(1+Z_s)S/2+\ldots,\\ Q&=Z_s^{\frac{3}{2}}(1+Z_s)^{\frac{1}{2}}(4\lambda)^{-\frac{1}{2}}S^{\frac{1}{2}}[1+S(5+4Z_s)/8+\ldots]. \end{aligned}\right\} \tag{46}$$

(iii) Radiative equilibrium. Kramers' opacity only (modified form).

The formulae are simple only for the modified Kramers' opacity.

$$\frac{dT}{dr} = -B\frac{\rho^2}{r^2T^6}, \tag{47}$$

$$N = \bar{\lambda}Q^2S^{-\frac{1}{2}}(1+4Z)(1+Z)^{-\frac{1}{2}}Z^{-\frac{5}{2}} - Z, \tag{48}$$

where the constant

$$\left.\begin{aligned} \bar{\lambda} &= \left(\frac{\mu}{\mathscr{R}}\right)^3\left(\frac{a}{3}\right)^2 B\left(\frac{4\pi aG}{3}\right)^{\frac{1}{2}}, \\ \frac{dZ}{dS} &= \frac{Z(Z+1)}{4Z+1}\,\frac{4N-1}{S(1+S-4Q)}. \end{aligned}\right\} \tag{49}$$

Near the surface

$$\left.\begin{aligned} N &= \tfrac{1}{4} + (1+4Z_s)S/4(3+Z_s) + \ldots, \\ Z &= Z_s + Z_s(1+Z_s)S/(3+Z_s) + \ldots, \\ Q &= Z_s^{\frac{1}{2}}(1+Z_s)^{\frac{1}{2}}(4\bar{\lambda})^{-\frac{1}{2}}S^{\frac{1}{2}}[1+(7+6Z_s)S/4(3+Z_s) + \ldots]. \end{aligned}\right\} \tag{50}$$

III. *Non-steady Stars*

The only case of this type considered so far is the homologous contraction under gravity of a star of uniform composition. There is supposed to be no nuclear energy production, radiation pressure is neglected, and the opacity is taken to be due to electron scattering only.

The equations reduce to the following form :—

Let $rt = z$, where t is the time measured from a suitable epoch.

$$M = \bar{M}(z), \qquad T = t\bar{T}(z), \qquad \rho = t^3\bar{\rho}(z), \qquad P = t^4\bar{P}(z). \tag{51}$$

Then

$$\left.\begin{aligned} \frac{d\bar{M}}{dz} &= 4\pi\bar{\rho}z^2, \\ \frac{d\bar{P}}{dz} &= -\frac{G\bar{M}\bar{\rho}}{z^2}. \end{aligned}\right\} \tag{52}$$

$$\left.\begin{aligned} \bar{P} &= \mathscr{R}\bar{\rho}\bar{T}/\mu, \\ \bar{P} &= -\frac{4\pi ac(\Gamma-1)}{3\kappa(1+X)(3\Gamma-4)}\,\frac{1}{z^2}\,\frac{d}{dz}\left(\frac{z^2\bar{T}^3}{\bar{\rho}}\frac{d\bar{T}}{dz}\right). \end{aligned}\right\} \tag{53}$$

Defining

$$S = 4\pi\bar{P}z^4/G\bar{M}^2, \quad Q = \bar{P}z/G\bar{\rho}\bar{M}, \quad 1-N = d\log\bar{\rho}/d\log\bar{P}, \tag{3'}$$

we have

$$\frac{d}{dS}\log\left[N(S+1-4N) - S(1+2S-4Q)\,\frac{dN}{dS}\right] = \frac{1}{S} + \frac{1-3N}{S(1+2S-4Q)} \tag{13'}$$

together with the usual equation

$$\frac{S}{Q}\frac{dQ}{dS} = \frac{S+N-Q}{1+2S-4Q}. \tag{4}$$

TABLE I

The uniform electron opacity solution $A=0{\cdot}218$

S	Q	N	r/r_s	M/M_s	T/T_c	ρ/ρ_c
0	0	0·2500	1	1	0	0
0·02	0·083	0·2529	0·676	0·980	0·151	0·013
0·10	0·132	0·2661	0·532	0·888	0·274	0·073
0·15	0·151	0·2734	0·493	0·842	0·322	0·115
0·30	0·204	0·2958	0·419	0·691	0·420	0·226
0·70	0·340	0·3541	0·325	0·437	0·571	0·429
1·03	0·453	0·4000	0·285*	0·328	0·652	0·527

* Limit of convective core of radius 1·58 in Emden units.

	$\frac{M_{\text{core}}}{M_s}$	$\frac{r_{\text{core}}}{r_s}$	r_s (Emden units)	$\frac{\mathscr{R}T_c r_s}{\mu G M_s}$	$\frac{\rho_{\text{mean}}}{\rho_c}$	$\frac{C}{M_s^3}\left(\frac{\mathscr{R}}{\mu G}\right)^4$
Present paper	0·328	0·285	5·54	0·80	0·049	0·0071
C. M. Bondi (7)	0·34	0·249	6·23	0·97	0·032	0·0092
L. R. Henrich (8)	0·31	0·283	5·56	0·77	0·050	0·0063

TABLE II

The uniform Kramers' opacity solution $A=0{\cdot}2351$

S	Q	N	r/r_s	M/M_s	ρ/ρ_c	T/T_c
0	0	0·23529	1	1	0	0
0·001	0·0458	0·23538	0·804	0·9987	$3{\cdot}8\times10^{-4}$	0·063
0·01	0·078	0·2362	0·673	0·987	$3{\cdot}2\times10^{-3}$	0·126
0·08	0·134	0·2425	0·484	0·885	0·042	0·271
0·20	0·184	0·2533	0·387	0·735	0·124	0·387
0·40	0·253	0·2707	0·315	0·563	0·257	0·498
0·80	0·386	0·3034	0·248	0·360	0·441	0·621
2·12	0·820	0·4000	0·170*	0·147	0·697	0·786

* Limit of convective core of radius 1·193 Emden units.

	$\frac{M_{core}}{M_s}$	$\frac{r_{core}}{r_s}$	r_s (Emden units)	$\frac{\mathscr{R}T_c r_s}{\mu G M_s}$	$\frac{\rho_{mean}}{\rho_c}$	$\frac{Br_s^{0.5}}{\mu^{7.5}M_s^{5.5}}\left(\frac{\mathscr{R}}{G}\right)^{7.5} \cdot 10^4$
Present paper	0·147	0·170	7·026	0·90	0·027	1·68
C. M. Bondi (7)	0·180	0·163	7·662	1·03	0·020	2·92
F. Hoyle and R. A. Lyttleton (2)	0·146	0·171	6·967	0·89	0·028	1·61
T. G. Cowling (1)	0·144	0·169	7·027	0·90	0·027	1·67

TABLE III

Electron opacity solutions for small values of S

A	Q(0·06)	Q(0·08)	Q(0·10)
0·125	0·063	0·070	0·075
0·150	0·077	0·084	0·091
0·175	0·090	0·099	0·107
0·200	0·103	0·113	0·122
0·225	0·117	0·128	0·137
0·250	0·131	0·144	0·154
0·275	0·145	0·160	0·173
0·300	0·160	0·176	0·192
0·350	0·188	0·210	0·231

TABLE IV

Kramers' opacity solutions for small values of S

A	Q(0·01)	Q(0·025)	Q(0·04)	Q(0·07)	Q(0·10)	N(0·10)	$\left(\frac{Q}{A}\right)_{0.10}$
0	0	0	0	0	0	0·2434	0·6147
0·1473	0·0495	0·0619	0·0698	0·0812	0·0900	0·2438	0·6111
0·2351	0·0784	0·0977	0·1105	0·1289	0·1440	0·2443	0·6124
0·3243	0·1072	0·1336	0·1510	0·1772	0·2000	0·2451	0·6166

PART II

1. The equations determining stellar structure are based on the fact that at every point of a star in a steady state the conditions of (i) mechanical equilibrium and (ii) energy equilibrium must be satisfied. Condition (ii) implies that the rate of outflow of energy must balance the local energy generation. A small violation of condition (i) can be shown to lead to significant changes in the star very much more quickly than a comparable violation of condition (ii), and (i) must therefore be satisfied much more accurately. Condition (ii) can take many forms which vary from one part of a star to another, whereas condition (i) is everywhere expressed by the equation of hydrostatic support

$$\frac{dP}{dr} = -\frac{GM\rho}{r^2} \tag{1}$$

together with the equation of conservation of mass

$$\frac{dM}{dr} = 4\pi r^2 \rho. \tag{2}$$

We shall therefore consider first the vital condition (i), and keep it separate from the subsidiary condition (ii), the various forms of which will be considered later. This separation enables one to make approximations in (ii) without impairing the accuracy with which (i) is satisfied.

Since the physical variables occurring in (1) and (2) must always be finite, it follows that M and P are always continuous functions of r. There is no such limitation on ρ and in fact it is easy to construct stellar models with one or more discontinuities in ρ.

Equations (1) and (2) have the important property that if they are satisfied by a set of functions $M=f(r)$, $\rho=g(r)$, $P=h(r)$, then the set $M=\beta f(\alpha r)$, $\rho=\alpha^3\beta g(\alpha r)$, $P=\alpha^4\beta^2 h(\alpha r)$ (where α, β are any two positive real numbers) will also satisfy the equations (1) and (2). This may be proved easily by direct substitution. This property is expressed by saying that the equations admit of two homologies.

Combinations of our variables can be constructed which are independent of α and β and these are known as homology-invariant (h-) variables. Since we have four physical (p-) variables and two homology parameters α, β, two h-variables independent of α, β and of each other can be constructed. Several such pairs of independent h-variables have been introduced by various authors in connection with Emden's equation.

It is advantageous to work in h-variables rather than in p-variables, since the homology constants which appear as constants of integration in the p-equations must be absent in the h-equations and these will accordingly be of lower order. We therefore work mainly in h-variables.

It is clearly desirable to choose as independent h-variable one which has no discontinuities throughout the star. Such a variable must not involve ρ and therefore can only depend on M, P and r, and the only non-dimensional h-variable which can be constructed from these is:

$$S = 4\pi \frac{r^4 P}{GM^2} \tag{3}$$

(or any function of S). Accordingly S will be our independent h-variable, taking the position corresponding to that of r among the p-variables. Since S has not been amongst the h-variables used by other writers in the past, we cannot use any of the pairs of h-variables previously introduced.

The choice of our second h-variable is arbitrary, but it is naturally desirable to select it so as to render the later equations as simple as possible. From this point of view it turns out that the most suitable choice is:

$$Q = Pr/GM\rho. \tag{4}$$

The continuity of Q will be examined later.

Equations (1) and (2) do not form a complete set, since they contain three dependent p-variables, and another condition is supplied by the energy transport equation. Correspondingly there is no direct connection between Q and S as a consequence of equations (1) and (2) only. It will be found useful to introduce another variable defined as:

$$N = 1 - \frac{d\log\rho}{d\log P} = 1 - \frac{1}{\rho}\frac{d\rho}{dr}\Big/\frac{1}{P}\frac{dP}{dr}. \tag{5}$$

Since N is unaltered by any change of scale in ρ, P or r, it may also be considered to be an h-variable. It is closely related to the polytropic index n and, under certain conditions, $N = 1/(n+1)$. We shall regard N and Q as functions of S.

It may be proved by substitution that, as a consequence of (1) and (2),

$$\frac{S}{Q}\frac{dQ}{dS} = \frac{S+N-Q}{1+2S-4Q}. \tag{6}$$

This equation is therefore the expression of the laws of hydrostatic support and mass conservation in h-variables, and it determines the variation of $Q(S)$. We shall look to the energy transport equation to supply us with the law of variation of N as a function of S, but by what has been said previously this is definitely a subsidiary condition and (6) is our principal equation, universally valid. Generally N is found to be a slowly varying function of S.

In order to consider a specific stellar model our procedure will be to find first the equations determining the variation of N (and of such auxiliary variables as it may be desirable to introduce) in the various zones of the star. The universally valid equation (6), together with these equations and the boundary conditions to be discussed in the next section, will then determine $Q(S)$ and $N(S)$. Once the problem has been solved in h-variables we must return to the p-variables. The following formulae (easily proved by substitution from (1) and (2)) are useful in showing the significance of the h-variables, and are the basis of the formulae (8) which are required for transforming from h-variables to p-variables:

$$\left.\begin{aligned} &\frac{r}{P}\frac{dP}{dr} = \frac{d\log P}{d\log r} = -\frac{1}{Q}, \quad \frac{r}{\rho}\frac{d\rho}{dr} = \frac{d\log\rho}{d\log r} = -\frac{1-N}{Q}, \\ &\frac{r}{M}\frac{dM}{dr} = \frac{d\log M}{d\log r} = \frac{S}{Q}, \quad \frac{r}{S}\frac{dS}{dr} = \frac{d\log S}{d\log r} = -\frac{1+2S-4Q}{Q}, \end{aligned}\right\} \tag{7}$$

$$\left.\begin{aligned} \log r &= \text{const.} - \int\frac{Q\,dS}{S(1+2S-4Q)} = \text{const.} - \int\frac{dQ}{S+N-Q}, \\ \log M &= \text{const.} - \int\frac{dS}{1+2S-4Q}, \\ \log P &= \text{const.} + \int\frac{dS}{S(1+2S-4Q)}, \\ \log\rho &= \text{const.} - \int\frac{(1-N)\,dS}{S(1+2S-4Q)}. \end{aligned}\right\} \tag{8}$$

Usually it is only necessary to carry out one of the quadratures (8). The other p-variables can then be found from the definitions of S and Q, and from the functional relation between N and the p-variables which arises as a consequence of the energy transport condition. This relation is discussed in the next section, and the various forms it can take are listed in the appendix to Part I. The constants of integration in (8) can be determined from the boundary conditions.

2. In order to specify the state of the material of the star more closely, it is necessary to introduce a number of additional p-variables. In particular the following are required :—the temperature T, the mean molecular weight μ, the hydrogen abundance X, the helium abundance Y and the luminosity (rate of flow of energy) $L(r)$.

There are a number of relations connecting the p-variables with one another, which we shall now describe.

The pressure and the density are related at each point by the equation of state. As long as we are dealing with a non-degenerate gas (i.e. except when we are considering white dwarfs) the equation is :

$$P = \mathscr{R}\rho T/\mu + \tfrac{1}{3}aT^4, \tag{9}$$

where $\mathscr{R}$ is the gas constant and a is Stefan's constant. The second term, the radiation pressure, is often, though not always, negligible.

X, Y and μ are connected by a relation which can often be represented with sufficient accuracy by

$$\mu = 4(2 + Y + 6X)^{-1}. \tag{10}$$

The energy transport equation shows how the flow of energy $L(r)$ depends on the local conditions. In a zone of the star in radiative equilibrium it is of the form

$$L(r) = -r^2 \frac{dT}{dr} F(\rho, T, \mu, X, Y). \tag{11}$$

The function F is highly complicated but it can be approximated by simple functions in many cases. The most important of these are listed in the appendix to Part I, where the equations satisfied by N as a consequence of each of these various simplified forms are also given.

In a zone in convective equilibrium, part of the energy transport is due to the convection currents. Equation (11) is still important for the purpose of checking that the radiative and convective modes of transfer are supplementary and not opposed. The convection transfer depends, however, on the detailed arrangement of the convective currents and is usually not investigated. A relation can be obtained from the consideration that the distribution of the p-variables must be close to the critical distribution which divides convectively stable and unstable arrangements. For a convective zone must be on the unstable side of this critical distribution, but it cannot be far from it, for otherwise the convection currents would become extremely powerful and so rearrange the material as to make it less unstable. The relation and its consequences are discussed in the appendix to Part I.

Finally we must consider how the distribution of sources $(1/4\pi \,.\, r^{-2}dL(r)/dr)$ is determined by the law of energy generation. Usually we are considering stars with nuclear liberation of energy which is believed to be governed by Bethe's law. *Qualitatively* we can deduce two facts from the extremely critical temperature dependence characteristic of this law. First, the bulk of the energy will be liberated in the hottest part of the star that contains an appreciable fraction of

hydrogen. Normally this is a small region surrounding the centre. Second, stability considerations show that most, if not all, of the energy-producing region must be in convective equilibrium. Since the equation governing convective equilibrium does not involve $L(r)$, it follows that the problem of the detailed distribution of the sources need not enter into the equations determining the structure of the star. The only remaining condition to be satisfied is then the *quantitative* one, that the total energy L produced in the interior equals the flow of energy through the outer (radiative) layers. This will be discussed at the end of the next section.

3. We now have to consider the conditions which the h-variables must satisfy at the centre and surface of the star and at the borders of two zones with different mechanisms of energy transport.

(i) Centre of the star.

Central values of all variables will be denoted by the suffix c. The behaviour of the p-variables is

$$r\to 0, \quad M\to 0, \quad \rho\to\rho_c, \quad P\to P_c, \quad T\to T_c, \quad Mr^{-3}\to 4\pi\rho_c/3.$$

Accordingly, $S\to\infty$, $Q\to\infty$ but $S/Q\to 3$.

In general N will tend to a definite limit N_c. It follows that near the centre $Q=Q_E(S;N_c)$, where $Q_E(S;N)$ is the special solution of equation (6) discussed in Section 4.

(ii) Surface of the star.

Surface values of all variables will be denoted by the suffix s. $r\to r_s$, $M\to M_s$, ρ, P and T tend to somewhat indefinite values which are very small compared with their average values in the star. Therefore, both S and Q will attain very small values there. In the case of the Sun the values would be of order 10^{-12} and 10^{-3} respectively. By considering the behaviour of the (S, Q) curves it can be seen that the continuation to $S=0$ of the solution which represents the star for $S>10^{-12}$ will always run to the point $S=0$, $Q=0$. The error involved in putting the surface values of S and Q equal to zero (corresponding to $P_s=0$, $T_s=0$) can be shown to be very small, involving an error in r_s of less than one part in 10^3, and it is similarly small for the other variables.

We shall therefore always put $S=0$, $Q=0$ at the surface of the star.

The behaviour of N may be ascertained from the energy transport equation valid near the surface, and it is found that N tends to a surface value N_s. Therefore $Q\sim AS^{N_s}$ near the surface where A is a constant not specified by the surface boundary conditions.

(iii) Interface.

The p-variables r, M, P, T, L are always continuous, while ρ, μ, X, Y need not be continuous. The continuity of r, M and P ensures the continuity of S; the continuity of P and T ensures by (9) the continuity of ρ/μ and hence of μQ. Q will therefore be discontinuous at a surface of discontinuity of μ. The continuity of L will, by means of the energy transport equation, determine the variation of N at the interface. It must be remembered in this connection that near the outside edge of a convective region the conditions are such as to decelerate the outward moving convection currents, and accordingly the energy transport will there be almost entirely by radiation. This condition determines the variation of N at the interface of a convective and a radiative region. In particular, if the composition is unchanged at the interface, N will be continuous there.

We can now evaluate the constants in (8) and find

$$\left.\begin{aligned} \log\frac{r_s}{r} &= \int_0^S \frac{Q\,dS}{S(1+2S-4Q)}, \\ \log\frac{M_s}{M} &= \int_0^S \frac{dS}{1+2S-4Q}, \\ \log\frac{P_c}{P} &= \int_S^\infty \frac{dS}{S(1+2S-4Q)}, \\ \log\frac{\rho_c}{\rho} &= \int_S^\infty \frac{dS(1-N)}{S(1+2S-4Q)}. \end{aligned}\right\} \tag{12}$$

These equations describe the variation of the p-variables for a stellar model for which Q and N have been determined as functions of S. The four scale constants r_s, M_s, P_c, ρ_c cannot, however, be assigned arbitrarily.

One relation between them is due to the fact that

$$\rho_c = \lim_{r\to 0} 3M/4\pi r^3.$$

Hence

$$\begin{aligned} \log \rho_c/\rho_{\text{mean}} &= \log 4\pi r_s^3\rho_c/3M_s = \lim_{r\to 0}\,[3\log r_s/r - \log M_s/M] \\ &= \lim_{S\to\infty} \int_0^S \frac{(3Q-S)\,dS}{S(1+2S-4Q)} = \int_0^\infty \frac{(3Q-S)\,dS}{S(1+2S-4Q)}. \end{aligned} \tag{13}$$

The other relation follows from the definition of Q :

$$\log Q = \log Pr/GM\rho = \log P_c r_s/GM_s\rho_c + \log r/r_s + \log P/P_c - \log M/M_s - \log \rho/\rho_c,$$

so that

$$\log\frac{P_c r_s}{G\rho_c M_s} = \log Q + \int_0^S \frac{(Q-S)\,dS}{S(1+2S-4Q)} + \int_S^\infty \frac{N\,dS}{S(1+2S-4Q)}. \tag{14}$$

If there are discontinuities in Q, suitable allowance for these has to be made through appropriate infinities in N. Equations (13) and (14) establish two relations between the four scale constants, so that (with a given variation of N and Q with S) there are only two free scale constants. A further limitation arises if Bethe's law is assumed to govern the rate of generation of energy.

The equation of radiative transfer applied near the surface establishes a connection between the total luminosity L_s, M_s and r_s (the mass-luminosity-radius relation). On the other hand, the variations of T/T_c and ρ/ρ_c with r/r_s follow by (12) if N and Q are known functions of S. Therefore, by integrating Bethe's law throughout the energy-producing part of the star, L_s can be found as a function of T_c, ρ_c and r_s. Equating these two expressions for L, we find another relation between the scale constants, leaving only one parameter free.

If account is taken either of the radiation pressure or of the guillotine factor (or some process involving the addition of different terms), then some further assumption has to be made (such as the adoption of a definite value for the ratio of radiation pressure to total pressure at the centre of the star) which fixes this last free parameter, so that only one star corresponds to a given solution in the h-variables. If, however, radiation pressure is neglected and a simple opacity law assumed, then we are left with a free parameter (usually taken to be the mass M_s). Therefore in such a case a series of stars corresponds to any solution in the h-variables.

4. The solutions of equation (6) for constant N are of great importance to the method of integration here presented, since any general solution consists of

portions of constant N solutions changing slowly from one value of N to the next. It is clear from its derivation that (6) for constant N is Emden's equation expressed in h-variables. The following well-known results may be briefly restated in these variables:

Only $Q \geqslant 0$, $S \geqslant 0$ are of physical importance, and for the simpler problems it is sufficient to consider only the ranges $S \geqslant 0$, $(1+2S)/4 \geqslant Q \geqslant 0$, $0{\cdot}40 \geqslant N \geqslant 0{\cdot}25$. In this region all the solutions start at $S=0$ with $Q \sim AS^N$, where A is an arbitrary positive constant.

There is a critical value A_c of A. If $0 < A < A_c$ the solution runs to infinity, and Q^2/S tends to a limit as $S \to \infty$. If $A > A_c$ the solution has a point of inflexion beyond which it crosses the line $1+2S-4Q=0$ with a vertical tangent. These two types of solutions are separated by the solution for which $A = A_c$. This is the Emden function and is denoted by $Q_E(S;N)$. For large S,

$$Q_E(S;N) = \tfrac{1}{8}S + O(1).$$

The results of graphical integrations of (6) for four constant values of N are given in the figures*. The integrations were carried out in the usual way by drawing the curves of constant dQ/dS and the locus of the points of inflexion which is a cubic most easily drawn in polar coordinates with $S = \frac{1}{2} - 2N$, $Q = \frac{1}{2} - N$ as origin.

For small S (say $S < 0{\cdot}1$) the curves are no longer useful and one can proceed either by numerical integration or by integrating graphically on log-log paper ($\log Q$ against $\log S$).

5. In this section we give brief derivations of the formulae of the appendix to Part I. The equations will be given the same numbers as they have there and in Part I.

$$\frac{dT}{dr} = -B\frac{\rho^\sigma}{r^2 T^\nu}. \tag{26}$$

We divide by

$$\frac{dP}{dr} = -\frac{GM\rho}{r^2},$$

and note that, in the absence of radiation pressure,

$$N = d\log T / d\log P.$$

Hence

$$N = \frac{B\rho^{\sigma-1}P}{GMT^{\nu+1}} = \frac{B}{G}\left(\frac{\mathscr{R}}{\mu}\right)^{\nu+1}\frac{\rho^{\sigma+\nu}}{MP^\nu},$$

$$\frac{r}{N}\frac{dN}{dr} = (\sigma+\nu)\frac{r}{\rho}\frac{d\rho}{dr} - \nu\frac{r}{P}\frac{dP}{dr} - \frac{r}{M}\frac{dM}{dr}$$

$$= -(\sigma-\nu)\frac{1-N}{Q} + \frac{\nu}{Q} - \frac{S}{Q} = -\frac{\sigma+S-(\sigma+\nu)N}{Q}.$$

Equations (9) and (27) follow immediately.

Multiplying the expression for N by $Q^{\nu+\sigma}S^{-\sigma}$, (25) and (28) are established.

A similar treatment establishes (31), from which (30) is deduced by logarithmic differentiation.

In the case of mixed opacities

$$-\frac{N}{Q} = N\frac{r}{P}\frac{dP}{dr} = \frac{r}{T}\frac{dT}{dr} = -\frac{C}{GMQ}\left(\frac{\mathscr{R}}{\mu}\right)^4\frac{\rho^4}{P^3}\left[1 + \frac{B}{C}\left(\frac{\mathscr{R}}{\mu}\right)^{3\cdot5}\frac{\rho^{4\cdot5}}{P^{3\cdot5}}\right]$$

by (32).

* See Introduction.

Let

$$1+\frac{B}{C}\left(\frac{\mathscr{R}}{\mu}\right)^{3\cdot5}\frac{\rho^{4\cdot5}}{P^{3\cdot5}}=\frac{1}{1-\omega}.$$

Hence

$$\frac{r}{N}\frac{dN}{dr}=-\frac{r}{M}\frac{dM}{dr}+[4(1-N)-3]\frac{r}{P}\frac{dP}{dr}+\frac{r}{1-\omega}\frac{d\omega}{dr}.$$

But

$$r\frac{d}{dr}\log\frac{\omega}{1-\omega}=\frac{r}{\omega(1-\omega)}\frac{d\omega}{dr}=[4\cdot5(1-N)-3\cdot5]\frac{r}{P}\frac{dP}{dr}=-\frac{1-4\cdot5N}{Q}.$$

Therefore

$$\frac{r}{N}\frac{dN}{dr}=-\frac{S}{Q}-\frac{1-4N}{Q}-\omega\frac{1-4\cdot5N}{Q},$$

and (33) follows from this.

Finally

$$\frac{SN^5}{Q^7}=\left[\frac{C}{GM}\left(\frac{\mathscr{R}}{\mu}\right)^4\frac{\rho^4}{P^3(1-\omega)}\right]^5 4\pi\frac{Pr^4}{GM^2}\left[\frac{GM\rho}{Pr}\right]^7$$
$$=\frac{4\pi C^5G\mathscr{R}^{20}\rho^{27}}{\mu^{20}r^3\rho^{21}(1-\omega)^5}=\frac{4\pi C^5G\mathscr{R}^{20}}{r^3\mu^{20}(1-\omega)^5}\left(\frac{\omega}{1-\omega}\right)^6\frac{C^6}{B^6}\left(\frac{\mu}{\mathscr{R}}\right)^{21},$$

from which (34) follows.

In order to derive (39), we write Lyttleton's equation (**6**) in the form

$$4Z+\frac{1}{\Gamma-1}\log T-\log\rho=\text{const.}$$

It follows that

$$T=[BZ\exp(4Z)]^{\frac{\Gamma-1}{3\Gamma-4}},$$
$$\rho=a\mu T^3/3\mathscr{R}Z,$$
$$P=(1+Z)aT^4/3Z,$$
$$Z(1+Z)^3=aP^3\mu^4/3\mathscr{R}^4\rho^4,$$
$$1-N=\frac{d\log\rho}{d\log P}=P\frac{d\rho}{dZ}\Big/\rho\frac{dP}{dZ}=\frac{(1+Z)(n+12Z)}{n+1+20Z+16Z^2},\qquad(41')$$

where $n=1/(\Gamma-1)$. Also

$$r\frac{d}{dr}\left(\log\frac{P^3}{\rho^4}\right)=-\frac{4N-1}{Q}=\left(\frac{1}{Z}+\frac{3}{1+Z}\right)r\frac{dZ}{dr}.$$

Hence

$$\frac{4Z+1}{(Z+1)Z(4N-1)}\frac{dZ}{dS}=\frac{1}{S(1+2S-4Q)}.$$

Integration and substitution leads to (39).

In order to discuss radiative equilibrium we consider the case when

$$\frac{dT}{dr}=-\frac{C}{r^2}\left(\frac{\rho}{T^3}\right)^{\nu}.$$

The case $\nu = 1$ corresponds to electron opacity, while $\nu = 2$ corresponds to the modified Kramers' law.

$$\frac{dP}{dr} = \frac{d}{dr}\left(\frac{\mathscr{R}\rho T}{\mu} + \frac{aT^4}{3}\right) = \frac{\mathscr{R}T}{\mu}\frac{d\rho}{dr} + \frac{\mathscr{R}\rho}{\mu}(1+4Z)\frac{dT}{dr}$$
$$= \frac{\mathscr{R}\rho T}{\mu P}(1-N)\frac{dP}{dr} - \frac{\mathscr{R}\rho}{\mu}(1+4Z)\frac{C}{r^2}\left(\frac{a\mu}{3\mathscr{R}Z}\right)^{\nu}.$$

Hence

$$-\frac{N+Z}{1+Z}\frac{dP}{dr} = \frac{N+Z}{1+Z}\frac{GM\rho}{r^2} = \frac{\mathscr{R}\rho}{\mu}(1+4Z)\frac{C}{r^2}\left(\frac{a\mu}{3\mathscr{R}Z}\right)^{\nu}.$$

Therefore

$$N+Z = \left(\frac{\mathscr{R}}{\mu}\right)^{1-\nu}\frac{C}{GM}(1+Z)(1+4Z)\left(\frac{a}{3Z}\right)^{\nu}$$
$$= \left(\frac{a\mu}{3\mathscr{R}}\right)^{1+\nu}\left(\frac{12\pi G}{a}\right)^{\frac{1}{2}} C\frac{Q^2(1+4Z)}{S^{\frac{1}{2}}Z^{\nu+\frac{1}{2}}(1+Z)^{\frac{1}{2}}},$$

by (36). Equations (43) and (48) follow immediately.

The equation

$$aP^3\mu^4/3\mathscr{R}^4\rho^4 = Z(1+Z)^3$$

holds, just as in the convective case. Equation (45) is deduced by logarithmic differentiation.

In the case of the contracting star we have

$$\bar{P} = -\frac{E}{z^2}\frac{d}{dz}\left[\frac{z^2\bar{T}^3}{\bar{\rho}}\frac{d\bar{T}}{dz}\right], \tag{53}$$

where E stands for the constant $4\pi ac(\Gamma-1)/3K(1+X)(3\Gamma-4)$.

Using the relation

$$\frac{z}{\bar{T}}\frac{d\bar{T}}{dz} = N\frac{z}{\bar{P}}\frac{d\bar{P}}{dz} = -\frac{N}{Q},$$

we obtain

$$\bar{P} = \frac{E}{z^2}\frac{d}{dz}\left[\frac{z\bar{T}^4}{\bar{\rho}}\frac{N}{Q}\right] = \frac{E\bar{T}^4}{z^2\bar{\rho}}\frac{N}{Q}\left[1 - \frac{5N-1}{Q} + z\frac{d}{dz}\log\frac{N}{Q}\right],$$

$$\frac{z^2\bar{\rho}\bar{P}}{E\bar{T}^4} = \frac{N}{Q}\left[1 - \frac{5N-1}{Q} - S\frac{1+2S-4Q}{Q}\frac{d}{dS}\log\frac{N}{Q}\right].$$

Equation (13′) is derived from this by differentiation and substitution from (4).

Newnham College, Cambridge:
1948 *December* 7.

Trinity College, Cambridge.

References

(1) T. G. Cowling, *M.N.*, **96**, 42, 1935.
(2) F. Hoyle and R. A. Lyttleton, *M.N.*, **102**, 218, 1942.
(3) L. H. Thomas, *M.N.*, **91**, 122, 1930.
(4) T. G. Cowling, *M.N.*, **94**, 768, 1934.
(5) M. H. Harrison, *Ap. J.*, **102**, 216, 1945.
(6) R. A. Lyttleton, *M.N.*, **106**, 228, 1946.
(7) C. M. Bondi, *M.N.*, **108**, 324, 1948.
(8) L. R. Henrich, *Ap. J.*, **98**, 192, 1943.

HIGH INTENSITY REFLECTION INTERFEROMETRY FOR WEAK SOURCES

S. Tolansky and J. Ranade

(Received 1948 December 15)

Summary

It is shown how the Fabry-Perot interferometer can be modified so that fringes can be used in reflection. The value of this procedure is that the high spectroscopic resolution and high dispersion of the interferometer become available without any effective loss in light, the arrangement being perhaps 30 times faster in light speed than when used as the normal transmission interferometer.

It is shown how the technique can be adapted to the measurement of wave-lengths and to the precision evaluation of the line-widths of weak sources.

Apart from solar studies, high resolution spectroscopic interferometry has as yet hardly found application in astrophysics. The reason is, of course, to be attributed to the question of available light intensities. It is first necessary to disperse the spectrum to be examined either before or after crossing with the interferometer and then, as is well known, the interferometer itself leads to additional considerable loss of light. If it were not for this, one could readily see considerable application to astrophysics. In particular, studies with the variable-gap silvered Fabry-Perot interferometer would be of very obvious value. It need only be recalled that a well-silvered interferometer varying from 1 to 10 mm. in plate separation offers a resolving power range of from 100,000 to 1,000,000, and with an associated high dispersion. With such simple equipment, high precision wave-lengths can be obtained, and what is perhaps of more interest, high dispersion studies of line-widths and line contours can be carried out.

It is the object of this paper to describe how in fact such observations can be made with a Fabry-Perot interferometer by employing *reflection* instead of the usual transmission fringes, and some laboratory applications are described. An earlier preliminary notice has already appeared* with some approximate calculations.

It will be shown that the particular feature distinguishing this reflection technique is that the interferometer then introduces practically no light loss at all. It will be seen, in what follows, that the decisive factor limiting applicability is the *absorption* of light in the thin film of highly reflecting silver which is deposited on the pair of parallel optical flats constituting the interferometer. This is an aspect usually avoided in the text-books dealing with the instrument.

The intensity of the fringes in transmission has already been treated (*loc. cit.*) and one finds that a good high definition Fabry-Perot interferometer rarely transmits more than a few per cent of the incident light. A reduction by a factor of 30 is a common experience. This is the principal objection to the use of the instrument and because of it faint light sources are excluded. For to this difficulty must be added the sensitivity of the instrument to variations in temperature, pressure, shock and mechanical change in springs, etc. holding the flats.

* *Physica*, **12**, 649, 1946.

These are such that exposures over more than, say, 4 hours usually exhibit disturbances. Since one cannot always tolerate the considerable light loss, the transmission instrument has not therefore been applied in spectroscopy to the weaker sources, such as, for instance, usually occur in astrophysical work.

Reflection fringes.—Although the use of two-beam *reflection* fringes in metrology, etc. is a commonplace, the *reflected* Fabry-Perot multiple-beam fringes have not apparently been used in high resolution spectroscopy, and apart from the preliminary notice in *Physica* (loc. cit.) there appears to be no mention in the literature of their use. In what follows, it will be shown that such reflection fringes can in fact be employed in a strictly limited number of ways, and in each case the essential striking fact is that the employment of the interferometer does not produce any effective reduction in intensity. It will be shown that the critical factor is the absorption in the film, but whereas in transmission it is *intensity* that is affected, in reflection it is *visibility* that is involved.

It can readily be shown that in the absence of absorption the reflection fringes are effectively complementary to the transmission fringes, consisting of fine narrow dark fringes on a broad bright background. Since the first reflected beam does not traverse a silver film, whilst the succeeding beams each traverse the first film twice, the first beam is out of phase with succeeding beams. A detailed analysis of the effects of this shows that such influences are only of consequence when the reflectivity is much too low to be considered at all suitable for the Fabry-Perot interferometer (see J. Holden, M.Sc. Thesis, Univ. Manchester, 1948). Thus in the absence of absorption it can be shown that to sufficient accuracy the reflected fringe intensity is given by

$$I = R + \left(\frac{T^2R + 2TR^2 - 2TR\cos\delta}{1 + R^2 - 2R\cos\delta} \right),$$

in which R, T are respectively reflection and transmission coefficients and δ the phase lag. This gives $I_{max} = 4R/(1+R)^2$ as the intensity of the maxima and $I_{min} = 0$ as the intensity of the minima; in fact, to see the graphical distribution, one merely inverts the familiar distribution of the transmission fringes. Now the quantity $I_{max} = 4R/(1+R)^2$ is almost unity for the R values to be used. Indeed, even if R is as low as 70 per cent, I_{max} has only fallen to 0·97. The maxima of the reflected fringes are therefore effectively as bright as if no interferometer had been inserted at all, whilst the troughs of the minima have true zero intensity. Clearly, if these reflected fringes can be used, then one is able to use the attendant high resolution without increasing exposure time at all.

When, however, the effect of absorption is taken into account, it is found to modify the *visibility* of the reflection fringes profoundly. Substitution for inclusion of absorption of a fraction A in the expression for the intensities leads to the following: the maxima instead of having the value

$$I_{max} = \frac{4R}{(1+R)^2} \quad \text{become} \quad I_{max} = \frac{4R}{(1+R)^2} \cdot \left(1 - A + \frac{A^2}{4}\right)$$

or closely enough $4R(1-A)/(1+R)^2$, since A is small compared with unity. That the effect of absorption on the intensity of the maxima is indeed slight, is shown in Table I, where the second row gives the values of I_{max} for the various reflectivities reported formerly for the green region with evaporated silver (see *Physica*, loc. cit.).

TABLE I

R (per cent)	60	70	75	80	85	90	94
I_{max}	0·89	0·94	0·94	0·95	0·95	0·93	0·93
I_{min}	0·007	0·01	0·01	0·02	0·08	0·27	0·76
I'_{min}	0·01	0·01	0·02	0·04	0·13	0·38	~0·93

In the region of practical reflectivities (80–95 per cent) the intensity of the maxima is merely some 5 per cent less than that of the incident light. Not so, however, is the effect on the minima. Instead of $I_{min}=0$ the effect of absorption leads to $I_{min}=RA^2/(1-R)^2$. The values for I_{min} are shown in row 3 in Table I, and it will be seen that whereas the minima are of the order of only 1 per cent of the intensity of the maxima for reflectivities below 75 per cent, they mount rapidly and at reflectivity $R=94$ per cent they have an intensity which is as great as some 80 per cent of the maxima.

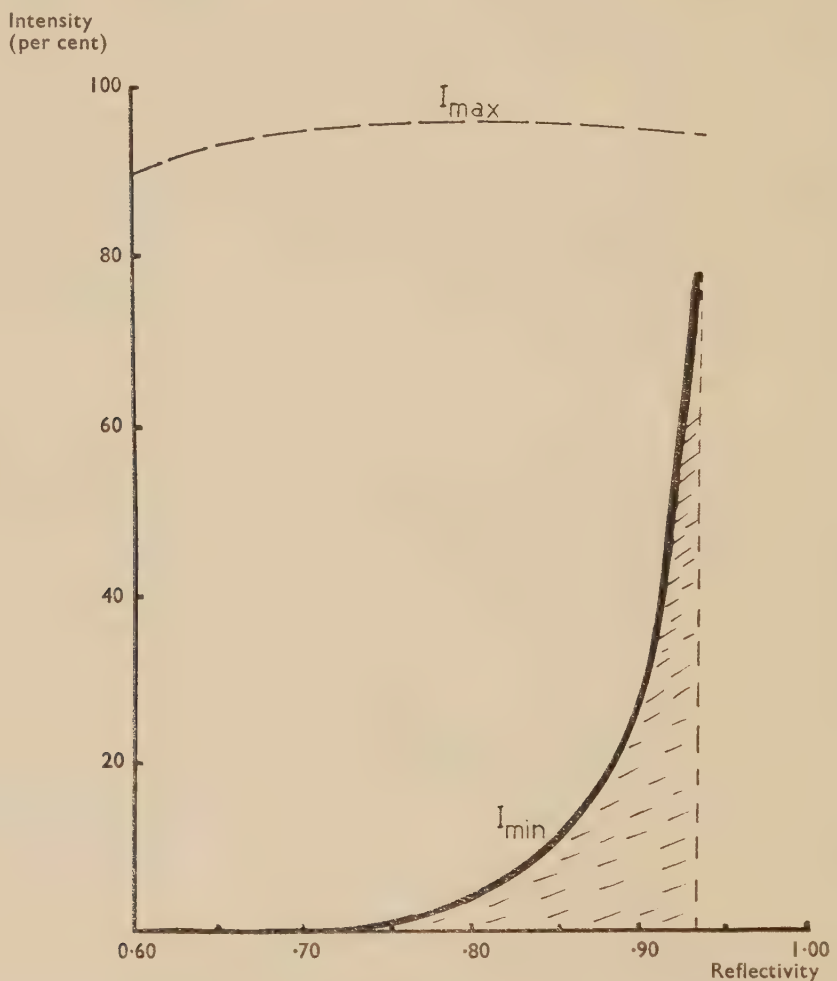

FIG. 1.

Fig. 1 shows the variations of I_{max} (upper dotted line) and I_{min} (continuous line) with change of R. The interpretation is clear. As the reflectivity increases, the effect of absorption is to reduce the visibility of the fringes. One can imagine the dotted line as representing the maximum, and fringes dipping down from this

level to reach the line of the minima. It is as if the dark fringe were diluted by the addition of the light represented by the shaded region below the curve of the minima. With the higher reflectivities the dilution is considerable and the visibility seriously affected.

Just as the intensity in the transmitted system is very sensitive to the absorption, so the visibility in the reflected system is indeed more sensitive. Fig. 2 shows the higher reflectivity region of Fig. 1 with an added curve (broken line), showing the effect of increasing the absorption fraction by only 1 per cent. The effect of this small increase is so great that, with R above 90 per cent, fringes are hardly visible at all. (These dotted minima are shown as I'_{min} in Table I.) Hence the greatest care is needed to avoid increasing the absorption in preparing the silver films. *The reflected system is much more sensitive to absorption than is the transmitted system* and thus experimentally more difficult to produce with high visibility.

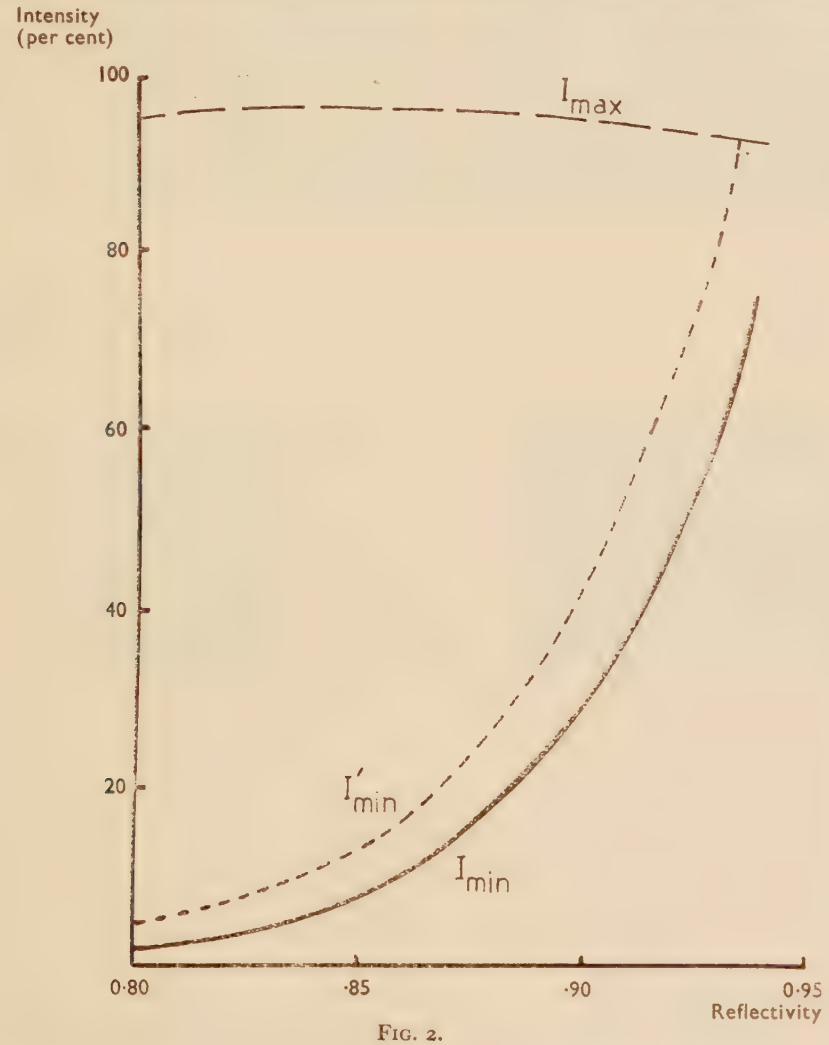

FIG. 2.

It is clear, from the curves, that at low reflectivities one obtains broad fringes with excellent visibility, whilst at high reflectivities one obtains narrow fringes which are difficult to see. In the earlier note published, only very approximate calculations

were made, yet the tentative results then reached about the higher and more important reflectivities are amply supported by the present more comprehensive conclusions. (The visibilities formerly given for the *lower* and *less* important reflectivities are somewhat inferior to those calculated here, but as, in any event, the lower reflectivities are not employed with the interferometer the difference is not significant.)

It is evident that in order to obtain adequate reflection definition the absorption must be low, thus the reflecting coefficient of the first mirror must necessarily be kept low. Fortunately, it is possible to compensate for this by making the reflectivity of the back face as high as possible, higher than that possible in a transmission instrument. If a Fabry-Perot interferometer consists of two different mirrors with reflectivities R_1, R_2, then the resolving power of the combination is, closely enough, equal to that of a symmetrical instrument, with reflectivity $R = \sqrt{(R_1 R_2)}$. By making the back mirror so thick as to be opaque, one obtains a reflectivity $R_2 = 95$ per cent, possibly slightly higher, hence, even if one adopts only 80 per cent for R_1, the combination equals a symmetrical interferometer with $R = 87$ per cent, which is adequate for many purposes and gives excellent fringes. The observed value of A is 3·5 per cent for $R_1 = 80$ per cent. The optimum R_1 adoptable from the viewpoint of visibility is 75 per cent, for which A has the low value 3 per cent. The combination $\sqrt{(R_1 R_2)}$ is then 84 per cent, which is still tolerable.

With either of these R_1 values it is seen from Table I that the conditions of visibility are excellent, whereas with the normal $R_1 = R_2 = 90$ per cent used in transmission, visibility in reflection is poor. This explains why the ordinary transmission instrument does not give good reflection fringes, and possibly accounts for their neglect in the past.

Experimental arrangements.—The three possible methods which present themselves according to requirements are shown in Fig. 3. Fig. 3 (*c*) shows the most economical form, for in this a 30° Littrow prism is used and the silvered face of this is used as one face of the interferometer. However, the prism face requires special working to the high degree of planeness needed for an interferometer. Tests made on existing prisms show that definition usually suffers through an insufficiently accurate figuring of the prism face. Both 3 (*b*) and 3 (*c*) suffer from the defect that only wave-lengths at minimum deviation (normal incidence) show symmetrical fringe patterns, the fringes skewing off-centre on progressively moving from minimum deviation, and one cannot tilt the fringes off-centre, a procedure which is often desired. Hence in the experiments described here the 3 (*a*) mounting is exclusively employed.

Observations.—The reflection fringes illustrated in Plate 5 (*a*) were given by a neon tube excited by a high-frequency discharge. The slit is made very broad and a number of the red lines are shown with the dark reflection fringes crossing the lines. The interferometer gap was 3 mm. and exposure time was less than 1 second. Attention may be drawn both to the excellent contrast (good visibility) and to the fringe sharpness. Resolving power is a quarter of a million and the separation between orders 1·66 cm.$^{-1}$. The dispersion on the original plate is about 1 A. per centimetre or so. It is emphasized that high resolution and high dispersion are secured *with no effective loss of light*, hence the exposure time is that which would have been required with no interferometer. With fringes of such quality it is easy to measure with precision wave-lengths to certainly better than

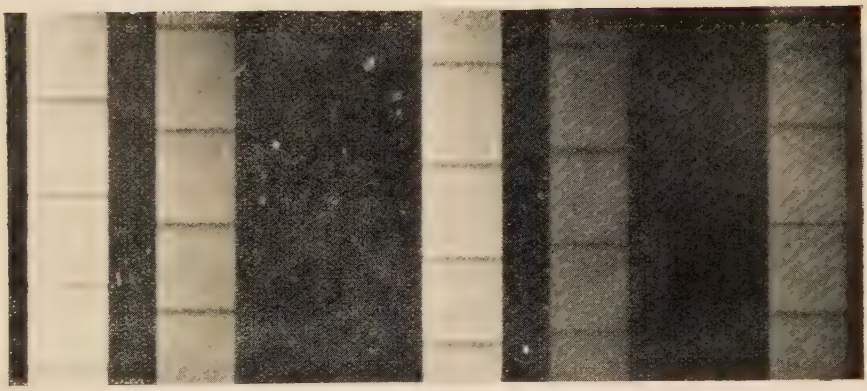

(a) Ne

(b) Hg

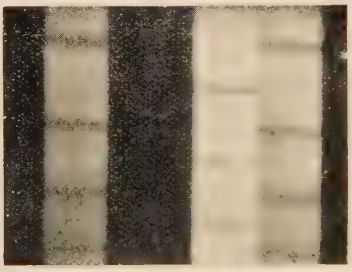

(c) Fe

0·001 A. by using standards in the normal manner, but then the centre of the fringe system would be thrown on to the slit in the routine manner and exact fractions evaluated.

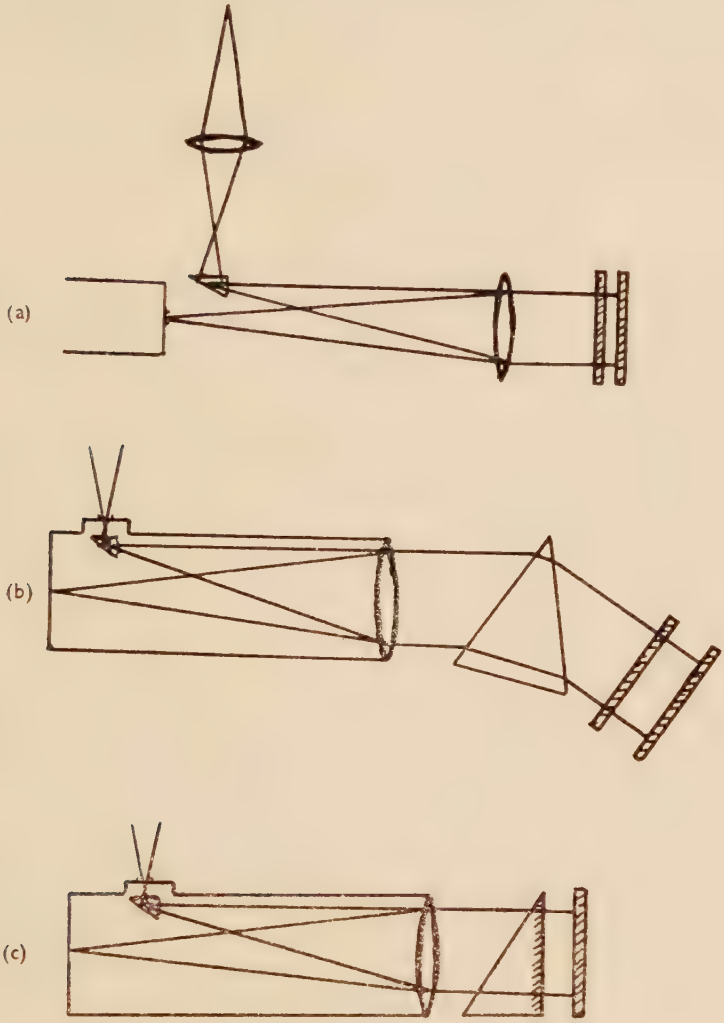

FIG. 3.

Plate 5 (*b*) shows the green and yellow lines of a mercury vacuum arc discharge. The slit width has been deliberately very much broadened to produce overlap of the two yellow lines, and it is apparent that even if the preliminary dispersion fails to separate lines, twin fringes can be seen, although visibility is impaired. The technique is thus capable of revealing hyperfine line structure but only in a very limited manner. For it is clear that when a line consists of more than one hyperfine structure component the background continuum of each fringe superposes and dilutes the minima of the other. Thus visibility suffers, and it follows that only close structure is revealed if the line in question has but very few components, each of comparable intensity. In this connection the doubling shown by many molecular band lines might offer a suitable object for study.

Line-widths.—There are many astrophysical and terrestrial weak sources about which line width information is desirable, and it should be possible also to estimate the temperatures in the upper atmosphere regions if reliable line-width data can be obtained from the feeble auroral lines, northern lights and night-sky spectra.

We have tested the application to widths on green line mercury sources in the following ways:—

(i) with a fixed interferometer, photographs have been taken of fringes from

(*a*) water-cooled vacuum arc,
(*b*) hot vacuum arc,
(*c*) hot high-pressure arc,

(ii) with a fixed interferometer, photographs have been taken of fringes from a hot high-pressure arc at successive stages in its warm-up to normal running pressure. The photographic speed of response is such that exposure is less than a second and a succession of photographs can thus easily be secured during normal warming-up time.

The increase in line-width leads to a fringe broadening readily recognizable, and we reproduce here in Fig. 4 microphotometer tracings made of adjacent pairs of fringes. In these the different traces are superposed but displaced in the vertical direction for clarity. The curve A in Fig. 4 (*a*) refers to the water-cooled vacuum arc and B to the hot vacuum arc. The increase in line-width is clearly shown in B. Fig. 4 (*b*) shows the high-pressure line source at various stages of broadening, A, B, C. Ultimately the source ran so hot that the interferometer gap used was too high to enable fringes to be recorded at all; i. e. the fringe width exceeded an order separation, and the fringes could not be seen. The slope of the zero line of the fringes arising because of non-uniform source does not significantly affect the recorded line-width. Fig. 4 (*c*) shows a series of fringes with a vacuum arc, A, B, C, D being given by currents of 1, 2, 3, 4 amps. respectively.

It is advisable to adapt the plate separations to the type of line-width to be studied. Inevitably, in view of the considerations already put forward in connection with hyperfine structure, it is apparent that the very line broadening itself appreciably reduces the visibility. But in this connection the flexibility of the variable gap Fabry-Perot is of value. The wider the line, i. e. the larger the fraction of an order occupied by the line, the more is the visibility affected. Conversely, when the line is narrowed, visibility improves. By reducing the plate separation, the fringe width can be shrunk and thus visibility retained as desired. One can continue this process until the instrumental fringe width is approached, in which case the effective instrumental fringe shape is then revealed. This is required for any specially precise evaluation of line-width. (According to usual practice, it is necessary to correct observed line width for instrumental fringe width.) Alternatively, a comparison spectrum of very sharp lines will reveal the instrumental width without the necessity for this procedure. It will be recognized that the numerical evaluation of line-width is more difficult experimentally than the precise determination of wave-length. On the other hand, the high dispersion is a great advantage, particularly since this is secured without loss of light. In Fig. 4 the separation between orders is 0·66 A.

No attempt has been made here to assess the true line-width as distinct from the combined instrumental and true line-widths which together form the fringe width, since the only object of this paper is to draw attention to the method and

not to make any specific measurements on mercury line-widths. The correction which needs to be made is not too difficult to apply and is best carried out directly by experiment. It can be done indirectly by calculation from a knowledge of the reflection and absorption factors, but this procedure is neither necessary nor advisable.

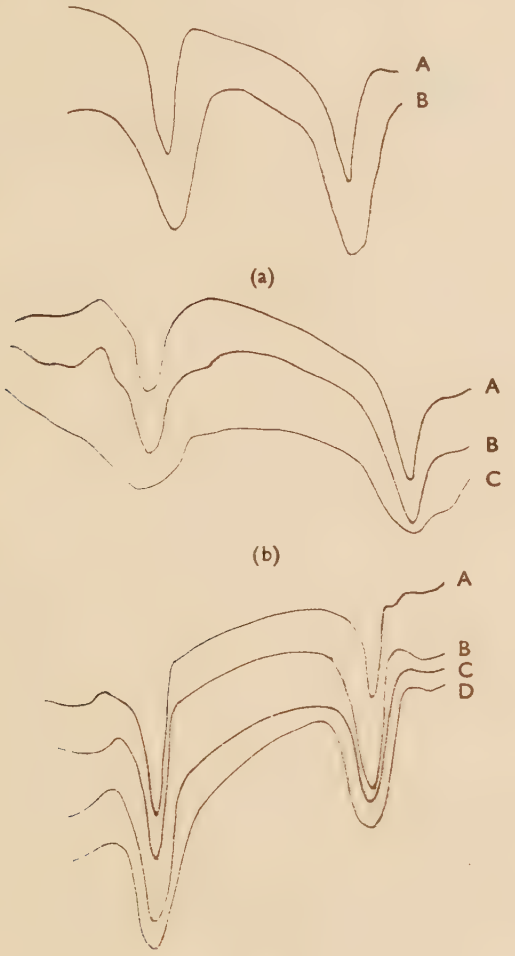

FIG. 4.

We have obtained excellent reflection fringes from an iron arc spectrum and from the Swan bands, thus demonstrating that the technique is adaptable to a many-lined complex spectrum providing the lines are separated by adequate preliminary dispersion. Plate 5 (*c*) shows fringes from an iron arc, using an instrumental gap of 1·5 mm., i. e. fringe separation 3·3 cm.$^{-1}$ and resolving power 125,000. Comparison with the neon or mercury lines in Plate 5 is striking, for despite the halving of the instrumental gap (which doubles the wave-number interval between orders) the fringes in Plate 5 (*c*) are much broader than those in Plate 5 (*a*), (*b*).

Royal Holloway College,
Englefield Green,
Surrey :
1948 *December* 14.

PHOTOMETRY OF NGC 5128

David S. Evans

(Received 1948 November 13)

Summary

Calibrated plates of NGC 5128 in red and blue light have been obtained and isophotes determined. These are approximately circular and show a brightness variation close to an inverse square law. It is suggested that the object consists of a concentrated source hidden behind obscuring matter and surrounded by a spherical mass of gas, and that it is probably not extra-galactic.

The nebula NGC 5128, position (1950) R.A. $13^h22^m.4$; Dec. $-42°45'$, is an object which has been the subject of much discussion in the past, and its nature has not yet been finally decided. It is a large bright object (photographic magnitude, according to Shapley and Ames *, 7·2) consisting of a luminous area unresolved into stars across which runs a broad, somewhat irregular belt of dark obscuring matter. Within this belt are disposed a number of irregularly shaped patches of luminosity, together with a number of stars which may either be foreground objects, or may be involved in this luminosity.

The Shapley-Ames Catalogue * classifies the nebula as irregular and of dimensions $10' \times 8'$. Shapley's catalogue † gives the dimensions as $25' \times 20'$. Gregory ‡ classifies the object as pretty bright, dimensions $7' \times 5'$ and gives the description, "a large patch of structureless and possibly gaseous nebulosity cut in two by a wide belt of absorbing matter through which appear several [illegible] and wisps of nebulosity". The same author gives a photograph §. Paraskevopoulos || gives a discussion of the literature in which he refers to a number of previous papers. He notes that H. D. Curtis ¶ classifies the object as an "edgewise spiral with a dark lane", whereas elsewhere ** the same author describes it as diffuse. Sir John Herschel †† had written "A similar but much more strongly marked case of parallel arrangement than that noticed by Mr Bond (in the Andromeda Nebula) is one in which two semi-ovals of an elliptically formed nebula appear cut asunder and separated by a broad obscure band parallel to the larger axis of the nebula, in the midst of which a faint streak of light parallel to the sides of the cut appears".

Dreyer ‡‡ described it as "Bifid, very bright, very large, very much extended in P.A. 122°·5". Paraskevopoulos discusses briefly a five-hour exposure taken at Arequipa, Peru, in 1926 with the 24-inch Bruce refractor, and a ten-hour exposure taken at Bloemfontein in 1934 with the 60-inch reflector. He gives a densitometer tracing across the centre of the second plate, but there is no calibration. He remarks, "It seems to me that the structure of NGC 5128 refutes the possibility

* H. Shapley and A. Ames, *Annals Harvard College Obs.*, **88**, 43, 1932.
† H. Shapley, *Annals Harvard College Obs.*, **88**, 93, 1934.
‡ C. C. L. Gregory, *Helwan Obs., Bull. No.* 21, p. 201, 1921.
§ C. C. L. Gregory, *Helwan Obs., Bull. No.* 22, p. 219, 1921.
|| J. S. Paraskevopoulos, *Harvard College Obs., Bull. No.* 898, 1935.
¶ H. D. Curtis, *Publ. Lick Obs.*, **13**, 45, 1918.
** H. D. Curtis, *Handb. Astrophys.*, **5**, 927, 1933.
†† J. Herschel, *Outlines of Astronomy*, London, 1849, p. 602.
‡‡ J. L. E. Dreyer, *Mem. R.A.S.*, **49**, Pt. 1, 143, 1888.

of its being an external galaxy", but it is difficult to reconcile this with his conclusion, "In view of this striking form, we might well be justified in calling the object 'a dark spiral'".

The real point at issue is whether the object is an external galaxy or not. The galactic coordinates (longitude 278°, latitude +18°) seem to leave the question somewhat open. The Shapley-Ames and Shapley catalogues classify it as external, but the investigation of Hubble * shows a gaseous emission spectrum. Using a 6° objective prism before a 10-inch Cooke lens giving a dispersion of 1·8 mm. from $H\beta$ to $H\epsilon$ he found the lines $H\beta$, λ4686, $H\gamma$ and $H\delta$ with the nebulium lines absent. Shapley † remarks, "N.G.C. 5128 is a 'pathologic' specimen—one of the external galaxies with peculiar spectrum. Any fully successful theory of galactic structure must take into account such abnormal forms". Hubble ‡ considers that the nebula may be a member of the "local group". In view of these varied opinions an investigation was undertaken to see whether surface photometry of the nebula might help to resolve the problem of its structure.

The Radcliffe telescope gives a scale of 22 seconds of arc per mm. at the Newtonian focus. The plates used in the present investigation were taken through a mask which exposed an area about 2·4 inches square on a quarter plate. The plates were then exposed for an equal time in a tube sensitometer adapted from an apparatus originally constructed by Redman. This imprinted twelve calibration spots on the previously protected parts of the plate. If a filter had been used for the exposure on the nebula it was also placed in front of the light source during the calibration exposure. The plates were put through the microphotometer by taking runs across the image of the nebula at intervals of 0·5 mm. and reduced by means of the calibration curve constructed from runs taken with the same microphotometer adjustments across the calibration spots. It is of some importance, in view of the consumption of time and material involved in reduction of these plates, to discover how much material is necessary for a determination of the isophotes of a nebula with reasonable accuracy. What are determined are "spot heights" on the contour map, and if the detail is complex it may be a matter of great difficulty to know how to join up the points determined. A print of the plate is of assistance, but, if the detail of complex topography is of importance, it is probably wise to put each plate through twice, taking runs in directions perpendicular to one another in the two cases. For regions of smooth variation of brightness a single plate is, as we shall see, probably sufficient if a check plate is available to enable blemishes to be discounted.

The plates reduced were as follows:—

Plate No.	Exposure	Emulsion	Date	J.D. No.	Filter
A 56	30 mins.	Zenith	1948 July 8	242 2741·76	None
A 57	66 mins.	Zenith	1948 July 8	242 2741·91	None
A 90	90 mins.	HP 3	1948 July 30	242 2763·80	Wratten 25

For each plate the zero of the magnitude scale was arbitrarily taken as the density of a particular calibration spot. To compare two plates it was therefore necessary to shift the levels at which isophotes were drawn, until the two sets of isophotes were in the best coincidence. Plates A 56 and A 57 were reduced independently, the runs being in perpendicular directions. Fig. 1 shows

* E. Hubble, *Contr. Mt. Wilson Obs., No.* 241, 1922.
† H. Shapley, *Galaxies*, Philadelphia, 1947, p. 217.
‡ E. Hubble, *The Realm of the Nebulae*, Oxford, 1936, p. 128.

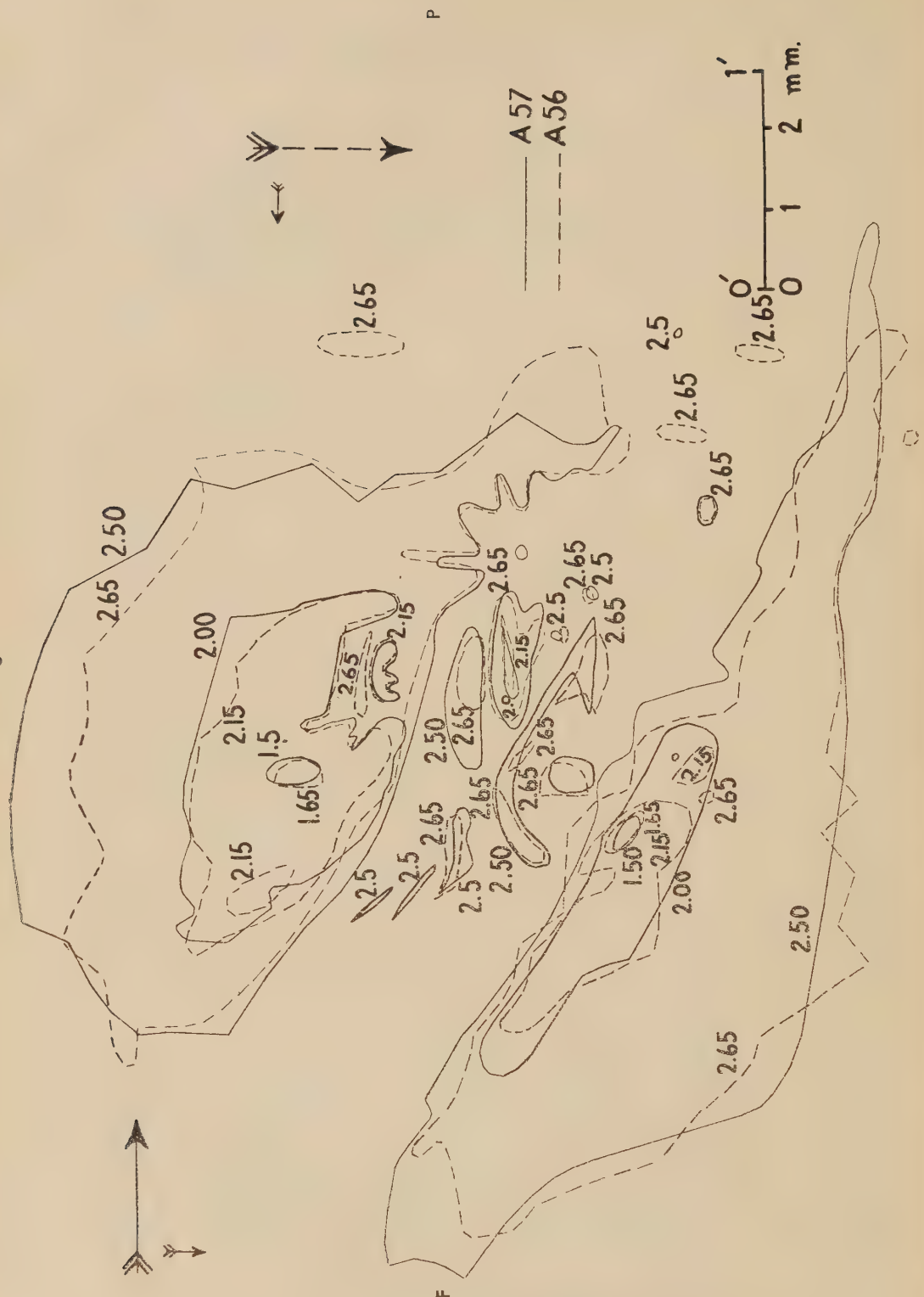
P
S
N
F
A 57
A 56
0 1 2 mm.
0' 1'
2.65
2.50
2.00
2.15
1.5
1.65
2.5
1.50
2.15

isophotes for the two plates, at half-magnitude intervals, brought into coincidence as explained above. The agreement is fairly satisfactory and seems to justify the conclusion that, carefully handled, a single plate will be adequate for most purposes. To draw isophotes for smaller magnitude intervals for the luminous patches in the absorbing band is a hopelessly complex task. On the other hand, such isophotes can be drawn for the outer regions, and the curves for an interval of 0·10 magnitudes for plate A57 are shown in Fig. 2. The north preceding

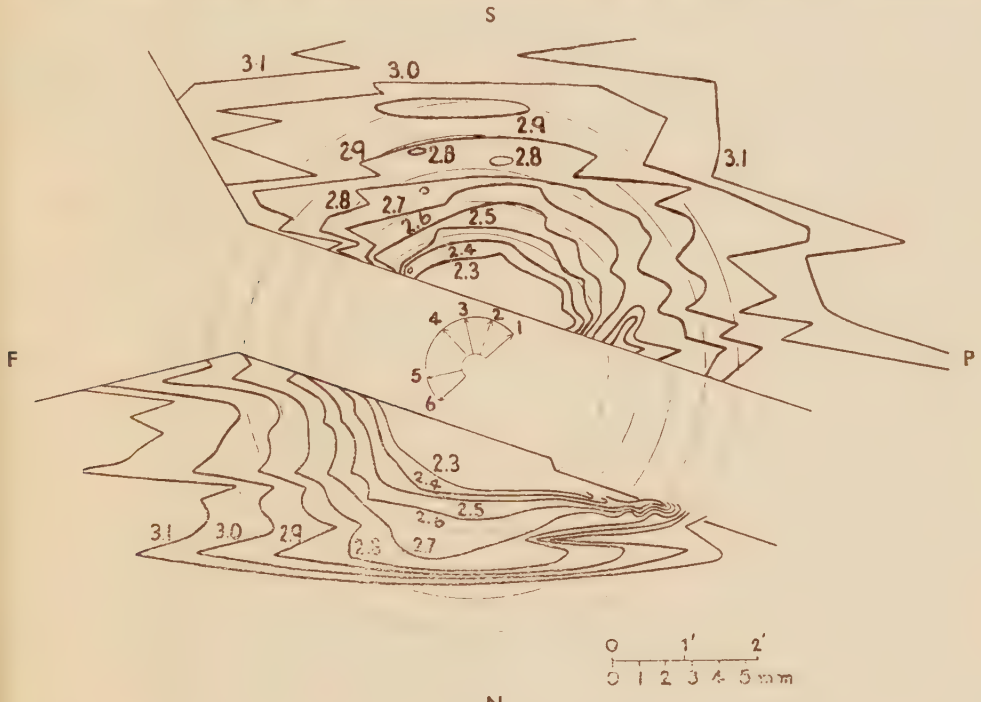

Fig. 2.

sector shows evidence of absorption, and so also, near the centre, does the south preceding sector. It is clear, however, as Paraskevopoulos seems to have first noted, that the general outline of the isophotes is fairly closely circular. The centre is marked on the diagram, and measures of the radial distance of each isophote in the six directions marked, have been taken. In one or two instances an irregularity of an isophote is cut more than once by a radius, and in such a case the mean of the several distances has been taken.

The results are as follows:—

Magnitude	Relative Brightness	Radius (mm. on plate)	R.M.S. error (mm.)	Radius (minutes of arc)
2·3	1·91	4·15	±0·08	1·52
2·4	1·74	4·70	±0·10	1·72
2·5	1·59	5·20	±0·10	1·91
2·6	1·45	5·59	±0·30	2·12
2·7	1·32	6·56	±0·37	2·40
2·8	1·20	7·48	±0·45	2·75
2·9	1·10	8·85	±0·70	3·25
3·0	1·00	10·72	±0·80	3·93

Sky fog estimated as 3·28±0·08 magnitudes = brightness 0·77±0·06.

These results are closely represented by the formula

$$I = 0{\cdot}85 + 19{\cdot}3/r^2,$$

where I means brightness in the units of the second column of the table, and r is in mm. on the plate. The constant 0·85 is fairly close to that deduced from the sky fog, but not as close as it should be in view of the estimated error of the determination. Adopting the value 0·77 we find the formula

$$I = 0{\cdot}77 + 22{\cdot}0/r^2$$

gives the best, but not a very good, fit. The rationale of these formulae, illustrated in Fig. 3, will be discussed presently. Now we merely note that the observed march of brightness is fairly close to an inverse square law.

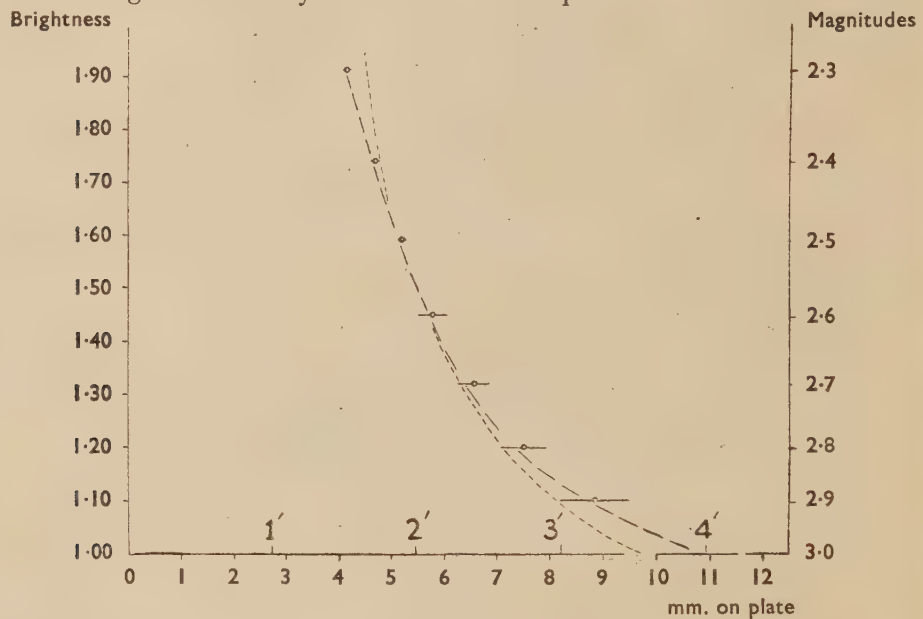

Fig. 3.
— — — $0{\cdot}85 + 19{\cdot}3/r^2$
- - - - - - $0{\cdot}77 + 22{\cdot}0/r^2$

The outline of the nebula is fairly closely circular and the outer parts of the isophotes of the two parts seem to be portions of the same curves. This supports the obvious impression that the nebula consists of a spherical luminous mass with the obscuring matter lying in front of it. Study of photographs suggests that this obscuring matter is in the form of a slab, extending some distance towards the observer and tilted slightly towards its northern edge. This suggestion is based on the facts that the brightest parts of the nebula are not equal in area and that the northern edge of the absorption is more sharply defined, as if it presented something approaching a definite edge outlined against the brightness. The isophotes for the red plate (A 90 on Fig. 4) add little to our knowledge except for one interesting point. There can be little doubt that the luminous central patches are reddened as compared with the rest of the nebula, since they appear relatively brighter on the red plate. It should also be noticed that the centre of the circular isophotes found on the blue plates lies in a direction near the centre of the group of luminous patches and that the outlying streaks on the absorption band point roughly towards the same centre.

P

S

N

F

D. S. Evans, Photometry of NGC 5128.

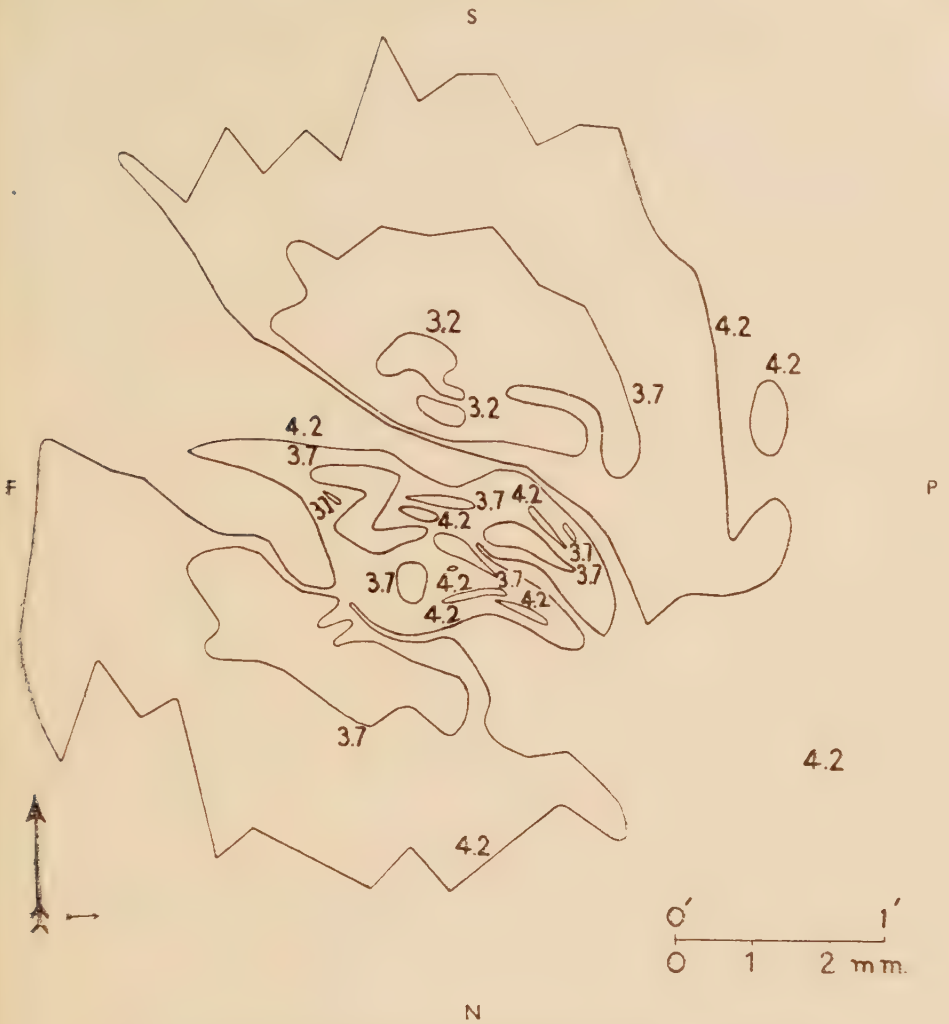

FIG. 4.—*Isophotes determined by using panchromatic plate and red filter. The arrow shows the direction of run in the microphotometer. Magnitude interval,* 0·5.

The obvious deduction from the closeness of the brightness variation to an inverse square law is that we have to deal with a point source concealed behind the absorbing material. On the other hand, if this is so, material must be present round the source to divert the light to the observer, and a somewhat closer discussion of the problem is clearly necessary. As a rough working model, consider a spherical mass of material which is such that a beam of light traversing it suffers a fractional intensity loss $\sigma\, ds$ in a distance ds. Let us further suppose that this loss takes place by pure scattering and that the energy abstracted from the original beam is re-emitted isotropically. If the mass is illuminated by a point source at its centre the intensity of direct light at distance r will be $(A/r^2)e^{-\sigma r}$ and the intensity of illumination of material at distance r due to direct illumination by the central source will be proportional to $(\sigma/r^2)e^{-\sigma r}$. There will in addition, of course, be an illumination due to scattered light, but this we can neglect as long as the scattering is not too high. What it comes to is that if we imagine an

observer at distance r, then in computing the brightness of his surroundings we count only the light which he receives from his central "sun" and neglect the general illumination of his "sky". To compute the brightness variation, as seen from an external point using this approximation, we name the various dimensions as in Fig. 5. Then the apparent brightness seen by the observer looking along a line whose perpendicular distance from the centre is p, is

$$B \sim \int_{y=0}^{2\sqrt{R_0^2-p^2}} \frac{\sigma}{r^2} e^{-\sigma r} e^{-\sigma y}\, dy.$$

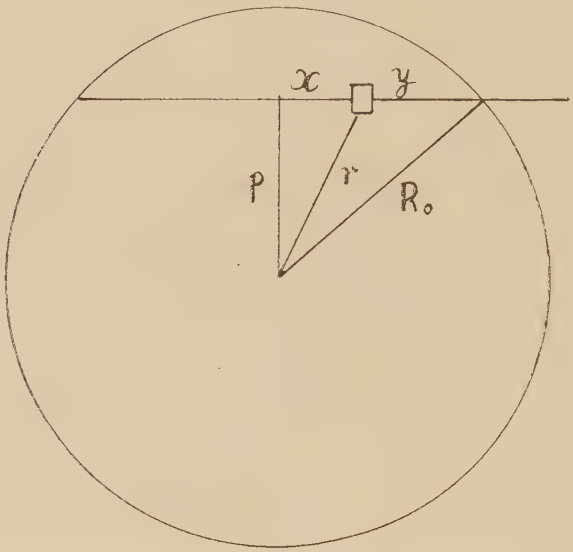

FIG. 5.—*Diagram showing notation for computation of surface brightness variation in model.*

If we write $x' = x/R_0$, $p' = p/R_0$, $\alpha'^2 = 1 - p'^2$, then

$$B \sim \int_{-\alpha'}^{\alpha'} \frac{e^{-\sigma R_0 \alpha'}}{(x'^2 + p'^2)} \exp\left[-\sigma R_0 \{(x'^2 + p'^2)^{\frac{1}{2}} - x'\}\right] dx'.$$

The further transformations $p' \tan\theta = \psi = \sqrt{(x'^2 + p'^2)} - x'$, $\sigma R_0 = \lambda$ reduce this to

$$B \sim e^{-\lambda\alpha'} \int_{\tan^{-1}\left(\frac{1-\alpha'}{p'}\right)}^{\tan^{-1}\left(\frac{1+\alpha'}{p'}\right)} \frac{d\theta}{p'} e^{-\lambda p' \tan\theta}.$$

The physical interpretation of λ is as follows: $e^{-\lambda}$ is the proportionate intensity of a collimated beam issuing from the centre which emerges at the surface of the system. The curves of B against p' for $e^{-\lambda} = 0{\cdot}5$ and $0{\cdot}1$ ($\lambda = 0{\cdot}7$, $2{\cdot}30$) and the limiting case for $\lambda = 0$ are illustrated in Fig. 6. In addition, an inverse square curve (shown dotted) has been fitted to the computed curves. It will be seen that in practice it would be impossible to distinguish these two types of curve, especially over a limited range of radius. That is to say that our model indicates that the observed variation should be closely represented by an inverse square

law. There are many obvious ways in which this mathematical model could be improved, but there seems little point in any further refinement.

It seems that our observed variation does entitle us to infer, if not a strict point source, at least a distribution of sources concentrated in a region which is small compared with the dimensions of the system *. The location of this system of sources is, as we have seen, in the same direction as the luminous patches within the absorbing band. This fact, and the reddening of the light from this region, suggest that these patches may represent light from the central source which has filtered out through rifts in the absorbing matter, and which has undergone reddening due to its passage through presumably dusty regions.

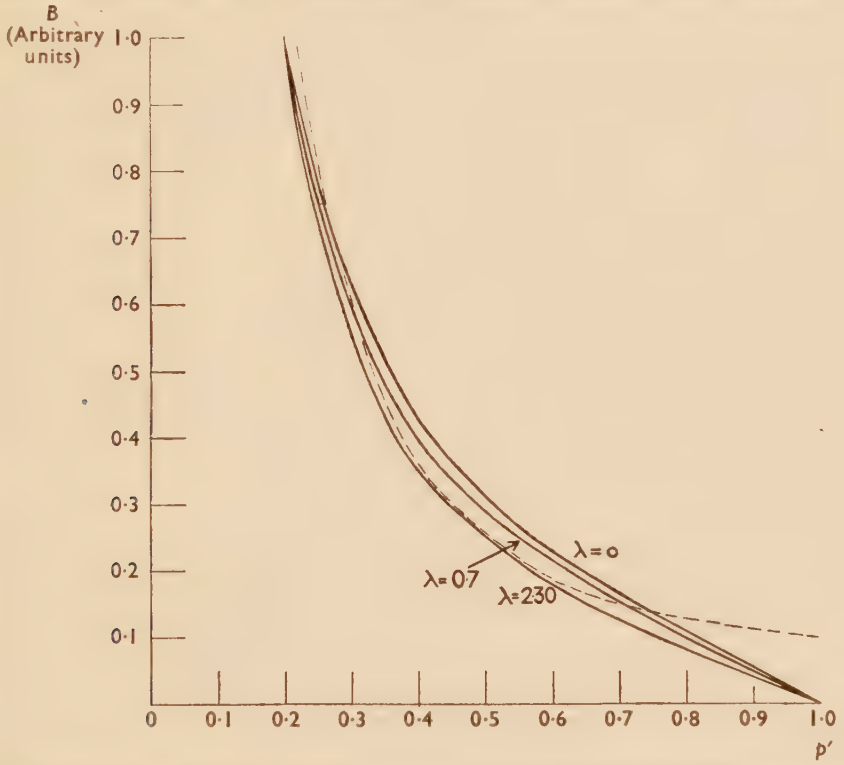

Fig. 6.—*Results of computations of surface brightness in model, compared with inverse square law.*

If NGC 5128 is extra-galactic, its great apparent size would indicate a very large system. It shows no sign of resolution into stars, and its spectrum is gaseous. It seems hardly possible therefore to classify it as extra-galactic. If we ask what known type of object fits the picture of a spherical gas cloud with a point source at its centre, the most obvious answer is "the planetary nebulae".

* It should be emphasized that the point in this discussion which is regarded as fundamental is the possibility of representation by an inverse square law. In empty space general considerations of potential theory entitle us to infer a concentrated source from an inverse square law of distribution of radiation intensity. In NGC 5128 the gaseous spectrum and the lack of resolution into stars suggest a primary light source not directly visible. The analysis of our model embodying a point source shows that light scattered by the surrounding gas cloud will still show a radial variation close to the inverse square law and suggests that the actual variation which would exist if the gas cloud were removed would follow this law.

It is true that the spectrum is not precisely that of a planetary nebula, but in other respects there is a similarity. This suggestion is, of course, highly speculative, and if verified it would lead on to deductions of some interest. The point of the suggestion is that it does open up more definite lines of thought for a further attack on this nebula, possibly at a later stage with the spectroscope as well. In addition the present merely exploratory investigation does suggest that work on similar lines on the apparently somewhat similar systems I 5267 and NGC 1316 might be profitable.

I am glad to acknowledge the help which discussions with Dr H. Knox-Shaw and Dr A. D. Thackeray have afforded me.

Radcliffe Observatory,
Pretoria:
1948 *November* 8.

RADIAL OSCILLATIONS OF A STELLAR MODEL

Chandrika Prasad

(Communicated by E. A. Milne)

(Received 1949 January 10)

Summary

Radial oscillations of a stellar model in which the density is proportional to $1-r^2/R^2$ have been considered. It has been shown that a solution is possible without recourse to numerical integration. The period and amplitude of oscillation have been found.

---

1. In a previous paper * the author has obtained the radial adiabatic oscillations of a star built on a particular model, namely a homogeneous interior with a point mass at the centre. In the present paper a similar investigation is made for a stellar model with a continuous distribution of density vanishing at the surface and without central singularity.

2. The differential equation for small radial oscillation is †

$$\frac{d^2\xi_1}{d\xi_0^2}+\frac{4-\mu}{\xi_0}\frac{d\xi_1}{d\xi_0}+\left\{\frac{n^2\rho_0}{\gamma P_0}-\frac{\alpha\mu}{\xi_0^2}\right\}\xi_1=0, \tag{1}$$

where ξ_1 is the amplitude of displacement $\delta\xi_0/\xi_0$; $\mu=g_0\rho_0\xi_0/P_0$, g_0, ρ_0, P_0 being respectively the mean values of gravity, density and pressure at a distance ξ_0 from the centre; $\alpha=3-4/\gamma$, γ being the ratio of specific heats and $n=2\pi\nu$, where ν is the frequency of the oscillation.

The boundary conditions require that the solution must be non-singular both at $\xi_0=0$ and $\xi_0=R$, the surface of the star.

We shall consider the model for which the density ρ_0 at any point is given by

$$\rho_0=\rho_c(1-\xi_0^2/R^2).$$

Then

$$M(\xi_0)=\tfrac{4}{15}\pi\rho_c(5\xi_0^3-3\xi_0^5/R^2).$$

This shows that $M=\frac{8}{15}\pi\rho_c R^3$, so that

$$\rho_c=\tfrac{5}{2}\bar{\rho}.$$

Also

$$g_0=\tfrac{4}{15}\pi G\rho_c(5\xi_0-3\xi_0^3/R^2)$$

and

$$P_0=\tfrac{4}{15}\pi G\rho_c^2\left(R^2-\tfrac{5}{2}\xi_0^2+2\frac{\xi_0^4}{R^2}-\tfrac{1}{2}\frac{\xi_0^6}{R^4}\right),$$

---

* *M.N.*, **108**, 414, 1948.

† A. S. Eddington, *The Internal Constitution of the Stars*, pp. 186 *et seq.*, 1926.

determining the constant of integration so that the pressure vanishes at the boundary of the star.

With these values we have, on putting $\xi_0 = Rx$,

$$\mu = \frac{x^2(5-3x^2)}{(1-x^2)(1-\frac{1}{2}x^2)} \quad \text{and} \quad \frac{n^2\rho_0}{\gamma P_0} = \frac{3n^2}{2\pi G\gamma\bar{\rho}R^2} \cdot \frac{1}{(1-x^2)(1-\frac{1}{2}x^2)}.$$

Substituting these in equation (1) we get the differential equation

$$(1-x^2)(1-\tfrac{1}{2}x^2)\frac{d^2\xi_1}{dx^2} + \frac{4-11x^2+5x^4}{x}\frac{d\xi_1}{dx} + (\mathcal{J}+3\alpha x^2)\xi_1 = 0, \tag{2}$$

where

$$\mathcal{J} = \frac{3n^2}{2\pi G\gamma\bar{\rho}} - 5\alpha. \tag{3}$$

3. Equation (2) has regular singularities at the origin, at $x=1$ and at $x=\sqrt{2}$. We have to find regular integrals which are finite in the range $0 \leqslant x \leqslant 1$. To solve this equation we shall adopt a method similar to that used by Kelvin* and Darwin for tides on a rotating globe.

The roots of the indicial equation are -3 and 0. To avoid singularity at the origin we must choose the latter. Assuming a solution in series,

$$\xi_1 = \sum_0^\infty a_k x^k,$$

we find that the terms in odd powers of x vanish, and that the coefficients of even powers are given by

$$10a_2 + \mathcal{J}a_0 = 0, \tag{4}$$

$$28a_4 - (25-\mathcal{J})a_2 + 3\alpha a_0 = 0,$$

$$\cdots \quad \cdots \quad \cdots \quad \cdots \quad \cdots$$

$$(2j+2)(2j+5)a_{2j+2} - \{j(6j+19)-\mathcal{J}\}a_{2j} + \{(j-1)(2j+7)+3\alpha\}a_{2j-2} = 0, \tag{5}$$

where j is a positive integer.

To bring it to a more convenient form put $a_{2j+2}/a_{2j} = N_{j+1}$, then it may be written as

$$N_{j+1} = \frac{j(6j+19)-\mathcal{J}}{(2j+2)(2j+5)} - \frac{(j-1)(2j+7)+3\alpha}{(2j+2)(2j+5)} \cdot \frac{1}{N_j} \tag{6}$$

$$= \tfrac{3}{2} - \frac{2j+15+\mathcal{J}}{(2j+2)(2j+5)} - \left(\tfrac{1}{2} - \frac{2j+12-3\alpha}{(2j+2)(2j+5)}\right)\frac{1}{N_j}. \tag{6'}$$

We shall show, in the first place, that N_j must tend either to the limit $\frac{1}{2}$ or to the limit 1. For this suppose that N_j (and thus N_{j+1} also) tends to the limit λ as j tends to infinity. Taking the limit of (6′) we have

$$\lambda = \tfrac{3}{2} - \tfrac{1}{2}\lambda^{-1},$$

which gives the roots $\frac{1}{2}$ and 1.

It can be easily shown that if N_j tends to the limit 1 then the series for ξ_1 diverges at $x=1$. Hence the conditions of our problem can be satisfied only if N_j tends to the limit $\frac{1}{2}$. This restricts us, as we shall see, to a determinate set of values of $\mathcal{J}$.

* For references and discussion of the method see H. Lamb, *Hydrodynamics* (6th ed.), p. 335, 1932.

The relation (6) may be put in the form

$$N_j = \frac{\dfrac{(j-1)(2j+7)+3\alpha}{(2j+2)(2j+5)}}{\dfrac{j(6j+19)-\mathcal{J}}{(2j+2)(2j+5)} - N_{j+1}}, \tag{7}$$

and by successive application of this we obtain N_j in the form of a convergent continued fraction *,

$$N_j = \frac{\dfrac{(j-1)(2j+7)+3\alpha}{(2j+2)(2j+5)}}{\dfrac{j(6j+19)-\mathcal{J}}{(2j+2)(2j+5)} -} \frac{\dfrac{j(2j+9)+3\alpha}{(2j+4)(2j+7)}}{\dfrac{(j+1)(6j+25)-\mathcal{J}}{(2j+4)(2j+7)} -} \frac{\dfrac{(j+1)(2j+11)+3\alpha}{(2j+6)(2j+9)}}{\dfrac{(j+2)(6j+31)-\mathcal{J}}{(2j+6)(2j+9)} -} \cdots \tag{8}$$

In particular this formula determines the value of N_1. But from (4) we have

$$N_1 = -\mathcal{J}/10.$$

Hence

$$\frac{\mathcal{J}}{10} + \frac{\dfrac{3\alpha}{28}}{\dfrac{25-\mathcal{J}}{28} -} \frac{\dfrac{11+3\alpha}{54}}{\dfrac{62-\mathcal{J}}{54} -} \frac{\dfrac{26+3\alpha}{88}}{\dfrac{111-\mathcal{J}}{88} -} \cdots = 0. \tag{9}$$

This equation determines the admissible values of $\mathcal{J}$. The constants a_2, a_4, a_6, . . . are then given by

$$a_2 = N_1 a_0, \qquad a_4 = N_1 N_2 a_0, \qquad a_6 = N_1 N_2 N_3 a_0, \ldots$$

It should be noticed that a_2, a_4, a_6, . . . are not found in succession by formula (5), as this would require us to start with *exactly* the right value of $\mathcal{J}$ and to observe absolute accuracy in subsequent stages of the work, otherwise the calculation will inevitably lead to values of N_j which approximate to the limit 1 †.

4. The solution of equation (9) was carried out in three stages. First it was found convenient to find N_1 for different values of $\mathcal{J}$ at intervals of 10, starting from 0. For this purpose N_{10} was calculated by an approximation and this value used to find N_9, N_8, N_7, . . . N_1, successively by formula (7). Graphs of the functions N_7, N_6, N_5, . . . were drawn, as these help in the drawing of the graph of the next lower function. By drawing graphs of N_1 and $-\mathcal{J}/10$ and finding the points of intersection, rough solutions of (9) were obtained. By taking values of $\mathcal{J}$ at intervals of 1 and interpolating, we find more accurate solutions. Lastly N_1 was calculated for two or three values of $\mathcal{J}$ close to the solution, starting from N_{14} or N_{18} (for larger values of $\mathcal{J}$). The final value of $\mathcal{J}$ satisfying (9) was then found by interpolation. These values of $\mathcal{J}$ for different modes of oscillation are given in Table I.

* It may not be quite clear from the above why N_j, as expressed by (8), should tend to $\frac{1}{2}$ and not 1. The reason is that the limiting form of (8) is the continued fraction

$$\frac{0{\cdot}5}{1{\cdot}5-} \frac{0{\cdot}5}{1{\cdot}5-} \frac{0{\cdot}5}{1{\cdot}5-} \cdots \tag{8'}$$

whose value is $\frac{1}{2}$, and it may be easily shown that the successive convergents of (8) and (8′), and hence the continued fractions themselves, differ only by terms of the order $1/j$.

† H. Lamb, *loc. cit.*

TABLE I

Values of $\mathcal{J}$ satisfying equation (9)

Mode of oscillation	0	1	2	3
$\alpha=0{\cdot}0$	0·00000	12·8089	31·335	55·656
$\alpha=0{\cdot}2$	−0·33458	12·4583	30·992	55·315
$\alpha=0{\cdot}4$	−0·67165	12·1083	30·648	54·974
$\alpha=0{\cdot}6$	−1·01122	11·7585	30·306	54·633

The expansions for the amplitude ξ_1 for different modes for the particular case $\alpha=0{\cdot}4$ are given below. For other values of α the results are similar.

$\xi_1=a_0(1+{\cdot}067x^2+{\cdot}019x^4+{\cdot}007x^6+{\cdot}003x^8+{\cdot}001x^{10}+\ldots)$ [0th mode]
$\xi_1=a_0(1-1{\cdot}21x^2-{\cdot}60x^4-{\cdot}28x^6-{\cdot}13x^8-{\cdot}06x^{10}-\ldots)$ [1st mode]
$\xi_1=a_0(1-3{\cdot}07x^2+{\cdot}57x^4+1{\cdot}29x^6+{\cdot}96x^8+{\cdot}58x^{10}+\ldots)$ [2nd mode]
$\xi_1=a_0(1-5{\cdot}50x^2+5{\cdot}85x^4+2{\cdot}00x^6-{\cdot}53x^8-1{\cdot}19x^{10}-\ldots)$ [3rd mode]

The values of $T\sqrt{(G\rho/6\pi)}$, where T is the period of oscillation, are given in Table II. These are calculated from the above values of $\mathcal{J}$ by the help of (3).

TABLE II

Values of $T\sqrt{(G\bar{\rho}/6\pi)}$

Mode	0	1	2	3
$\alpha=0{\cdot}0$	∞	0·2419	0·1547	0·1161
$\alpha=0{\cdot}2$	1·0257	0·2281	0·1479	0·1115
$\alpha=0{\cdot}4$	0·6995	0·2146	0·1411	0·1068
$\alpha=0{\cdot}6$	0·5493	0·2017	0·1343	0·1021

From the results obtained above it would be noticed that for the zero'th mode the amplitude remains nearly constant and the model considered approximates to the homogeneous model in this respect, but the period of the zero'th mode is much less than that of the homogeneous model. Table III gives a comparison of the periods for the present model, the author's point-mass model *, the standard polytrope † and Sterne's three models ‡, for the particular case $\alpha=0{\cdot}4$. The sequence of periods is similar for other values of α also.

TABLE III

Values of $T\sqrt{(G\bar{\rho}/6\pi)}$ for $\alpha=0{\cdot}4$

Model \ Mode	0	1	2	3
Homogeneous	0·9014	0·2096	0·1329	0·0986
Present	0·6995	0·2146	0·1411	0·1068
Point mass	0·7465	0·1906	0·1181	0·0863
Sterne's 2nd	0·5929	0·2159	0·1382	0·1023
Polytropic	0·2774	0·1909	0·1428	0·1142
Sterne's 3rd	0·4662	0·1832	0·1167	0·0859

* *Loc. cit.*, p. 416.
† Calculated from the results of M. Schwarzschild, *Ap. J.*, **94**, 245, 1941.
‡ T. E. Sterne, *M.N.*, **97**, 592, 1937.

On consideration of Table III, which has been arranged in order of increasing density condensation *, we are drawn to the conclusion that the point-mass model and Sterne's third model, both of which have a discontinuity in their density distributions, show a disparity in their periods. The periods of zero'th mode of these two models are higher than would be expected from their density condensations; and the periods of the higher modes are lower than the corresponding periods of other models. The periods of the remaining four models, which have a continuous density distribution, show a gradation in accordance with their density condensations. The periods of higher modes of the present model and the polytrope, both of which have a zero density at the surface, are generally higher than for the other models.

As a comparison, the periods of δ Cephei (actual period 5·37 days) calculated from the above table for the successive models, are 7·8, 6·1, 6·5, 5·1, 2·4 and 4·0 days respectively. The present model gives 6·1 days, in fair agreement with the actual value; but if a lower value of α is chosen the period would be larger.

In conclusion I wish to express my sincere thanks to Professor E. A. Milne for his kind interest and suggestions for improvement. I am also indebted to my friend Dr S. K. Roy for referring me to Kelvin's work.

Queen's College, Oxford:
1949 *January* 5.

* The ratio of the mass within a sphere of half the radius to the total mass, or alternatively, the ratio of the whole radius to the radius of the sphere containing half the mass, may be taken as a measure of the density condensation of a star. Any other formula would give a similar result.

PRESSURE AND TEMPERATURE CYCLES IN THE REVERSING LAYERS OF CEPHEID VARIABLES

W. N. Abbott

(Communicated by F. J. M. Stratton, F.R.S.)

(Received 1948 April 8; received in final form 1948 December 31)

Summary

The object of this paper is to draw attention to some interesting relations which exist between gas pressure and temperature variations in the reversing layers of Cepheids of different types. From these data, a pulsation of the reversing layer appears, which is out of phase with the pulsation of the photosphere.

Five Cepheids have been considered. They are η Aquilae, U Vulpeculae, U Aquilae, W Geminorum and W Sagittarii (**1**). The mean absolute magnitudes $\bar{M}$, the distances d and the masses μ have been computed from the Shapley period-luminosity and the Eddington mass-luminosity relations. Radii at maximum light, R_1, have been computed from the temperatures at maximum, T_1, given by the line spectra at maximum.

The Sun's surface temperature was taken as 6200 deg. K. and the surface temperatures of the stars were taken to be those of the line spectra, that is, reversing layer temperatures, which mainly interest us. Temperatures corresponding to spectral class were taken from Schaub's table (**2**).

Table I gives the basic data, the Sun's radius being taken as $6{\cdot}951 \times 10^{10}$ cm.

TABLE I

Basic Data

Star	$\bar{M}$	d (parsecs)	μ (10^{34} grams)	$\frac{R_1}{R_\odot}$	Spectral Class
η Aquilae	$-1{\cdot}77$	146·7	1·598	28·2	F3–G5
U Vulpeculae	$-1{\cdot}85$	1063·5	1·742	26·0	F8–G4
U Aquilae	$-1{\cdot}74$	479·5	1·707	22·4	F8–G8
W Geminorum	$-1{\cdot}85$	558·2	1·742	19·7	F5–G5
W Sagittarii	$-1{\cdot}81$	200·7	1·575	17·1	A9–G1

The varying values of the radii of the stars were deduced from R_1 and from the radial velocity curves, the variations in the areas of the curves being the variations in the stars' radii (corrected for the radial velocities v_0 of the stars' centres of gravity).

Where R_n and $R_{n-\frac{1}{2}}$ are radii at times separated by half a day,

$$R_n - R_{n-\frac{1}{2}} = \int_{n-\frac{1}{2}}^{n} (v - v_0)\, dt.$$

Computations of ΔR were made at half-day intervals and when added successively gave the radius R at time n. These radii are given in Table II in units of 10^{12} cm.

In Table III are given, for each star, two quantities. The first is the mean density $\rho_m = \mu/V$, and the second is the acceleration of gravity, g, in the reversing layer, calculated from $g = -\frac{4}{3} f \pi \rho_m R$, where $f = 6{\cdot}66 \times 10^{-8}$ c.g.s. units.

TABLE II

Radii, in units of 10^{12} *cm.*

Phase (days)	η Aquilae	U Vulpeculae	U Aquilae	W Geminorum	W Sagittarii
0·0	1·8910	1·8073	1·5565	1·3680	1·1921
0·5	1·9623	1·7943	1·6377	1·4207	1·2531
1·0	2·0327	1·7597	1·6964	1·4617	1·2950
1·5	2·0923	1·6880	1·7521	1·4941	1·3330
2·0	2·1355	1·5779	1·7927	1·5170	1·3968
2·5	2·1661	1·5083	1·8260	1·5291	1·4031
3·0	2·1838	1·4876	1·8389	1·5312	1·4239
3·5	2·1885	1·5066	1·8290	1·5257	1·4153
4·0	2·1890	1·5571	1·7989	1·5033	1·3764
4·5	2·1799	1·6258	1·7411	1·4652	1·3050
5·0	2·1441	1·6828	1·6573	1·4172	1·2082
5·5	2·0716	1·7312	1·5483	1·3511	1·1087
6·0	1·9741	1·7658	1·4904	1·2764	1·0525
6·5	1·8941	1·7917	1·5184	1·2288	1·0720
7·0	1·8751	1·8064	1·5565	1·2531	1·1196
7·5		1·8120		1·3105	1·1788

TABLE III

Mean density (ρ_m) *in units of* 10^{-3} *g. cm.*$^{-3}$ *and acceleration in reversing layer* (g) *in c.g.s. units*

Phase (days)	η Aquilae		U Vulpeculae		U Aquilae		W Geminorum		W Sagittarii	
	ρ_m	g	ρ_m	g	ρ_m	g	ρ_m	g	ρ_m	g
0·0	0·564	299	0·702	354	1·062	448	1·621	620	2·210	738
0·5	0·504	276	0·720	360	0·951	433	1·448	598	2·008	704
1·0	0·455	253	0·760	374	0·834	395	1·324	540	1·730	638
1·5	0·417	244	0·863	407	0·752	367	1·242	536	1·584	591
2·0	0·392	234	1·061	467	0·701	350	1·190	504	1·380	529
2·5	0·378	229	1·212	516	0·661	336	1·166	498	1·365	535
3·0	0·373	228	1·262	526	0·651	334	1·147	490	1·330	532
3·5	0·372	228	1·210	510	0·663	338	1·169	500	1·328	526
4·0	0·372	228	1·100	487	0·690	345	1·200	503	1·460	561
4·5	0·374	233	0·970	442	0·772	375	1·319	539	1·693	620
5·0	0·388	249	0·880	414	0·894	413	1·460	578	2·137	735
5·5	0·429	275	0·800	386	1·102	477	1·822	689	2·760	854
6·0	0·494	297	0·755	372	1·223	509	2·000	711	3·218	902
6·5	0·560	322	0·721	361	1·120	475	2·240	770	3·036	853
7·0	0·577	299	0·699	353	1·061	448	2·117	740	2·680	831
7·5			0·701	355			1·842	675	2·292	755

We may now proceed to compute the gas pressure p_G in the reversing layer, as a function of phase.

We will use the method developed by Tiercy (**3**), in his memoir, where he computes p_G by successive additions of Δp_G at half-day intervals. Pressures thus computed form an independent whole, and as far as temperature is concerned are only dependent upon the temperature of the reversing layer at maximum light.

We assume that, during the pulsation, the overall height of the atmosphere above the reversing layer (or the photosphere) is proportional to the photospheric radius. This is legitimate, considering that we cannot imagine a tenuous gaseous atmosphere being pushed up and dragged down by the photosphere

without participating in proportion to the general movement, whatever the cause of this may be. This purely dynamical assumption, however, in no way implies the pulsation proper of the dense reversing layer, or the mode of pulsation, for the behaviour of the reversing layer is certainly as dependent upon the effective temperature variations of the adjacent photospherical surface, as it is on the variations of the gas pressure.

We assume from Tiercy (**3**) the equation

$$dp_G = K\rho_m g dR, \tag{1}$$

where dR is not the variation in height of the atmosphere, but is the variation of the radius of the reversing layer.

The value of K must be determined. Tiercy shows that if R becomes λR, by using the perfect gas equation and assuming that λ differs little from unity, then

$$\Delta p_G = p_G\left(\frac{1-\lambda^3}{\lambda^3}\right).$$

If λ is for example 1·01 (i. e. if the radius is increased by one per cent), then

$$\Delta p_G = -0{\cdot}029401 p_G.$$

Substituting this value in equation (1) gives $K = \dfrac{-2{\cdot}9401 p_G}{g_1\rho_1 R_1}$, the suffix 1 denoting values at maximum light.

If we take maximum light as phase 0, and if we put $\Delta R = nR_1/100$ and $R_1 = 1{\cdot}0$, then for any phase interval,

$$\Delta p_G = Kg\rho_m\left(\frac{n}{100}\right) = \frac{-2{\cdot}94}{g_1\rho_1}\cdot g\rho_m\left(\frac{n}{100}\right)p_G.$$

The gas pressure at phase n is thus obtained by successive algebraic additions of Δp_G during the succeeding phases.

We need now at least an approximate value for the gas pressure at phase 0. We take

$$p_G = Lk\rho_2 T_1, \tag{2}$$

where $L = 6{\cdot}064 \times 10^{23}\,\text{mole}^{-1}$, $k = 1{\cdot}3709 \times 10^{-16}\,\text{erg deg.}^{-1}$ and ρ_2 and T_1 are density and effective temperature of reversing layer at maximum light.

This relation (2) is the only link that we have between the scale of temperatures estimated from the observational data throughout each cycle, and the scale of gas pressures which are being derived from the variations of g and ρ_m which we have already found.

We get an approximate value of the density ρ_2 of the reversing layer at maximum light by using Homer Lane's relation (**4**) $\rho_2 = 0{\cdot}032\rho_1$.

In Table IV are given values of the gas pressure, in c.g.s. units, of the reversing layers of the five stars.

Reversing Layer Temperatures.—Nothing would have been easier than to derive temperatures from gas pressures simply by using the perfect gas equation. This would not, however, have given any additional data. Temperatures must be taken directly from observational data.

Unfortunately information from spectral class is not very precise, since fluctuations and disagreements of as much as two sub-classes are the rule. As a result we shall derive temperatures using the reversing layer temperature at maximum (from spectral type) and the luminosity relation. We shall assume that the reversing layer temperatures vary as the bolometric effective temperatures.

TABLE IV

Gas pressure in c.g.s. units

Phase (days)	η Aquilae	U Vulpeculae	U Aquilae	W Geminorum	W Sagittarii
0·0	803	775	1368	2096	3193
0·5	720	792	1295	1871	2726
1·0	653	841	1156	1723	2463
1·5	606	956	1064	1618	2270
2·0	575	1193	1005	1550	2118
2·5	554	1393	960	1515	1997
3·0	543	1462	945	1506	1924
3·5	539	1402	956	1517	1958
4·0	539	1246	992	1582	2110
4·5	545	1076	1069	1687	2448
5·0	570	962	1122	1851	3087
5·5	621	879	1386	2157	3999
6·0	710	828	1566	2600	4753
6·5	800	792	1477	2933	4483
7·0	824	773	1368	2752	3905
7·5		767		2388	3314

If L is the luminosity, T the effective temperature and ΔM the absolute (or apparent) magnitude variations (**5**), then we have:—

$$L = 4\pi R^2 H \qquad \text{and} \qquad H = \sigma T^4, \qquad \text{where} \qquad \sigma = 5{\cdot}6 \times 10^{-5},$$

$$M_2 - M_1 = 2{\cdot}5 \log_{10} \frac{L_1}{L_2} = 2{\cdot}5 \log_{10} \frac{R_1^2 H_1}{R_2^2 H_2}.$$

We have accordingly

$$0{\cdot}4\Delta M - 2 \log_{10} \frac{R_2}{R_1} = \log_{10} \frac{H_2}{H_1} = 4 \log_{10} \frac{T_2}{T_1}$$

or

$$\log_{10} T_2 = 0{\cdot}1\Delta M - 0{\cdot}5 \log_{10} \frac{R_2}{R_1} + \log_{10} T_1.$$

Temperatures of the reversing layers are given in Table V.

TABLE V

Reversing layer temperatures

Phase (days)	η Aquilae	U Vulpeculae	U Aquilae	W Geminorum	W Sagittarii
0·0	7200	6500	6400	6800	7600
0·5	7000	6400	6180	6650	7180
1·0	6750	6490	5820	6500	6880
1·5	6440	6450	5623	6410	6760
2·0	6400	6380	5545	6440	6660
2·5	6220	6230	5350	6270	6525
3·0	6040	6100	5250	6050	6430
3·5	5950	5920	5140	6100	6330
4·0	5850	5600	5080	6055	6260
4·5	5780	5230	5100	6075	6230
5·0	5725	5120	5225	6150	6350
5·5	5920	5130	5465	6250	6650
6·0	6350	5160	5760	6470	6750
6·5	6780	5360	6150	6655	7100
7·0	7380	5625	6400	6870	7670
7·5		5380		6910	7600

Gas Pressure and Temperature Cycles.—In Fig. 1 gas pressures (p_G) have been plotted against temperatures (T). The curves, whose areas and orientations vary progressively, show the cyclic variation of these quantities. Further, no less interesting from the point of view of evolution is the logarithmic relation which appears to exist between the mean gas pressure and mean temperature and spectral type. The orientation as well as the area of these curves are both related to what we may consider as the pulsation proper of the reversing layers of these classical Cepheids.

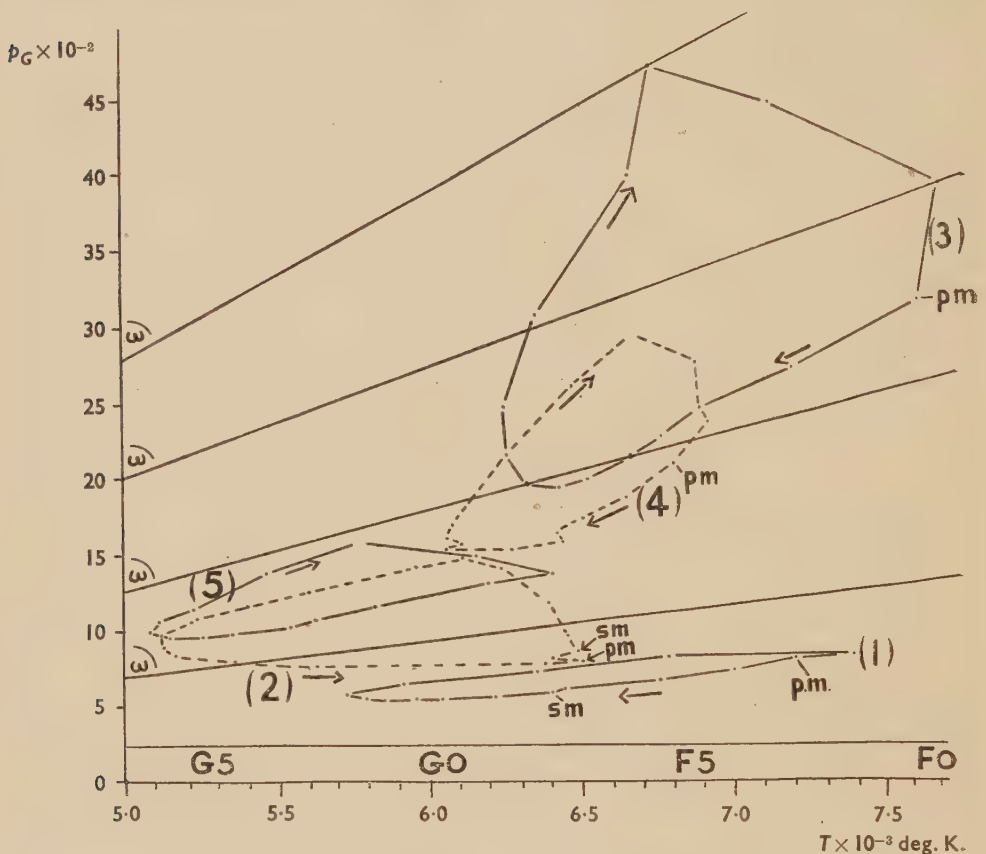

FIG. 1.—*Gas pressure and temperature cycles in the reversing layers of the Cepheids.*
pm: primary maximum.
sm: secondary maximum.
(1) *η Aquilae.*
(2) *U Vulpeculae.*
(3) *W Sagittarii.*
(4) *W Geminorum.*
(5) *U Aquilae.*

Pulsation of the Reversing Layer.—If the gas pressures and temperatures are substituted in the perfect gas equation $v = R'T/p_G$, ($R' = 8{\cdot}313 \times 10^7$), we can follow the behaviour of the atomic volume of the matter of the reversing layer during the cycle.

In Fig. 1, lines parallel to the ordinate axis are isotherms. The ratio T/p_G, duly multiplied by a factor depending on the ratio of unit lengths along the two axes (which in the case of Fig. 1 is 2), defines a sheath of oblique lines radiating from the coordinate origin (not shown in the figure). These lines could be termed

"isochores", in the sense that they are lines of equal atomic volume, and there exists one through any point of the diagram. These oblique lines form with the ordinate axis an angle ω given by $\tan\omega = 2T/p_G$ (i.e. $\tan\omega$ is proportional to v, the atomic volume), whence $v = (R\tan\omega)/2$, and we can say that, roughly, the variation of the atomic volume is given by the variation in the angle.

If now, $\mathcal{M}$ is the total mass of the reversing layer, and $\mathcal{A}$ is the mean atomic weight and $\mathcal{V}$ is the volume of the reversing layer, then $\mathcal{V} = \mathcal{M}.v/\mathcal{A}$, where $\mathcal{M}$ and $\mathcal{A}$ are constants.

TABLE VI

Values of "atomic volume" of reversing layers in units of 10^6 *cm.*^{3}

Phase (days)	η Aquilae	U Vulpeculae	U Aquilae	W Geminorum	W Sagittarii
0·0	744·8	697·5	389·0	269·3	197·8
0·5	808·8	671·7	396·5	295·1	218·6
1·0	858·7	642·6	418·1	314·4	231·9
1·5	883·7	558·8	438·9	327·5	247·7
2·0	925·2	446·4	458·9	345·0	261·0
2·5	933·5	371·6	463·9	344·1	271·8
3·0	924·4	346·6	463·0	333·4	277·6
3·5	916·9	350·8	460·3	334·2	268·5
4·0	902·0	373·2	425·6	317·6	266·9
4·5	881·1	404·0	396·5	299·3	211·1
5·0	834·6	442·2	387·4	276·0	171·2
5·5	791·2	485·6	327·5	240·2	138·0
6·0	743·2	517·9	305·0	207·0	118·0
6·5	704·1	562·8	345·8	188·7	131·3
7·0	744·0	605·2	389·0	207·8	162·9
7·5		636·8		240·2	190·4

In Table VI are given values of v throughout each cycle. Total volumes can be obtained by multiplying by the factor $\mathcal{M}/\mathcal{A}$. These values of v are plotted in Fig. 2 and show the pulsation proper of the reversing layer for each star.

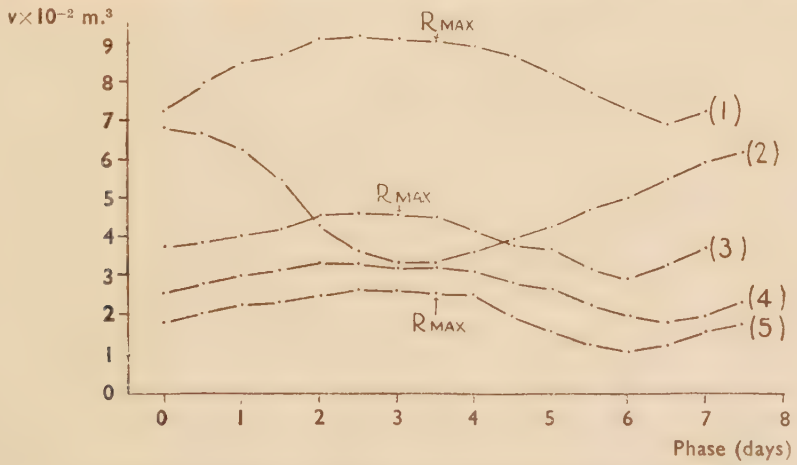

FIG. 2.—*Curves of the atomic volume of matter in the reversing layers of the Cepheids.*

(1) *η Aquilae.*
(2) *U Vulpeculae.*
(3) *U Aquilae.*
(4) *W Geminorum.*
(5) *W Sagittarii.*

R_{max} : *Phase of maximum radius of photosphere.*

There is a point of interest to be noted. If we plot the radius R against phase (the pulsation curves of the photosphere), we perceive that the phases of the maximum volume of the star and of the reversing layer do not coincide. The maximum of the star's volume corresponds to a phase slightly after the secondary maximum, while the maximum of the reversing layer volume coincides with the secondary maximum of the light curve. The case of U Vulpeculae, if exact, is exceptional. However, the coincidence of the maximum volume of the reversing layer with the secondary maximum might be due to the "puff" of radiated energy which clearly seems to occur at that phase. But the problem of the secondary maxima of the Cepheids is a theme to be discussed separately.

Athens :
1948 *March* 22.

References

(1) η Aquilae : T. S. Jacobsen, *Lick Obs. Bull.*, **379,** 138, 1926.
U Vulpeculae : Vernon Robinson, *H.B.*, **872,** 11, 1930.
U Aquilae : R. F. Sanford, *Ap. J.*, **72,** 46, 1930.
W Geminorum : R. F. Sanford, *Ap. J.*, **72,** 46, 1930.
W Sagittarii : E. Baker, *Astronomy*, Van Nostrand, N.Y., p. 350.
(2) *Astrophysik*, Akad. Verlag., Leipzig, p. 182.
(3) G. Tiercy, *Mem. Osservatorio Astrofisico di Arcetri*, **44,** 34, 1927.
(4) H. Lane, *A.J.*, **1,** 57, 1870.
(5) ΔM has been measured from the graphs of the light curves. These have been taken from :
η Aquilae : E. E. Markwick, quoted by Grouiller, *Bulletin Astronomique*, 2^{e} *série*, **1,** 350, 1922.
U Vulpeculae : Curve by the author ; "The secondary maxima of the regular variables." Thesis, Athens, not published, 1946.
U Aquilae : E. C. Pickering, *Ap. J.*, **72,** 46, 1930.
W Geminorum : J. van der Bilt, *Ap. J.*, **72,** 46, 1930.
W Sagittarii : E. Baker, *Astronomy*, van Nostrand, N.Y., p. 350.

A THERMODYNAMIC CONSIDERATION IN RELATION TO ACOUSTIC ENERGY IN STELLAR MODELS

T. Gold

(Received 1949 February 16)

Summary

Thermodynamic limitations of the generation of acoustic energy in stars are discussed. It is shown that noise can never become the sole agent of outward energy transport, and that it is unlikely ever to play a major part in this process.

It has recently been suggested (**1, 2**) that the transfer of energy in stars may, under some circumstances, be achieved by acoustic waves. Processes do undoubtedly occur in which acoustic energy is liberated, but it is difficult to gain insight into the details of such processes. For this reason it is of interest to consider the general limitations which would be imposed on any such energy liberation by the second law of thermodynamics.

Acoustic energy is, from the thermodynamic point of view, "free" energy, as its transfer is not by necessity associated with a transfer of entropy. This is true whatever the spectral distribution of the noise may be, so long as we do not include frequencies which are so high that the extinction distance becomes short compared with the wave-length. Accordingly any thermal process which leads to the liberation of acoustic energy is subject to the thermodynamic limitations of a heat engine ; and the maximum possible efficiency, in terms of free energy available per unit of thermal energy supplied at the temperature T_1, is given by

$$\eta = \frac{T_1 - T_2}{T_1}, \tag{1}$$

where T_2 is the temperature at which heat is ejected. It follows that in the steady state case, where there is a continuous source of thermal energy within a closed region, there cannot be a net outflow of acoustic energy without a net outflow of heat at least $T_2/(T_1 - T_2)$ times as great.

In a recent paper by Richardson and Schwarzschild (**2**) a stellar model of red giants is discussed and analysed in detail ; it is there supposed that a convective core gives rise to acoustic energy as a result of turbulence, and that this core is surrounded by an isothermal zone in which the outward transport of energy is entirely acoustic. It will be seen that such a model is in direct conflict with the previous consideration. Taking the figures for the temperatures which are assumed there, namely 3×10^7 degrees at the centre and $1{\cdot}5 \times 10^7$ degrees at the boundary between the noise-producing core and the supposed isothermal zone, we find that at least half the energy requires to be transported away as heat; and that the surrounding zone cannot, in fact, approach an isothermal condition.

The previous considerations set an upper limit to the efficiency with which mechanical energy can be generated; they are independent of the type of mechanism employed, and only a perfect mechanism could attain this efficiency. In fact,

a system of convection currents is far from being a perfect generator of noise. Free energy must continuously be supplied to keep the system of convection currents moving against the frictional effects of turbulence and viscosity. Furthermore, a part of the heat supplied is transferred outwards by radiation and plays no part in the generation of mechanical energy. One may hence expect that the efficiency of noise generation falls far short even of that given by equation (1). Acoustic waves can hence not become a major agent of energy transport.

Trinity College,
Cambridge :
1949 *February* 13.

References

(1) M. Schwarzschild, *Ap. J.*, **107,** 1, 1948.
(2) R. S. Richardson and M. Schwarzschild, *Ap. J.*, **108,** 373, 1948.

ERRATA

M.N., **107,** No. 3, Harold Jeffreys' paper :

P. 260, fifth line of *Summary*, *for* less *read* more.
P. 261, equation (6), *for* c^2 *read* c^3.

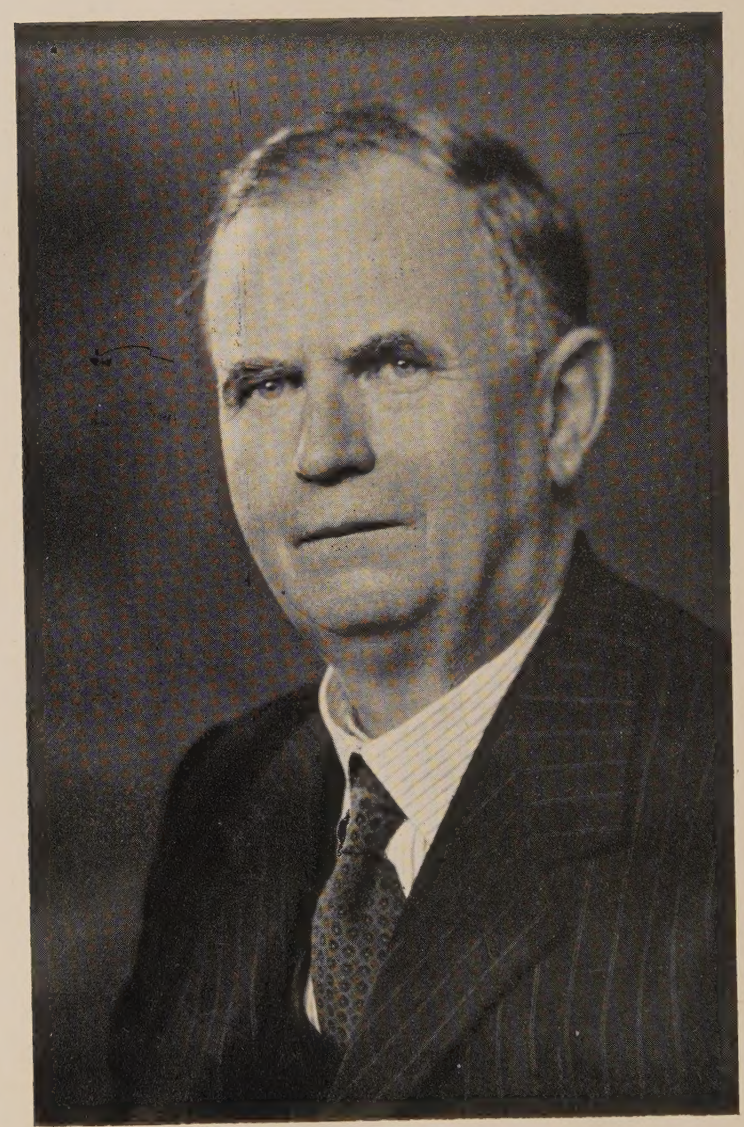

Professor W. M. H. Greaves, M.A., F.R.S.,
President, 1947–1949